UNIVERSIDADE DE SÃO PAULO
INSTITUTO DE FÍSICA DE SÃO CARLOS

Paulo Cesar Ventura da Silva

Epidemic modeling with host behavioral responses

São Carlos

2021

Paulo Cesar Ventura da Silva

Epidemic modeling with host behavioral responses

Thesis presented to the Graduate Program in Physics at the Instituto de Física de São Carlos da Universidade de São Paulo, to obtain the degree of Doctor in Science.

Concentration area: Basic Physics

Advisor: Prof. Francisco Aparecido Rodrigues

Corrected version
(original version available on the Program Unit)

São Carlos
2021

Silva, Paulo Cesar Ventura da
Epidemic modeling with host behavioral responses / Paulo Cesar Ventura da Silva; advisor Francisco Aparecido Rodrigues - corrected version -- São Carlos 2021.
181 p.

Thesis (Doctorate - Graduate Program in Basic Physics) -- Instituto de Física de São Carlos, Universidade de São Paulo - Brasil , 2021.

1. Epidemic models. 2. Behavioral responses. 3. Multiplex networks. 4. Agent-based modeling. 5. Metapopulations. I. Rodrigues, Francisco Aparecido, advisor. II. Title.

ACKNOWLEDGEMENTS

I express my sincere gratitude...

To the outstanding teachers and professors that I had during my life, especially the passionate physics teachers that I had during high school.

To professor Francisco, whose kindness and creative ideas are greatly responsible for the results in this thesis. Huge gratitude to professor Yamir Moreno, who cordially received me for an internship in Zaragoza/Spain and helped me with academic and life aspects.

To my friends and colleagues from multiple work-related groups that I joined during the PhD, especially those who helped me through the learning of an entirely different research area. To all my collaborators, with whom I had the pleasure to share ideas and tasks: Federico Vazquez, Fátima Velásquez-Rojas, Alberto Aleta, Colm Connaughton, Eric Tokuda, Luciano da Fontoura Costa and Kirstin Roster.

My well-being was also ensured thanks to my friends from CAIFSC, Integração Musical and Parkour São Carlos, activities that I had beyond the PhD.

To my father, who had the full role of parenting during most of my childhood, and to my adorable family.

To the financial support from FAPESP, through grants 2016/24555-0 (main PhD funding) and 2019/11183-5 (internship abroad). Research carried out using the computational resources of the Center for Mathematical Sciences Applied to Industry (CeMEAI) funded by FAPESP (grant 2013/07375-0).

"I think the next century
will be the century of complexity."
Stephen Hawking

ABSTRACT

SILVA, P. C. V. **Epidemic modeling with host behavioral responses**. 2021. 181p. Thesis (Doctor in Science) - Instituto de Física de São Carlos, Universidade de São Paulo, São Carlos, 2021.

Epidemics have always been the cause of significant economic and life losses. Among the multiple developments of science against infectious diseases, mathematical and computational models are increasingly important, especially after the development of complexity and network science. The study and forecasting of epidemics are highly influenced by behaviors of host populations, which are unpredictable and difficult to incorporate. In this thesis, we contribute to the substantial volume of works dedicated to solving this problem. First, we approach the coupling between disease and information spreading on multiplex networks. We propose a rumor-like model for the information and a flexible ratio of time scales between disease and information. We show that increasing the time scale of the information reduces the disease prevalence. We also show that stiflers may cause an increase in both infection and information levels. This problem is then further studied with more general models of asymmetrical interaction between contagion phenomena. We show that our previous results on the time scale depend on the form of interaction between the spreading processes. We also study in more depth these models, numerically describing their transient oscillations and deriving analytical expressions for their steady states and phase transitions. We then switch to systems with host mobility, which is an important ingredient of epidemic spreading. We first develop an individual-based mobility and epidemic model, into which behavioral responses are incorporated as an avoidance of infectious hosts. We show how this reduces the disease spreading in different regimes of our model. In particular, for when mobility evolves much faster than epidemics, we derive a semi-analytical approach to describe the model's bifurcation diagrams, verifying the existence of a bistable region and relating the dynamics to some metrics of the underlying networks. Finally, we move to larger scales and describe mobility as net flows between homogeneous populations. In this metapopulation scheme, we propose a model for behavioral responses that directly reduce the disease reproduction number. We show that our model can generate different outbreak sizes between subpopulations. Then we use it to compare strategies in which each subpopulation responds independently (locally), or the whole population follows the same response curve (globally). We show which strategy is more effective in different scenarios, for both a random geometric graph and two metapopulations constructed from real data. With the variety of topics that we approached, we hope to contribute significantly to the problem of disease-behavior coupling.

Keywords: Epidemic models. Behavioral responses. Multiplex networks. Agent-based modeling. Metapopulations.

RESUMO

SILVA, P. C. V. **Modelagem epidêmica com respostas comportamentais dos hospedeiros**. 2021. 181p. Tese (Doutorado em Ciências) - Instituto de Física de São Carlos, Universidade de São Paulo, São Carlos, 2021.

Epidemias sempre foram a causa de perdas econômicas e vitais significantes. Entre os múltiplos avanços da ciência contra doenças infecciosas, modelos matemáticos e computacionais são cada vez mais importantes, especialmente após o desenvolvimento da ciência de redes e complexidade. O estudo e previsão de epidemias é muito influenciado por comportamentos da população hospedeira, que são imprevisíveis e difíceis de se incorporar. Nesta tese, contribuímos para o grande volume de trabalhos dedicados a resolver esse problema. Primeiramente, abordamos o acoplamento entre a propagação de doenças e informação em redes multiplex. Propomos um modelo de rumor para a informação, bem como uma razão flexível entre as escalas de tempo da doença e da informação. Mostramos que aumentando a escala temporal da informação se consegue uma redução de casos da doença. Também mostramos que *stiflers* podem aumentar tanto os níveis da informação quanto da doença. Depois estudamos esse problema mais a fundo com modelos mais gerais de interação assimétrica entre fenômenos de contágio. Mostramos que nossos resultados anteriores com a escala de tempo dependem do formato da interação entre os processos de propagação. Também estudamos esses modelos em mais detalhe, descrevendo numericamente suas oscilações transientes e derivando expressões analíticas para os estados estacionários e transições de fase. Mudamos então para sistemas com mobilidade de hospedeiros. Desenvolvemos um modelo de mobilidade individual, em que respostas comportamentais são incorporadas na forma de esquiva de hospedeiros infectados. Mostramos como isso reduz a propagação da doença em diferentes regimes do modelo. Em particular, para quando a mobilidade progride mais rápido que a doença, derivamos uma abordagem semi-analítica para descrever os diagramas de bifurcação, verificando a existência de uma fase biestável e relacionando a dinâmica com algumas métricas das redes subjacentes. Finalmente, descrevemos a mobilidade como fluxos entre populações homogêneas. Nesse esquema de metapopulação, propomos um modelo para respostas comportamentais que diretamente reduzem o número de reprodução. Mostramos que nosso modelo pode gerar surtos de tamanhos diferentes em cada subpopulação. Então o usamos para comparar estratégias em que cada lugar responde de forma independente (localmente) ou em que toda a população segue a mesma curva (globalmente). Mostramos qual estratégia é mais eficiente em diferentes cenários, tanto para um grafo geométrico aleatório quanto para duas metapopulações de dados reais. Com tal variedade de tópicos explorados, esperamos contribuir para o problema da interação doença-comportamento.

Palavras-chave: Modelos epidêmicos. Respostas comportamentais. Redes multiplex. Modelagem de agentes. Metapopulações.

LIST OF FIGURES

LIST OF TABLES

LIST OF ABBREVIATIONS AND ACRONYMS

ANAC	National Agency of Civil Aviation
ANTT	National Agency of Terrestrial Transport
BA	Barabasi-Albert
CM	Configuration model
DBMF	Degree-based Mean Field
DFE	Disease-Free Equilibrium
DK	Daley-Kendal
ER	Erdős-Rényi
GDP	Gross Domestic Product
HIV	Human Immunodeficiency Virus
HMF	Heterogeneous Mean Field
IBGE	Brazilian Institute of Geography and Statistics
LT	Long-term scenario
MMCA	Microscopic Markov Chain Approach
MT	Maki-Thompson
RGN	Random geometric network
SF	Scale-free
SEIR	Susceptible-Exposed-Infectious-Removed
SIS	Susceptible-Infectious-Susceptible
SIR	Susceptible-Infectious-Removed
SIRS	Susceptible-Infectious-Removed-Susceptible
ST	Short-term scenario
UCM	Uncorrelated configuration model
WS	Watts-Strogatz

CONTENTS

1 INTRODUCTION

Throughout history, humankind changed the way it develops its scientific knowledge about the Universe multiple times. In the Classical Era of Western history, a highly philosophical approach prevailed, with experimentation based on simple observations. In the Middle Ages, it was strongly bound to religion and dedicated to understanding the constructions of God. It was only after the Renaissance that modern science was born, with personalities like Nicolaus Copernicus, Galileo Galilei and Isaac Newton using experimentation as the base to develop knowledge, defining the scientific method as we know.

Early scientists of the Modern Era were considerably generalists, in the sense that they contributed to our understanding of nature in multiple aspects, from the motion of celestial bodies to the behavior of living beings. However, as the knowledge accumulated, science was partitioned into multiple areas and sub-branches, such as biology, chemistry and physics. Nowadays, we still recognize the branches of science, and researchers tend to be experts with deep knowledge in a specific branch and research topic. However, parallel to the specialization of science, we see an increasing tendency to *interdisciplinarity*, the integration between two or more areas of knowledge to answer complex common questions. Some new areas were actually born in the overlap between multiple scientific branches. This is the case of the *science of complex systems*, or *complexity science*, as sometimes mentioned.

The concept of complexity itself is older than its dedicated scientific area. In physics, a system is said to be complex when it has multiple components that interact in such a way that cannot be described by a unique, higher rule. Spin glasses, which are sets of particles with magnetic spin that display apparently random orientations, are examples of complex systems typically studied by physicists. The abundance of such systems in condensed matter physics led some specialists in this area to consider the concept in a broader context. For example, Phillip Anderson defended that complexity is what lies in between areas of science in a famous paper called “More is different”, published in 1972.[7] For example, physics provides fundamental laws that govern elementary particles and atoms; therefore, in a reductionist view, it should be able to describe any phenomena studied in chemistry. Similarly, living beings are made of atoms, ions and molecules, so the chemistry should explain the entire biology, and so on. None of this is true because, according to Anderson, the complex organization of particles, atoms and molecules leads to entirely new phenomena at higher scales.

These new behaviors that arise from the complexity of interactions are called *emergent phenomena*, and are often considered as fundamental to the definition of complex systems. *Self-organization*, which is when the system as a whole exhibits an ordered behavior, even though its components are disordered, is another feature of complex systems. Over time, some scientists recognized that complexity was the subject of a proper research field for itself. In a later article

published in 1991, Anderson writes[8] p. 11):

> A movement is under way toward joining together into a general subject all the various ideas about ways new properties emerge. We call this subject the science of complexity. Within this topic, ideas equal in depth and interest to those in physics come from some of the other sciences.

He was pointing not only to the fact that complexity was a new scientific branch, but also that problems from other areas rather than physics could be studied in the same fashion. In fact, the global climate, social groups, cities, the human brain, economics and ecosystems do all display complex patterns of interactions, emerging phenomena and self-organization. In the following years after Anderson's publication, the world would witness the consolidation of complexity science as an interdisciplinary research field, dedicated to solving problems arising from multiple contexts, from the micro to the macroscopic world.

In most cases, a complex system is associated with a subjacent *complex network*. These entities are represented as graphs, with vertices representing units of the complex system and edges representing the relationships, connections or interactions between them. For networks that underlie complex systems, these interactions are typically complicated, seemingly random, and do not follow a simple rule for all entities – thus, the name *complex* networks. The study of these networks themselves, with the use of statistical tools and the definition of useful metrics, constitutes another research area itself called *network science*.

The fundamentals of network science come from graph theory, which is an older and well-established field of mathematics. However, graph theory and network science took different directions, mainly due to their different goals. According to Iñiguez and others,[9] p. 2):

> Graph theory has focused on providing rigorous proofs for graph properties, such as graph enumeration, coloring, and covering (with applications ranging from chemistry to circuit design). Current network science, instead, is more akin to phenomenological physics by focusing on observations of real-world networks and ad hoc mathematical concepts to quantify them, with the goal of gaining intuition of their underlying generative mechanisms. Due to its aim of pursuing rigorous arguments, graph theory has so far concentrated on structures that are more analytically treatable, like random or dense graphs, whereas network science focuses on the most common features seen in data, such as sparsity and inhomogeneities in the structure and temporal behavior of large but finite networks.

The authors of the same paper also argue that both areas developed a gap between them, with disruption within research questions and academic communities. They also think that filling this gap in the next years could bring important advances to both fields.

By joining network and complexity science, major scientific developments have been achieved in the last two decades. The human brain, one of the most intriguing systems that we

know, can be better understood with models and descriptive metrics from network science.[10] In economics, recognizing product trades and stock markets as complex systems provide important indices and predictive algorithms[11–12] that have solid applications to the real world. Moreover, infectious diseases in human and animal populations can now be tracked daily and forecasted, thank to the acknowledgment that complex interaction patterns between hosts are fundamental to correctly understand epidemic spreading.[13–15]

In this thesis, we focus on the application of complex systems and networks to epidemic spreading. Epidemics are known to cause several life and economic losses. One single bacterial species, *Yersinia pestis*, caused multiple pandemics throughout human history, including the Plague of Justinian (from 541 to 549) and the Black Death (from 1346 to 1353), some of the deadliest epidemic episodes known. *Influenza-like illnesses* (ILI) have also caused great pandemics, notably the Spanish Flu (1918 to 1920) and COVID-19 (2019 until present), claiming millions of souls each. Other diseases, such as AIDS, dengue fever and tuberculosis, do not usually cause major worldwide outbreaks, but remain endemic for very long periods, constantly causing damages and life losses. Finally, animal and plant diseases, such as the classical swine fever and the citrus greening disease, can also cause substantial economic losses and production outages.

In the toolbox that science offers against infectious diseases, including drugs, vaccines, individual prevention methods and vector control, mathematical and computational models are progressively gaining importance. Disease forecasting can help to guide control policies and prepare resources (such as hospital beds and protection equipment). However, forecasting is one major but not the ultimate goal of epidemic modeling. Relatively simple models can be used to study strategies of targeted quarantining and immunization, the effect of mobility and host interaction patterns, and the interplay between epidemic spreading and some behavioral traits like opinion, rumors, vaccine hesitancy and self-protection.

Models for epidemic spreading can also be adapted to a variety of other phenomena, in what Pastor-Satorras and others[16] refer to as the "epidemic metaphor". The authors also write[16] p. 927):

> The spread of information, cultural norms, and social behavior can be conceptually modeled as a contagion process. How blackouts spread on a nationwide scale or how efficiently memes can spread on social networks are all phenomena whose mathematical description relies on models akin to classic epidemic models.

Indeed, the so-called *rumor models*, which mimic how people start and stop spreading rumors,[17] consist a famous adaptation of epidemic models. We can refer as *spreading phenomena* or *contagion processes* to any of these systems that can be reasonably modeled based on epidemic models.[16]

1.1 The research problem and our contribution to it

Despite the great advances in the field of epidemic modeling over the last years, the area still struggles with one of its essential features: the crucial influence of host behavior, especially in human populations. Incorporating the unpredictability of human behavior is recognized as a major challenge,[18] both for disease forecasting and other applications of epidemic models. In fact, Moran and others[19] argue that epidemic forecasting is more difficult than weather forecasting, which, despite being subject to heavily chaotic systems, has little influence from human and animal behavior in the short term. During new outbreaks of emerging diseases, such as Ebola and COVID-19, it can be even more difficult to incorporate behavior, as it is highly dependent on decisions made by policymakers and has profound impacts on the disease dynamics.

In spite of the general unpredictability of human behavior, some of its features and patterns can be observed from empirical data, and then converted into a modeling framework. For example, models of opinion dynamics and rumor spreading can be used to describe the spread of disease-related information on physical and virtual social media, which then influence the disease dynamics. Mobility is also modified during emerging outbreaks, and the current availability of mobility data makes it possible to incorporate and predict these changes.

For the work reported in this thesis, we embraced the challenge of the disease-behavior relationship in multiple aspects. Our primary goal is to contribute to the knowledge in the topic from a mostly theoretical aspect, with potentially important insights extracted from simple models. To achieve this goal, we explored new and trending techniques in the field such as multiplex networks, agent-based temporal networks and microscopic Markov Chains, as well as established tools such as metapopulations, homogeneously mixed populations and some tools from dynamical systems.

1.2 Structure of the text

Multiple works were developed during the PhD course that culminated into this thesis, and this is reflected in the structure of the manuscript. The next chapter, “Fundamentals”, is dedicated to presenting the underlying theory that is common to most of the manuscript, divided into two main topics: populations (Section 2.1), represented by complex networks, and epidemic dynamics (Section 2.2), including multiple approaches to fundamental epidemic models.

In the following chapters, we expand from the basic concepts and present our contributions. In Chapter 3, two works regarding the interaction between spreading phenomena, with emphasis on the asymmetrical interplay between disease and information, are presented and discussed. In Chapter 4, we expose two more works that have in common the inclusion of host mobility and protective behavioral responses.

Despite the overlapping points, these works are based on their specific range of previous works, and consequently we present our literature review within each chapter, instead of

a single dedicated one for all subjects. The discussions are also presented after each work. Finally, in Chapter 5, we recall the main conclusions and discuss the takeaways from our work. Importantly, we remark that there are appendixes in which we develop some calculations and experiments that are not focal to the main text.

2 FUNDAMENTALS

Nowadays, the spread of epidemics is considered a complex system, because it is sustained through complex patterns of contacts between hosts. These patterns have been shown to cause emergent phenomena, such as the propagation of the disease even for very small transmission rates in some complex topologies. Therefore, it is expected that complex networks are one of the fundamental ingredients of our work.

In this chapter, we present the theoretical basis that is shared by all works developed in this thesis. We divide this chapter by the two main components that we use to construct an epidemic model: the *population* and the *dynamics*. For the population (Section 2.1), we present the fundamentals of network theory, which may be of common interest for readers from other areas of complexity science. For the dynamics (Section 2.2), we present two of the most fundamental epidemic models, focusing on the SIS (which is the most used during the rest of the thesis). We describe multiple theoretical approaches for these models, including homogeneously mixed populations and some mean field approaches for static networks. We also discuss in brief multiple methods for stochastic simulations.

2.1 Modeling populations

Up to the end of the 20th century, most mathematical models for disease spreading, ecosystem dynamics and information propagation were based on homogeneously mixed populations, regular lattices or simple random graphs without heterogeneity. A homogeneously mixed population assumes that all its elements interact with each other at equal rates (or probabilities), or in an all-to-all scheme (all elements interact). By the second half of the 20th century, some researchers from social sciences already employed graphs to represent human populations.[20] In ecology[21] and epidemiology,[22] some groups also considered *metapopulations*, but they were usually connected in a homogeneous scheme as well.

At the beginning of the 21st century, triggered by important results from seminal works,[6,23] it was evidenced that many real-world systems, when represented as graphs, were far from random in many aspects, such as the distribution of numbers of links (degree) and statistical correlations. It was also unveiled that dynamical systems, when held on top of these graph representations, have fundamentally different properties from when executed on homogeneous populations. This led to the consolidation of network and complexity science as an authentic area of the knowledge.

Since then, an incredible amount of works have tried to describe and unveil the diverse properties that can be present on complex networks. In this section, we review some of the most important concepts learned from this emerging field, aiming to set the ground for the rest of this

thesis. For a more detailed introduction, we guide the reader to some important references on the subject.[24–29]

2.1.1 Complex networks – basic concepts

In this chapter, we shall use the terms graph and network interchangeably. A graph $\mathcal{G}$ is composed by a set of N nodes (or vertices) $\mathcal{V}$, connected by links (or edges) from a set $\mathcal{E}$ with M elements. For a simple (undirected) graph, each element of $\mathcal{E}$ is an unordered pair of nodes $(i, j) \in \mathcal{V}^2$. A subgraph of $\mathcal{G}$ is any subset of $\mathcal{V}$, along with all edges $(i, j) \in \mathcal{E}$ such that i and j belong to the subset. Networks can be represented by an adjacency matrix $\mathbf{A}$, whose elements are defined as:

$$A_{ij} = \begin{cases} 1 & (i,j) \in \mathcal{E} \\ 0 & (i,j) \notin \mathcal{E} \end{cases}. \tag{2.1}$$

Therefore, $\mathbf{A}$ stores non-null values for the pairs of nodes that are linked, and $A_{ij} = A_{ji}$ for an undirected graph.

We can denote as $\mathcal{N}_i$ the *neighborhood* of node i, this is, the set of nodes that are connected to i . The number of links that emerge from a node i is called the *degree* k_i of this node, and can be extracted from the adjacency matrix as $k_i = \sum_{j=1}^{N} A_{ij}$. The average degree $\langle k \rangle = \frac{1}{N} \sum_{i=1}^{N} k_i = \frac{2M}{N}$ tells how well connected are the nodes of a network, and is a starting metric to compare different networks.

2.1.1.1 Centrality

For many applications, nodes with higher degrees are usually more *important* for the dynamics that is held on the network. For instance, with epidemic models, high-degree nodes are often influential spreaders, meaning that they can contract and transmit a disease more easily.[30] This idea of *importance* of a node for a given dynamics or structural properties can be generalized to what is called *centrality*. A centrality is usually a locally applied metric (meaning that it applies to a single node, edge or a small subgraph), which somehow encodes the importance of each element for a given context. The idea of "importance" is vague, thus better explained with examples.

The *closeness centrality*, defined initially by Bavelas,[31] is calculated for *connected* graphs (i.e., graphs in which all nodes can be accessed from all other nodes by following the existing links) as:

$$l_i = \frac{1}{\sum_{j=1}^{N} d_{i,j}}, \tag{2.2}$$

where d_{ij} is the distance between nodes i and j, often regarded as the minimum number of links that must be followed from i to reach j (the *shortest path length*). This centrality metrics effectively tells how close, in average, a given node is from all other nodes. Another example, the *betweenness centrality*[32] is defined as:

$$b_i = \sum_{j,k \in \mathcal{V}, j \neq k} \frac{n_{jk}(i)}{n_{jk}}, \tag{2.3}$$

where n_{jk} is the total number of shortest paths connecting j and k, while $n_{jk}(i)$ is the number of such shortest paths that pass through node i. This measures how much a given node is an important intermediate when moving between random nodes of the network, and has notable importance, for example, for traffic networks, where nodes with high b_i are subject to heavier loads of traffic.[33]

Other popularly known definitions of centrality include: the *eigenvector centrality*,[34] which measures how important a node is for a random walk process on the network; the *harmonic centrality*,[35] which is a variant of the closeness centrality that applies for non-connected graphs; the *PageRank centrality*, which modifies the eigenvector centrality to work with directed (i.e., non-reciprocal) links and long-range jumps; the *non-backtracking centrality*,[36] another modification to the eigenvector centrality that compensates for localization effects, among many others. For a detailed description of centrality measures, we refer to Chapter 7 of [26] and references therein.

2.1.1.2 Clustering and correlations

Interactions in real-world complex systems are not independent of one another; this produces statistical features that can be captured by appropriate metrics. For example, on the network of friendships of a school, individuals from the same classroom are more likely to be friends and, even inside a, classroom there are "clubs" of mutual friendship. For large online social networks, famous people usually interact more with other famous individuals than with "anonymous" people. Finally, nodes of a network with spatial constraint (e.g. highway networks between cities) are more likely to connect with closer nodes, which leads to clusters of highly connected nodes by proximity. These features can be captured by a number of statistical metrics, of which we discuss two important ones: *clustering* and *assortativity*.

Clustering quantifies the tendency of a network to present triangles, i.e., triples of nodes entirely connected to each other. One measure of the clustering is called *transitivity*, and applies to an entire network as follows[24,26]:

$$T = \frac{3 \cdot \text{number of triangles}}{\text{number of connected triples}}. \tag{2.4}$$

By connected triples, we understand a subgraph of three nodes that has at least two (but not necessarily three) links. With the factor 3 on the numerator, the metric falls between 0 and 1, and only reaches 1 in a complete graph (i.e., with each node linked to every other). Networks with high transitivity present many nodes with the property that "a friend of my friend is also my friend". For a different perspective of the same phenomenon, a local metrics called *clustering coefficient* is defined, for nodes $i \in \mathcal{G}$ with $k_i \geq 2$, as:

$$c_i = \frac{2e_i}{k_i(k_i - 1)}, \tag{2.5}$$

where e_i is the number of edges on the subgraph formed by node i and all of its neighbors. Notice that $k_i(k_i - 1)/2$ is the maximum possible value for e_i, meaning that $0 \leq c_i \leq 1$. Also, by convention, $c_i = 0$ if $k_i < 2$.

To quantify the connectivity between individuals with similar degrees, another metric can be conveniently defined: the *degree assortativity*.* It is an adaptation of the Pearson correlation coefficient to measure the tendency that hubs (i.e., highly connected nodes) have to connect with other hubs (positive correlation) or low-degree nodes (negative correlation). As defined by Newman,[26,37] it is expressed as:

$$r = \frac{\sum_{ij \in \mathcal{G}} (A_{ij} - k_i k_j / 2M) k_i k_j}{\sum_{ij \in \mathcal{G}} (k_i \delta_{ij} - k_i k_j / 2M) k_i k_j}, \tag{2.6}$$

where δ_{ij} is the Kronecker delta, yielding 1 if $i = 0$ and 0 otherwise. The numerator quantifies the co-occurrence of high-high or low-low degrees between neighbors, subtracted by the expectancy from a null model (given by $k_i k_j / 2M$), and the denominator represents the variance of this quantification, to normalize the metrics into the $[-1, 1]$ interval. For example, networks of scientific coauthorship and film actor collaborations tend to have a strong assortative pattern[38] ($r > 0$), while metabolic and neural networks tend to be dissortative ($r < 0$), for instance, with highly interacting proteins often making many connections with lowly interacting ones.[39]

2.1.2 Basic network models

To construct a complex network, it is necessary to either extract it from real-world data or to produce a synthetic one. For the latter case, a considerable variety of models have been and are still being proposed. More than just algorithms to construct graphs, these models often prove useful to understand the creation and evolution dynamics of real systems. This happens, for example, when the model defines procedures inspired on a real mechanism, and the resulting network presents features that are actually observed on the system in which it was inspired.

* Here we focus on the correlations between degrees, but assortativity can be defined for any scalar property of nodes.

In this subsection, we present some of the most popular models used by network scientists to produce simple synthetic networks. These models will also be used through the next chapters of this thesis.

2.1.2.1 Erdős-Rényi model – The "random network"

One simple way to construct an arbitrarily large network was studied by the Hungarian mathematicians Paul Erdős and Alfréd Rényi, in a series of papers.[40–43] It consists of simply connecting pairs of nodes at random, with uniform probabilities. The graph generated by the *Erdős-Rényi* (ER) model is sometimes called a "random network" ,[29] although this term is more appropriately attributed to any graph constructed with a random process.

In a construction algorithm called $G(N, p)$ model, each pair of nodes is queried once to form a connection, which may be established with probability p. This produces a graph for which the final number of links M is a random variable, with average $\langle M \rangle = p \cdot N(N-1)/2$. As the probability is uniform, every node $i \in \mathcal{V}$ is statistically similar, and the degree distribution is a binomial:

$$p(k) = \binom{N-1}{k} p^k \left(1-p\right)^{N-1-k}. \tag{2.7}$$

The $G(N, p)$ is preferred for analytical purposes, because each link is created independently of one another. However, its construction has $\mathcal{O}(N^2)$ computational complexity, while the desired often has very low p (meaning that most link creation events will fail). If computational cost is a concern, or if an exact number M of links must be given, the so called $G(N, M)$ model may be used instead. In this algorithm, at each step, two nodes i and j are randomly selected to form a link, and the steps are repeated until M links are formed. If i and j are already connected, the step is repeated; this means that, as the graph is constructed, the choice of new links is no longer independent of existing ones. Therefore the actual distribution differs from 2.7, but the statistical differences between $G(N, p)$ and $G(N, M)$ tend to zero as M (or $\langle M \rangle$) tends to infinity. Yet, the $G(N, M)$ algorithm is considerably cheaper for sparse graphs, this is, when $M \ll N^2$.

The ER model, due to its simplicity, lacks several statistical properties of real social systems, and is often not regarded as a *complex* network. For example, its expectancy for the clustering coefficient is:[29]

$$\langle C_i \rangle = \frac{\langle M \rangle}{2N^2} = \frac{\langle k \rangle}{N} \tag{2.8}$$

which, for a large population in which the number of contacts $\langle k \rangle$ is limited, tends to zero as $N \to \infty$. This happens because every node is equally likely to interact with each other node, whereas large social populations impose spatial and organizational constraints to the links,

resulting in non-vanishing clustering. Another feature from social groups is the heterogeneity of contacts, in contrast to the homogeneous degree distribution of the ER model.

2.1.2.2 Barabasi-Albert model, scale-free networks and the configuration model

In 1998, an analysis over an empirical survey of citations in scientific papers was made by Redner,[44] showing that the distribution of papers according to their numbers of citations displayed a fat-tailed distribution. Albert and others[45] found a similar pattern in the number of links of webpages in the World-Wide-Web at that time. These and other similar results in different networks were aggregated by Barabasi and Albert[23] in a paper that is considered foundational of the contemporary network science.

In the same papers, the authors propose a network construction algorithm that could reproduce the fat-tail pattern with a power law degree distribution. In this model, currently known as the *Barabasi-Albert* (BA) model, the network is grown from an initially small set of m_0 nodes with an arbitrary connectivity (provided that all nodes have at least one link). At each step of the algorithm, a new node is added with $m \leq m_0$ links to the other existing nodes. These links are chosen following a *preferential attachment* rule: the probability that a node i already present is linked to the new node is given by:

$$p_{\text{link}}(k_i) = \frac{k_i}{\sum_{j \in \mathcal{V}} k_j}, \tag{2.9}$$

therefore proportional to the current degree of i.[†] This means that highly connected nodes are more likely to receive more links during the network construction, making their degrees even higher – a "rich-gets-richer" phenomenon.

With these two ingredients – growth over time and preferential attachment – included, and for sufficiently large N, the degree distribution of the network converges to[23,29]:

$$p(k) = \frac{2m^2}{k^3}, \tag{2.10}$$

*w*hich is a power law with exponent -3. Although real networks, when subjected to a power-law fit of their $p(k)$, typically presents values greater (less negative) than -3, the BA model is a great example of the process mentioned in the head of this section: a network construction model inspired on real mechanisms that reproduces features of the systems in which they apply. For example, the network of scientific citations is constantly growing as new papers are added, and highly-cited papers are more likely to be further cited by the new ones.

In general, networks that display a degree distribution shaped as $p(k) \propto k^{-\gamma}$ (with $\gamma > 0$) are named *scale-free* (SF) networks. The BA baseline model, despite its historical im-

[†] To prevent link repetitions, nodes that were already linked are excluded from the choice of the next ones.

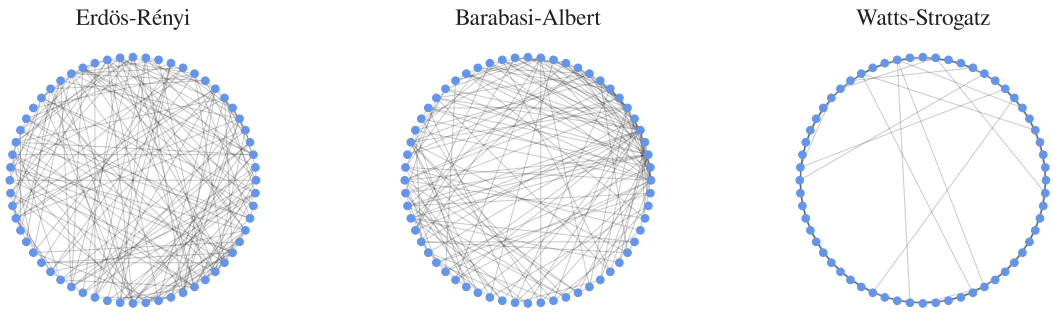

Figure 1 – Samples of different network models. The ER is constructed using $G(N, p)$ algorithm with $p = 0.1$; the BA graph is made with $m = 3$; the WS has $k = 4$ and $p = 0.1$.All graphs have $N = 60$ nodes and have average degrees of $\langle k \rangle \approx 6$.

Source: By the author.

portance, is limited in terms of versatility to construct an SF network (for example, it can only produce an exponent $\gamma = 3$). One common approach to overcome this is the *configuration model* (CM),[46] an algorithm that allows the creation of random networks with arbitrary degree distribution $p(k)$ or, more specifically, a given sequence $\{k_1, k_2, ..., k_N\}$ of degrees. In a simple implementation of this algorithm, the index i of each node is repeatedly placed k_i times in a container such as a list. Then, at each step, two entries of this list are chosen and the corresponding nodes are linked. It is only required that the sum $\sum_{i \in \mathcal{V}} k_i$ is an even number so, by the end of the process, each node i will have exactly k_i links. This implementation does not prevent multiple links between the same pair of nodes, or even self-loops (this is, links with the same node at both ends). This can either be avoided during the construction by discarding unwanted iterations, or after the construction by degree-preserving rewiring.[47]

Scale-free (SF) networks can be constructed with the CM by drawing k_i values from a power-law probability distribution $p(k_i) \propto k_i^{-\gamma}$. Specifically for the generation of SF networks, one common additional step is to constrain the values of k_i to be no greater than $\sqrt{N}$. Catanzaro[48] and others, who proposed this constraint, showed that otherwise the SF networks produced by the CM can present strong degree-degree correlations (assortativity), and for this reason the use of $k_i \leq \sqrt{N}$ is known as the *Uncorrelated Configuration Model* (UCM). Uncorrelated networks serve as useful null models for the analysis of network properties and dynamical systems.

2.1.2.3 The Watts-Strogatz (WS) “small-world” model

Another network construction model inspired in a real-world property was proposed by Duncan Watts and Steven Strogatz in 1998.[6] Since decades before, there was already a common belief that every person in the world could be reached, by following acquaintance

links, by no more than six steps. Although this sentence is imprecise and not strictly true, the hierarchical and highly connected structure of the present global population indeed allows for short acquaintance paths between individuals of geographically distant communities.[49] Yet, as already mentioned, large-scale social networks still have highly clustering coefficients, unlike ER networks with similar average degrees.

Aiming to mimic these features – low shortest paths and high clustering – Watts and Strogatz proposed a network that starts from a ring configuration. Each node is (conceptually) put in the vertices of an N-sized regular polygon, and connected to its k immediate neighbors both to the clockwise and counterclockwise directions, totaling $2k$ links for each node. This configuration has high clustering coefficient (as the neighbors of a node share a significant amount of links), but still present large average distances due to the sequential aspect of the ring. Then a rewiring procedure is executed: each edge starting from a node may have its other end redirected to another randomly selected node, and this occurs with probability p for each edge. Watts and Strogatz show that, for an intermediate scale of values of p, the average shortest path of the network, given by:

$$\langle d \rangle = \frac{1}{N(N-1)} \sum_{i \neq j \in \mathcal{V}} d_{ij}, \tag{2.11}$$

is considerably reduced from the basic ring (i.e., with $p = 0$), while the average clustering is kept high. This algorithm, now known as the *Watts-Strogatz* (WS) model, is therefore a straightforward way to reproduce the relationship between clustering and distances found in real social networks.

For visualization, in Figure 2.1.2.2, we show one sampled graph from each network model described up to this point. All samples have $N = 60$ nodes, and the parameters are such that their average degree are around 6. In the Erdős-Rényi graph, links are random and fill the inside of the circular layout more or less homogeneously. In the BA network, though (in which nodes are sorted by their time of creation), a small set of nodes concentrate more links than the rest. In the WS network, most links are between close nodes, but some few links from the rewiring process help to reduce average distances.

2.1.2.4 Random Geometric Networks (RGN)

For the WS model, we use a geometric shape (a polygon) to visualize the initial arrangement of the nodes. We can, however, use a geometric space to establish connections between nodes, especially if we want to reproduce the features of a real system in which nodes are embedded in space (such as cities, streets and transport stations). One simple and popular way to do this is called a *random geometric network* (RGN).[50]

In order to construct a two-dimensional RGN, we start by uniformly distributing nodes at random in a rectangular space of dimensions L_x and L_y. Then we connect pairs of nodes

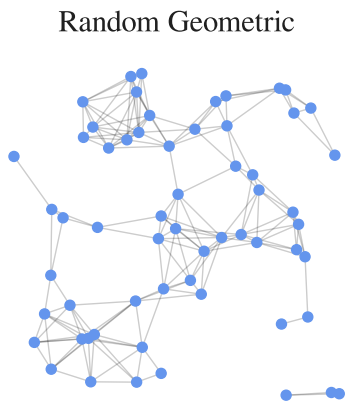

Figure 2 – Example of an RGN with $L_x = L_y = 1$, $d = 0.2$ and $N = 60$ nodes. The average degree is $\langle k \rangle \approx 6$, as in the network samples of Figure 2.1.2.2.

Source: By the author.

whose Euclidean distance is smaller than a given value d. Periodic boundary conditions are optional, but desired if border effects are to be avoided. Using this algorithm, the resulting networks present homogeneous properties among nodes, but a strong spatial character. Just like an ER graph, the expected degree distribution is binomial. However, and unlike the ER model, the average clustering coefficient is typically high due to shared neighborhoods, and average shortest path length is also high due to the spatial constraint of the links (assuming that d is at least one order of magnitude smaller than the dimensions of the space).

In Figure 2 We show an RGN with the nodes' in their positions that were used for the network construction. It is visible that triangles (this is, fully connected triples of nodes) are very frequent, which explains the high clustering coefficient. In the borders, we also find nodes that are many steps away from some other nodes and, thus, the average shortest path distance is high.

2.1.3 Directed, weighted and bipartite networks

The basic definition of network given in Section 2.1.1 can be extended in several ways, usually with the goal of capturing additional features that are observed in the real system being modeled. This is important to better understand the underlying system and its dynamics.

The links (edges), as described so far, are a symmetric relationship between two nodes (vertices), meaning that if node i is connected to j, then j is also connected with i. We can also say that every edge $(i, j) \in \mathcal{E}$ is an unordered pair, and the adjacency matrix $\mathbf{A}$ is symmetric. We can relax this condition by imposing a *direction* into the links: we now regard $(i, j) \in \mathcal{E}$ as an *ordered* pair, in which case we say that i *points to* j. This sentence does not imply that j

points to i.[‡] A network with this property is called a *directed* network.

For directed networks, many of the metrics must be redefined. For example, the degree can now refer to three concepts: the *incoming* degree k_i^{in} of links that point to i, the *outgoing* degree k_i^{out} of links that emerge from i, and the *total* degree $k_i = k_i^{\text{in}} + k_i^{\text{out}}$. Besides concepts already defined by graph theoreticians for directed graphs, researchers have worked to redefine existing and create new metrics that are useful for complex directed networks ,[51–54] the PageRank being one such example. Many real systems can be more adequately represented as directed networks: the links through the WorldWide Web, scientific citations, metabolic networks (of chemical reactions between components of a cell[55]), some online social networks such as Twitter and Instagram, flights between airports, and many others.

For some systems, it is also convenient to define the *weight* of each link. Mathematically, this can be done by including a third entry to the elements of $\mathcal{E}$, now represented as (i, j, w_{ij}), where w is usually a scalar value. Networks with weighted links are called *weighted networks*.[56] The general idea is that some links are more "intense" than others, but the actual interpretation of the weights is up to each system. For example, transport and traffic systems usually have different traffic flows between its linked elements, such as volume of people moving between cities, or numbers of flights between airports. In networks of predator-prey relations, some species may interact more or less frequently with some others, and the frequencies can be quantified as weights. Metabolic networks can also be weighted, by considering the fluxes w_{ij} of each reaction from metabolite i to j,[57] where the links are also directed.

It is always important to understand the impact of including or disregarding one of these extensions to the basic definition of a network. Some systems, like the metabolic network, can have weights that span different orders of magnitude ,[57] thus requiring the incorporation of link weights for detailed analysis. Others, such as migration flows between cities of a small region, could safely disregard the direction of the links for simple applications, with the advantage of having no net flows between the cities. It is responsibility of the researcher to adequately comprise the necessary and sufficient features of a model.

In some situations, we want to only consider interactions between disjoint groups of elements. For example, in vector-borne diseases, such as dengue and schistosomiasis, the transmission occurs by interactions between different species – the host and the vector species.[58] The relevant links between individuals, therefore, are only between a host and a vector. This system can be modeled as a *bipartite* network. Mathematically, we now consider two sets of nodes, $\mathcal{U}$ and $\mathcal{V}$, and the links $(i, j) \in \mathcal{E}$ are such that $i \in \mathcal{U}$ and $j \in \mathcal{V}$. Other previously mentioned systems can also have a bipartite representation. For example, the network of co-authorship can have $\mathcal{U}$ as the set of researchers and $\mathcal{V}$ as the set of scientific papers, and then have links (i, j) for each scientist i that has authored a paper j. The regular network between scientists, con-

[‡] The exact terminology may vary depending on the context. For example, in a directed online social network, we can say that i follows j.

nected by those who share at least one paper, is therefore a projection of the bipartite network, with the latter carrying more information than its projection. As usual, the choice between considering the whole bipartite network[59] of projecting it into a simpler structure[60] depends on the considered system and the desired precision of the results.

2.1.4 Multilayer and multiplex networks

An important generalization to the concept of networks, especially popular in the last decade, is that of *multilayer* and *multiplex* networks.[61–63] A multilayer network (often named just as "multilayer") is a composite structure of multiple layers, each one being a network itself in its basic definition. Each layer encodes its set of links between its own nodes, which are called intra-layer links, but there can also exist links between nodes of separate layers, which are called inter-layer links. Mathematically, the multilayer network can be represented as a set of graphs $\mathbf{G} = \{\mathcal{G}_\alpha = (\mathcal{V}_\alpha, \mathcal{E}_\alpha) : \alpha \in \{1, ..., M\}\}$ and a set of inter-layer links $\mathbf{E} = \{(i, j) \in \mathcal{V}_\alpha \times \mathcal{V}_\beta;\ \alpha, \beta \in \{1, ..., M\},\ \alpha \neq \beta\}$.[62] The adjacency structure can be represented as a rank-4 tensor, two indices for the layers and two for the nodes. Reference[61] provides detailed mathematical description of multilayer networks, as well as some generalized metrics for this type of structure.

It is arguable that a multilayer network could be represented as a single regular network, where nodes are grouped into communities, and links are classified according to the communities to which its pertaining nodes belong.[63] However, it is of conceptual value to represent the multilayer network as composed of multiple individual networks, especially when modeling real systems. For example, we can represent the public transportation of multiple cities as a multilayer network, with each layer representing a single city, and each node representing a transport stop. The intra-layer links describe transport lines of a city, usually managed by the city's own transport department, while inter-layer links are lines between cities, often managed by transport companies. In this example, intra and inter-layer links are *different*, thus justifying the use of multilayers instead of regular networks with communities.

An important particular case of multilayer networks is called *multiplex* networks,[63] which satisfy the following conditions: (i) every layer has the same number of nodes, and (ii) each pair of layers either is connected such that each node of a layer is linked to exactly one node on the other layer, or not connected at all. In other words, there is a one-to-one correspondence between nodes of a connected pair of layers. With this property, it is very common to interpret a multiplex network as follows: each node and its correspondents in other layers represent the same entity (an individual, a transport node, a protein, etc), and each layer represents a different connection structure between these entities.

For example, multiple social media platforms can be represented as a multiplex network, with each layer as a different platform. Individuals that do not have an account in one of the platforms can be set as an isolated node. Notice that each layer may have different features,

such as directed or weighted links, justifying the use of a multiplex network instead of a single network with communities. Another relevant example for this thesis is of multiple interacting spreading phenomena. Diseases, as well as information, have their own means of propagation (direct contact, airborne, sexually transmissible), and to represent multiple diseases we can use a separate layer for the transmissible contacts of each one.

Finally, dynamical systems in multilayer and multiplex networks are proven to display interesting emerging phenomena. Nicosia and others[64] proven that an explosive phase transition occurs in a coupled system of neural (synchronization) and nutrient transport dynamics, each one held in one layer of a two-layer multiplex. De Arruda and others[65] study localization phenomena for disease spreading in multilayers (a single disease that can cross the layers), describing multiple susceptibility peaks caused by localization on the layers instead of the nodes, and a barrier effect for a system of three layers.

2.1.5 Temporal networks

We address here yet another way to extend the basic definition of a network. A *temporal network* is simply any network whose structure, which can either be the nodes and links, varies over time.[66] Indeed, most real complex systems are not static in time but, depending on the ratio between the time scale of the system changes and that of the dynamics of interest, the static graph can be a good assumption. Nonetheless, there are a number of situations in which neglecting the dynamic nature of a network can lead to imprecise results.[67] For a detailed analysis of the topic, we refer to this review [66] by Holme and Saramäki.

There are multiple ways to define a network with temporal dynamics. The evolution of time can be discrete, so at each time step t the system is represented by a given graph $\mathcal{G}_t$. This can be used to represent, for example, a network of flights between airports in more detail than a static network, where (for example) each time step considers the flights that departed during one day. For continuous time evolution, we can regard each creation and annihilation of a node or link as an event ϵ, which occurs at a given time t_ϵ. This could depict, for example, interactions between people in a party, hospital or other social gatherings. Yet under continuous time, the interactions themselves could be regarded as instantaneous events, as in the representation of a network of emails, by considering each message as a network link, regarded as instantaneous.[68] The mathematical definition for each of these formulations is different (in terms of sets of nodes and links), so we do not present them here.

Temporal networks can be either obtained from real data or synthesized using models. The Barabasi-Albert model itself,[23] which is more commonly used for the resulting static network, was inspired on how real systems typically evolve by the constant inclusion of new elements, and can be used as a model of dynamic network. Stehlé and others [69] proposed a model for continuous-time dynamic networks that mimics social interactions, with agents that alternate between being alone or interacting in groups. By considering a memory effect, their

model produces heterogeneous patterns of interactions, with some agents being very socially active and others tending to be more isolated. Starnini and others [70] proposed a discrete-time dynamic network, also based on agents and inspired on social interactions. Each agent performs a random walk on a 2D space, alternating between being inactive, performing the random walk alone of gathering around "attractive" agents (each agent has a social attractiveness score, with higher values making neighbors to stop around it).

With the mentioned model, Starnini and the collaborators reproduced the behaviors and parameters of some empirical distributions from the SocioPatterns dataset,[71] a research collaboration that aims to collect data of human activity and social dynamics in field. For a variety of environments, like schools, hospitals, workplaces and scientific conferences, they used radiofrequency identification (RFID) on each individual to detect proximity between subjects, within a radius of 1 to 2 meters and only when both subjects are facing each other. The contacts are aggregated in time intervals of 20 seconds, making each of their dataset a valuable sample of a social temporal network.

Several examples of applications of temporal networks to epidemic modeling can be found in the literature. Yet using the SocioPatterns data, Stehlé and others [72] simulated an epidemic model on top of the dynamic network of a scientific conference. Considering different levels of aggregation of the data over time, they showed that the temporal ordering of the contacts itself was not very important for the resulting dynamics in this case, but that the weights of the aggregated contacts, based on total interaction times, was crucial to obtain correct outcomes. On the side of synthetic networks, a framework called *adaptive networks* was used in the context of epidemic models ,[73–76] being particularly popular between 2005 and 2015. These works typically consider a network in which each node tries to avoid contagion by changing their contacts, usually rewiring their links from infectious to susceptible individuals. Interesting phenomena, such as bistability [73] and epidemic bursts ,[75] were reported from these types of systems. Adaptive networks are examples of temporal networks whose evolution is mostly guided by another dynamical system running on top of them. Finally, we mention epidemic models based on networks of random walker agents, such as in Frasca and others.[4] We extensively cover these models in Section 4.1.2.

2.2 Modeling epidemic and information dynamics

Despite the inherent complexity of events that lead to disease transmission, mathematical and computational models can be a useful tool to study epidemic spreading in a population level. These models can range from simplistic ones, which translate epidemic spreading into a very minimal set of features, to much more complex and realistic ones, which try to capture most of the relevant details of the propagation of a real disease.

The earliest epidemic model that we know was developed by Daniel Bernoulli in 1766, published in 1766.[77] In this work, Bernoulli pondered the the collective risks and benefits of

the inoculation (a precursor of vaccines) against smallpox, a deadly and widespread disease by the second half of the 18th century. His model included demographic aspects, such as birth and death rates, and disease parameters that depended on the age of individuals, making it notoriously complex for a pioneer work. He concluded that, despite the individual risks of inoculation, its universal application would increase the life expectancy from 26.6 to 29.8 years.

Later, in the 1920 decade, works like those of Kermack and McKendrick[78] and of Reed and Frost[79] founded the basis of contemporary epidemic modeling.[§] During the 20th century, the mathematical modeling of epidemics slowly evolved into a research area, and a summary of important works from this era was made by Anderson and May in 1992.[80]

By the beginning of 21st century, a great revolution in epidemic modeling was witnessed, pulled by the development of network science,[24,28,30–81] the advance of computational power and the access to large-scale real data. Elaborate and realistic models are nowadays used as predictive tools for global and local epidemics,[82,83] while simpler and often minimalist models are used to understand the dynamics of these models, as well as specific aspects of disease spreading such as effect of mobility, immunization strategies and behavioral responses.

In this section, we describe different frameworks through which epidemic models are defined. They vary in terms of the population type (structured or homogeneously mixed) and the progression of time (discrete or continuous), and can be defined by deterministic equations or stochastic processes.

2.2.1 Homogeneously mixed populations

The framework that was dominant in most works during the 20th century[80,84] was that of homogeneously mixed populations. It is based on a simple hypothesis: each individual of a given population is equally likely to interact with any other individual at any time. This makes no distinction between individuals, and imposes no structure of contacts to the population.

In this section, we discuss the most fundamental epidemic models in a homogeneous mixing framework. The hypothesis can be applied for both discrete and continuous time evolution, as well as for stochastic simulations. However, here we only deal with a continuous time and deterministic formulation, which is the most used.

Let us first introduce one of the simplest epidemic models: the *Susceptible-Infectious-Susceptible* (SIS). In this model, individuals are put into compartments according to their disease status: *susceptible* (S), which does not have the disease and could catch it, and *infectious* (I), which has the disease and can transmit it. Susceptible individuals contract the disease upon contacts with infectious. Let N be the number of individuals and define $\beta \in \mathbb{R}_+$ as the product between the rate at which each individual makes contacts with others and the probability that each contact between S and I individuals results in a transmission. The expected rate at

[§] Reed and Frost presented their model in 1928, but did not have interest in publishing it, which was only made in 1952 by Abbey.[79]

which new infections occur is $\beta \cdot N_S \cdot N_I/N$, where N_S and N_I are respectively the numbers of susceptible and infectious individuals, and the factor N_I/N comprises the probability that each contact made by a susceptible points to an infectious individual.

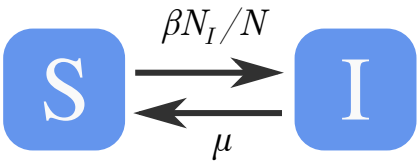

Figure 3 – Schematic representation of the compartment transitions in the SIS model, where S stands for *susceptible* and I represents *infectious*. Along with each arrow is the transition rate for a homogeneously mixed population with continuous-time evolution.

Source: By the author.

In the basic SIS model, infectious individuals can heal from the disease spontaneously, at a constant rate $\mu \in \mathbb{R}_+$. When healed, individuals go back to the susceptible compartment, meaning that no immunity is considered in this simple disease model. Figure 3 depicts the possible compartment transitions in the SIS, with their respective rates. Putting together all elements, the rate equations for the evolution of N_S and N_I read as:

$$\dot{N}_S = -\beta N_S \frac{N_I}{N} + \mu N_I \tag{2.12}$$

$$\dot{N}_I = +\beta N_S \frac{N_I}{N} - \mu N_I. \tag{2.13}$$

With the additional constraint that $N_S + N_I = N$ (constant), the two equations can be reduced to one:

$$\dot{N}_I = \beta(N - N_I)\frac{N_I}{N} - \mu N_I. \tag{2.14}$$

So the system is effectively one-dimensional. We can also divide it by N and write it in terms of the fractions of the population at each compartment, $\rho_S = N_S/N$ and $\rho_I = N_I/N$:

$$\dot{\rho}_I = \beta(1 - \rho_I)\rho_I - \mu\rho_I. \tag{2.15}$$

We also name ρ_I as the *disease prevalence*, a concept from epidemiology. Although it is difficult to solve Equation 2.15 in time, it is straightforward to find the value of ρ_I such that

new infections and recoveries are balanced. This is a fixed point of the underlying dynamical system, and can be found by setting $\dot{\rho}_I$ to zero:

$$0 = \rho_I(\beta(1 - \rho_I) - \mu). \tag{2.16}$$

An immediate solution is $\rho_I = 0$, meaning that if there are no infectious individuals at all, there is no epidemic dynamics. This can be named as the *healthy state*, and often as *disease-free equilibrium* (DFE) in math literature. For the analogous stochastic model, it is also an *absorbing state*, meaning that once visited it cannot be left (by the lack of infectious units).

Another solution can be obtained by setting to zero the term inside the parenthesis in Equation 2.16, which solves as:

$$0 = \beta(1 - \rho_I) - \mu \quad \Leftrightarrow \quad \rho_I = 1 - \frac{\mu}{\beta}. \tag{2.17}$$

The value $\rho_I = 1 - \mu/\beta$ corresponds to the *endemic stationary state*, in which new infections and heals cancel out. This expression is also related to the concept of herd immunity, which we discuss further on. A very important epidemiological parameter can also be defined at this point: the *basic reproduction number* R_0. It is defined as the number of secondary infections produced by a primary infectious individual, assuming that the population is fully susceptible. In the simple framework of homogeneously mixed populations, it can be shown to be $R_0 = \beta/\mu$.

The reproduction number defines whether and how strongly a disease can propagate. One can verify this for the homogeneously mixed population with a stability analysis of the mentioned fixed points (stationary states). For the SIS, this is as simple as taking the derivative of the right-hand side of Equation 2.15 with respect to ρ_I, then evaluating its signal. Using the product rule, we have that:

$$\frac{\mathrm{d}\dot{\rho}_I}{\mathrm{d}\rho_I} = \beta(1 - \rho_I) - \mu \, + \, \rho_I \cdot (-\beta) \; = \; \beta(1 - 2\rho_I) - \mu. \tag{2.18}$$

By replacing ρ_I with its value at the fixed point, a positive value of $\mathrm{d}\dot{\rho}_I/\mathrm{d}\rho_I$ indicates that the system is unstable at that point, while a negative value implies that it is stable. For the DFE, with $\rho_I = 0$, Equation 2.18 evaluates as $\beta - \mu$. Therefore, the disease-free equilibrium is stable if, and only if:

$$\beta - \mu < 0 \quad \Leftrightarrow \quad R_0 = \frac{\beta}{\mu} < 1. \tag{2.19}$$

Indeed, if the number of secondary cases produced by a primary one is smaller than 1, the disease cannot be sustained and vanishes. Otherwise, if $R_0 > 1$, the DFE is unstable. On the other hand, it can be shown that the endemic solution at $\rho_I = 1 - 1/R_0$ is positive and stable if $R_0 > 1$, but negative (unphysical) and unstable if $R_0 < 1$. Indeed, when the function $1 - 1/R_0$

Figure 4 – Schematic representation of the transitions in the SIR model, where S stands for *susceptible*, I for *infectious* and R represents *removed*. Along with each arrow is the transition rate for a homogeneously mixed population with continuous-time evolution.

Source: By the author.

crosses the x axis at $R_0 = 1$, it exchanges the stability with the DFE fixed point $\rho_I = 0$. In the theory of dynamic systems, this characterizes a *transcritical bifurcation*.[¶] In physics literature, $R_0 = 1$ is referred as a critical point, where a phase transition occurs. For epidemiology, it is also usual to name this point as *epidemic threshold*. Regardless of the name, this is an important point at which the epidemics change from a vanishing condition to a stable endemic stationary state.

We use homogeneously mixed populations to present yet another important model for theoretical epidemiology: the *Susceptible-Infectious-Removed* (SIR). In this model, besides S and I, the *removed* (R) compartment is included to consider individuals that are either fully immune to the disease or were removed from the dynamics by other means (such as death). While infections occur exactly the same way as in SIS, the only difference of the SIR model is that infectious individuals move (with rate μ) to the R compartment rather than S, meaning that each individual can catch the disease only once. Figure 4 represents the compartment transitions in this model.

The dynamic equations, already written in terms of fractions $\rho_S = N_S/N$, $\rho_I = N_I/N$ and $\rho_R = N_R/N$, read as:

$$\dot{\rho_S} = -\beta\rho_S\rho_I \tag{2.20}$$

$$\dot{\rho_I} = \beta\rho_S\rho_I - \mu\rho_I \tag{2.21}$$

$$\dot{\rho_R} = \mu\rho_I. \tag{2.22}$$

The constraint $\rho_S + \rho_I + \rho_R = 1$ makes the system effectively two-dimensional. Even though the definition of the SIR is very similar to that of SIS, its dynamics has a fundamental

¶ We use this and some other concepts of dynamical systems during other chapters of this thesis, for which we refer the reader to Kuznetsov[85] for more details.

difference: there is no endemic stationary state, as individuals do not return to the susceptible compartment. If the disease ever spreads, it causes the population to be less susceptible over time, making it eventually vanish. One can use a separation trick to calculate the fraction of the population that will have caught the disease by the end of the process. Dividing both sides of Equation 2.20 by both side of Equation 2.22, we get:

$$\frac{\dot{\rho_S}}{\dot{\rho_R}} = \frac{-\beta\rho_S\rho_I}{\mu\rho_I}, \tag{2.23}$$

where we assumed that ρ_I is not strictly zero. From Equations 2.20 and 2.22, we also deduce that ρ_S always decreases with time while ρ_R increases. This monotonic behavior allows us to write ρ_S as a composite function of ρ_R, which is then a function of the time t. This, in turn, allows us to apply the inverse chain rule to the left-hand side of Equation 2.23, which along with simplifications to its right-hand side yields:

$$\frac{\mathrm{d}\rho_S}{\mathrm{d}\rho_R} = -R_0\rho_S. \tag{2.24}$$

Dividing both sides by ρ_S (which can be safely assumed as greater than zero) and integrating on $\mathrm{d}\rho_R$, with a variable change from ρ_R to ρ_S on the left-hand side, we get:

$$\int_{\rho_S(0)}^{\rho_S(t)} \frac{1}{\rho_S}\mathrm{d}\rho_S = -R_0 \int_{\rho_R(0)}^{\rho_R(t)} \mathrm{d}\rho_R, \tag{2.25}$$

which solves on both sides as:

$$\ln\left(\frac{\rho_S(t)}{\rho_S(0)}\right) = -R_0(\rho_R(t) - \rho_R(0)). \tag{2.26}$$

We can impose some initial conditions to have a final expression. Let us assume that the epidemic starts with a very small fraction of infectious units $\rho_I(0) = \delta \to 0$, with the rest of the population susceptible $\rho_S(0) = 1 - \delta$ and $\rho_R(0) = 0$. Then:

$$\ln\left(\frac{\rho_S(t)}{1-\delta}\right) = -R_0(\rho_R(t) - \rho)R(0). \tag{2.27}$$

This expression holds for any time t, but we are specifically interested in the end of the process, say, at time $t \to \infty$. By then, all infectious population will have vanished, thus $\rho_S(\infty) = 1 - \rho_R(\infty)$. Using this on Equation 2.27, converting the logarithm to its definition, and finally taking $\delta \to 0$, we get:

$$\rho_R(\infty) = 1 - e^{-R_0\rho_R(\infty)}, \tag{2.28}$$

which is a transcendental equation on $\rho_R(\infty)$. Again, there is a trivial solution $\rho_R(\infty) = 0$, which represents the case in which the disease is not able to cause a macroscopic outbreak. Another solution emerges if $R_0 > 1$, which can be graphically visualized as the crossing between the functions $f(x) = x$ and $g(x) = 1 - e^{-R_0 x}$. Therefore, as with the SIS model, there is a phase transition between a disease-free and an epidemic phase at $R_0 = 1$.

Models with homogeneously mixed population allow the discussion of another important concept in epidemiology: *herd immunity*.[86] This is a state in which the population has enough immunity to prevent the disease from spreading, even though not all individuals are immune, and is achieved when the *effective* reproduction number (R) is at most 1. Under homogeneous mixing, the effective reproduction number only considers the fraction of the population that is not susceptible: $R = \rho_S \cdot R_0$. For example, in the SIS model, setting the condition that $R = 1$ gives us $1 - \rho_S = \rho_I = 1 - 1/R_0$, which is exactly the disease prevalence at the endemic stationary state.

After the first epidemic models on networks,[87] and backed up by real data,[72] it became clear that interactions between hosts are very structured and far from homogeneous, with important implications into epidemic spreading. Nevertheless, the homogeneous mixing hypothesis is still of great use for contemporary works, with its analytical tractability as the main strength. Important results are still obtained using this hypothesis,[88–90] being particularly popular among mathematicians. It is also commonly employed for each subpopulation of a metapopulation, which are approached in Section 4.1.3.

2.2.2 Networks: Heterogeneous Mean Field (HMF)

Before the 21st century, most works with epidemic models either assumed complete homogeneous mixing between individuals, or divided the population into other groups (like age ranges, locations, etc) inside which homogeneous mixing was still assumed. In a seminal paper published in 2001, Romualdo Pastor-Satorras and Alessandro Vespignani[91] considered complex networks for the contacts between hosts, and came to a striking conclusion: *complexity itself* could enhance the epidemic spreading in a network of contacts.

To reach their conclusions, the authors developed an analytical and numerical formulation for epidemic spreading on networks, currently known as *Heterogeneous Mean Field* (HMF) or *Degree-based Mean Field* (DBMF).[16] It is still very useful until nowadays, as a simple and powerful framework to assess the effect of heterogeneous topologies on epidemic models. It is based on a reductionist assumption that all nodes with the same degree are statistically equivalent (for this section, "node" and "individual" represent the same thing). This is particularly accurate for configuration model networks, in which the only property that defines a node before the network construction is its degree. We take the SIS model as an example to describe the HMF formulation, but with some additional tools it can be useful for SIR-like models too (see Section 17.8 of [26]). Let $\rho_k = \rho_k(t)$ be the fraction of individuals with degree k that are in-

fectious at time t. Assuming continuous-time evolution, the rate equation for ρ_k can be written as:

$$\dot{\rho_k} = \beta k \Theta_k \cdot (1 - \rho_k) \; - \; \mu \rho_k, \tag{2.29}$$

where β is now the transmission rate for each contact between S and I individuals (in opposition to the previous section, where β also incorporated the rate of contacts, for simplicity), and μ is the healing rate of a single I individual. Θ_k is defined as the probability that a link that comes from a node with degree k points to an infectious node, and in principle depends both on the connectivity between degrees and the disease prevalence. For simplicity, we can also assume that there are no degree-degree correlations in the network, meaning that the probability $P(k'|k)$ that a link starting from a node with degree k points to a node with degree k' does not depend on the starting node's degree k. It is possible, yet more complicated, to develop the theory on correlated networks.[92–93] Otherwise, $P(k'|k)$ can be proven to be:

$$P(k'|k) = \frac{k' \, p(k')}{\langle k \rangle}, \tag{2.30}$$

where $\langle k \rangle = \sum_k kp(k)$ and $p(k)$ is the network's degree distribution. The dynamic variable Θ_k is evaluated as the probability that a k node points to a k' node multiplied by the probability that the k' node is infectious:

$$\Theta_k = \sum_{k'} P(k'|k) \rho_{k'} \; = \; \sum_{k'} \frac{k' p(k')}{\langle k \rangle} \, \rho_{k'} \; = \Theta. \tag{2.31}$$

Notice that Θ looses its dependence on k, becoming a single dynamic variable valid for all nodes. If we start with a guess for Θ, update ρ_k for every existing k using Equation 2.29, then update Θ with Equation 2.31 and repeat this update cycle, we get an iterative method to find the stationary values of the system. The overall prevalence is then given by $\sum_k p(k)\rho_k$.

Besides this numerical evaluation, one can analytically calculate the SIS epidemic threshold for the HMF on uncorrelated networks with an interesting trick. By multiplying both sides of Equation 2.29 by $kp(k)/\langle k \rangle$, then summing over all k values, we get:

$$\sum_k \frac{kp(k)}{\langle k \rangle} \, \dot{\rho_k} = \beta \Theta \sum_k \frac{kp(k)}{\langle k \rangle} \cdot (1 - \rho_k) \cdot k \; - \; \mu \sum_k \frac{kp(k)}{\langle k \rangle}. \tag{2.32}$$

The left-hand side of Equation 2.32 is simply the time derivative of Θ, whereas simplifications to the right-hand side lead to:

$$\dot{\Theta} = \frac{\beta \Theta}{\langle k \rangle} \left[\langle k^2 \rangle \; - \; \sum_k k^2 \rho_k k p(k) \right] \; - \mu \Theta, \tag{2.33}$$

which is an equation for the time evolution of Θ, yet it still carries explicit dependence on ρ_k due to the second term inside square brackets. However, as we mentioned, we are interested in calculating the epidemic threshold, around which the disease prevalence asymptotically goes to 0. When all the prevalences ρ_k are sufficiently small, the mentioned term is negligible when compared to $\langle k^2 \rangle / \langle k \rangle$, and the dynamics of Θ asymptotically tends to:

$$\dot{\Theta} \simeq \theta \left[\beta \frac{\langle k \rangle}{\langle k^2 \rangle} - \mu \right], \tag{2.34}$$

Which is a linearized rate equation. The stability analysis is then straightforward: if $\beta \langle k^2 \rangle / \langle k \rangle - \mu > 0$, then variable Θ grows out of the linear regime around $\Theta = 0$, meaning that an epidemic outbreak occurs. Otherwise, if $\beta \langle k^2 \rangle / \langle k \rangle - \mu > 0$, then Θ vanishes over time and the epidemic dies out. We can then state that the epidemic threshold is given by the following condition:

$$\beta \frac{\langle k^2 \rangle}{\langle k \rangle} - \mu = 0 \quad \Leftrightarrow \quad \frac{\beta}{\mu} \frac{\langle k^2 \rangle}{\langle k \rangle} = 1. \tag{2.35}$$

This led Pastor-Satorras and Vespignani[91] to a striking conclusion about scale-free networks, which was reinforced by many subsequent works. For scale-free networks with exponent between 2 and 3, the second moment of the degree $\langle k^2 \rangle$ diverges as $N \to \infty$, meaning that, for sufficiently large N, even a very small transmission rate β would render the system above its epidemic threshold. This conclusion was later questioned, and partially reviewed under the concept of eigenvector localization and Griffiths effects on networks.[94–97] These works point that, although the system may be above the threshold for propagation, the disease is likely limited to a very small subgraph with incredibly high connectivity.

Another way to interpret the result from Equation 2.35 is to regard $\beta \langle k^2 \rangle / \mu \langle k \rangle$ as a good approximation for the basic reproduction number R_0 when it is close to 1. If we replace $\langle k^2 \rangle$ by the degree's *coefficient of variation*, given by $c_v = \sigma_k / \langle k \rangle = \sqrt{(\langle k^2 \rangle - \langle k \rangle^2) / \langle k \rangle^2}$, we get that:

$$R_0 \approx \frac{\beta}{\mu} \langle k \rangle (c_v^2 + 1). \tag{2.36}$$

We can interpret this result as follows: the disease will propagate more if (i) the number of contacts, given by $\langle k \rangle$, is greater, and (ii) the diversity of degrees on the network, represented by c_v^2, is higher. In other words, heterogeneity (or complexity) itself can favor the propagation of a disease.

2.2.3 Networks: Quenched Mean Field (QMF)

Another mean field approximation for epidemic models on networks, apparently more detailed than the HMF, was proposed by Chakrabarti and others[98] in 2008. Instead of assuming

that nodes with the same degree are equivalent, it retains the whole structure of the network of contacts. An approximation is then assumed on the dynamical system itself, rather then on the network structure. This approach, in its version with continuous-time evolution, is better known as *Quenched Mean Field* (QMF).

We again use the SIS model to illustrate the formulation. Let $A_{i,j}$, with $i, j = 1, ..., N$ be the adjacency matrix elements of an undirected and unweighted graph $\mathcal{G}$. As in Section 2.2.2, we define β as the transmission rate of a contact between S and I nodes, and μ as the recovery rate of I nodes. Denote as $\rho_i = \rho_i(t)$ the probability that node i is infectious at time t. Assuming that two nodes $i, j \in \mathcal{V}$ are connected, the probability ρ_i increases over time with rate $\beta \cdot P(X_i = S, X_j = I|t)$, where $P(X_i = S, X_j = I|t)$ is the joint probability that, at time t, node i is susceptible and node j is infectious.

To exactly address this system as a continuous-time Markov chain, we should consider all the joint probabilities $P(X_i = A_i \,|\, i = 1, ..., N)$, where each A_i can either be S or I. This is a total of 2^N states to keep track of, making the state space prohibitively large for analytical and computational purposes in the case of medium and large graphs (see [99] for an exact approach to the 2^N problem). Instead, one first approximation is to consider that the dynamic probabilities ρ_i are statistically independent of each other,[‖] meaning that any joint probability can be broken as products between individual probabilities. For example, using this approximation, we write that $P(X_i = S, X_j = I|t) = (1 - \rho_i(t)) \cdot \rho_j(t)$, so dynamical correlations that exist between the states of nodes i and j are neglected.

Under this approximation, we can join the contributions of each neighbor of node i to its infection probability, as well as its own recovery rate, to write the time evolution of $\rho_i(t)$ as:

$$\dot{\rho}_i = \sum_{j=1}^{N} A_{ij}\beta(1 - \rho_i)\rho_j \; - \; \mu\rho_i. \tag{2.37}$$

This defines a non-linear dynamical system for the N individual infection probabilities ρ_i instead of the whole Markov chain of size 2^N, making the system numerically tractable. Methods for integration of differential equations, such as Runge-Kutta,[100] can be employed along with initial conditions to solve the time evolution of the system under the QMF hypothesis (i.e., no dynamical correlations).

It is also possible to extract the epidemic threshold with a stability analysis over the DFE (disease-free equilibrium). The Jacobian matrix element J_{ik}, given by $\partial\dot{\rho}_i/\partial\rho_k$, is evaluated from Equation 2.37 as:

$$J_{ik} = \frac{\partial\dot{\rho}_i}{\partial\rho_k} = A_{ik}\beta(1 - \rho_i) \; - \; \delta_{ik}\,[\mu \; + \; \sum_j A_{ij}\beta\rho_j], \tag{2.38}$$

‖ This does not mean that the probabilities evolve independently. Their evolution is tangled, but they are independent in a statistical sense.

where δ_{ik} is the Kronecker delta. As the system is N dimensional, the stability analysis consists into finding the signal of the Jacobian's leading eigenvalue evaluated at the fixed point. In the DFE, all probabilities ρ_i are zero, and the matrix elements are evaluated as:

$$J_{ik} = A_{ik}\beta - \delta_{ik}\mu \tag{2.39}$$

or, in a matrix form:

$$\mathbb{J} = \beta\mathbb{A} - \mu\mathbb{I}_N, \tag{2.40}$$

where $\mathbb{I}_N$ is the identity matrix with size N. Denoting the leading eigenvalue of a matrix $\mathbb{M}$ as $\Lambda_0(M)$ (this is, $\Lambda_0(M)$ is the eigenvalue with greatest real part), then the DFE will be unstable if $\Lambda_0(\mathbb{M}) = \beta\Lambda_0(\mathbb{A}) - \mu > 0$ or, equivalently, $\beta\Lambda_0(\mathbb{A})/\mu > 1$. The epidemic threshold itself is defined as:

$$\frac{\beta\Lambda_0(\mathbb{A})}{\mu} = 1. \tag{2.41}$$

As we did for the HMF in Section 2.2.2, we can interpret $\beta\Lambda_0(\mathbb{A})/\mu$ as the approximate value of the basic reproduction number R_0 around the critical condition of $R_0 = 1$. This means that, according to the QMF, networks with larger leading eigenvalue of its adjacency matrix are more favorable to the spread of a disease. In general terms, the value of $\Lambda_0(\mathbb{A})$ is greater for networks with higher connectivity, but this is not a universal rule.

For scale free (SF) networks built with the configuration model (CM) (degree distribution $p(k) \sim k^{-\gamma}$), it is shown that its leading eigenvalue diverges as $N \to \infty$, for any $\gamma > 2$.[101–103] This again means that the disease can be sustained for a long time even with very small propagation rates. However, Goltsev and others[94] showed that the leading eigenvector of $\mathbb{A}$ is highly concentrated on a finite set of nodes around the greatest hub (node with highest degree). Therefore, if β is small but above the critical value, the disease activity is also concentrated around these subsets. This condition is known as *disease localization*, and is a current topic of research.[65,97,104,105] The details of how the disease localizes were further unveiled by Pastor-Satorras and Castellano,[104] who shown a finite localization pattern for $\gamma > 5/2$ but a mesoscopic one for $\gamma < 5/2$.

Another tricky point about the conclusions of the QMF is its divergence from the HMF for $\gamma > 3$. In this regime, $\langle k^2\rangle/\langle k\rangle$ is finite for SF networks and, therefore, the epidemic threshold should be non-vanishing according to HMF. These differences also arise from subtleties of each mean field treatment, and were addressed by Ferreira,[95] Mata[106] and others.

2.2.4 The Microscopic Markov Chain Approach (MMCA)

Another popular theoretical approach for epidemic models on networks is a discrete-time version of the QMF. Initially proposed by Wang and others,[103] it was revisited by Gómez and others[107] and then employed in a multitude of works, and is often known as the *Microscopic Markov Chain Approach* (MMCA). To exemplify the method, we use again the SIS model due to its simplicity. Here we disregard events of instant reinfection, in which an infectious individual can recover and then be infected again in a single time step.

Let again $\mathcal{G}$ be an unweighted and undirected graph, with $\mathcal{V}$ as its set of N nodes and A_{ij} as its adjacency matrix elements, $i, j \in \mathcal{V}$. This time, we define β as the *probability* (rather than rate) of disease transmission, during a single time step, in a given contact between S and I individuals. μ is the probability that an I node recovers and becomes S during one time step. Let $\rho_i = \rho_i(t)$ be the probability that node $i \in \mathcal{V}$ is infectious at time t, where now $t = 0, 1, ...$ evolves discretely. Assuming that node i is susceptible, the probability that it catches the disease from node j at time t is given by $A_{ij}\beta\rho_j(t)$, where A_{ij} tells if i and j are neighbors. The probability that node i does *not* catch the disease from any node is then the product of the probabilities that it does not catch the disease from any neighbor, given by $\prod_j(1 - A_{ij}\beta\rho_j(t))$. Therefore, given that i is susceptible, the probability that it catches the disease at time t from any source node is written as:

$$q_i(t) = 1 - \prod_{j=1}^{N}(1 \; - \; A_{ij}\beta\rho_j(t)). \tag{2.42}$$

As in the QMF approach, we disregard correlations between the state of neighboring nodes. This way, the states of node i and its neighbors are statistically independent, and the probability that it moves from S to I at time t is simply the probability that it is susceptible, $1 - \rho_i(t)$, multiplied by $q_i(t)$ from Equation 2.42. The difference equation for the evolution of ρ_i is, therefore:

$$\rho_i(t+1) = (1 - \rho_i(t)) \cdot q_i(t) \; + \; \rho_i(t) \cdot (1 - \mu). \tag{2.43}$$

This map defines a dynamical system of dimension N, instead of the 2^N exact Markov chain. Computationally, Equation 2.43 defines an iterative method to find the time evolution and the steady state of the system. It is usually fast and stable, making this a very convenient tool to study more advanced models in complex networks. We use this approach to study the coupling between disease and information, as presented in Section 3.2.

The epidemic threshold can, again, be determined by a stability analysis of the DFE (where $\rho = \sum_i \rho_i = 0$). This consists in evaluating the leading eigenvalue of the Jacobian matrix. The system's map is given by a set of functions $f_i : [0,1]^N \to [0,1]$ such that $\rho_i(t + 1) = f_i(\{\rho_j(t) \,|j \in \mathcal{V}\})$ (i.e., f_i is the right-hand sides of Equation 2.43). The Jacobian matrix

element is $J_{ik} = \partial f_i / \partial \rho_k \,|_{\rho=0}$. Let us first calculate the derivative of q_i with respect to ρ_k with given $k \in \mathcal{V}$:

$$\left.\frac{\partial q_i}{\partial \rho_k}\right|_{\rho=0} = -(-A_{ik}\beta) \cdot \left.\prod_{\substack{j=1 \\ j\neq k}}^{N} (1 \; - \; A_{ij}\beta\rho_j(t))\right|_{\rho=0} = +A_{ik}\beta. \tag{2.44}$$

Then the jacobian matrix at the DFE fixed point is then given by:

$$\begin{aligned} J_{ik} &= -\,\delta_{ik} \cdot q_i|_{\rho=0} + (1-\rho_i)|_{\rho=0} \cdot \left.\frac{\partial q_i}{\partial \rho_k}\right|_{\rho=0} \; + \; \delta_{ik} \cdot (1-\mu) \\ &= A_{ik}\beta \; + \; \delta_{ik}(1-\mu). \end{aligned} \tag{2.45}$$

In matrix form: $\mathbb{J} = \beta\mathbb{A} + (1-\mu)\mathbb{I}_N$, where again $\mathbb{I}_N$ is the N x N identity matrix. As the system is discrete in time, we need to compare the leading eigenvalue of $\mathbb{J}$ with 1. If $\Lambda_0(\mathbb{J}) > 1$, the DFE is unstable and the system has an epidemic outbreak; otherwise, the DFE is stable and the epidemics extinguishes. The critical condition (epidemic threshold) is given by:

$$\Lambda_0\mathbb{J} = \beta\Lambda_0(\mathbb{A}) + (1-\mu) = 1 \quad \Leftrightarrow \quad \frac{\beta\Lambda_0(\mathbb{A})}{\mu} = 1, \tag{2.46}$$

which turns out to be the same condition as that of the continuous-time QMF approach (Equation 2.41), except that now β and μ are probabilities instead of rates. The discussions about vanishing thresholds, disease localization and related concepts remain the same as those presented in Section 2.2.3.

2.2.5 Discrete-time Monte Carlo simulations

The analytical and numerical methods described so far are very useful ways to study simple epidemic models in homogeneously mixed and structured (networked) populations. They are deterministic, meaning that every run will always return the same result, and provide some important analytical insights such as the formulae for the epidemic threshold. However, these methods are all subject to some degree of approximation in order to be tractable, specially those aimed at large networked populations. Mathematical approximations can be avoided through the use of stochastic simulations, which promote the dynamics of the models as they are proposed.

For discrete-time evolution, it is usually intuitive to implement a Monte Carlo simulation knowing the model's rules. The basic principle is to draw random numbers that determine which or how many events will occur at each time step, then execute the state changes. We now briefly describe how to implement Monte Carlo simulations of the SIS model, both on homogeneously mixed populations and on networks of contacts.

In homogeneously mixed populations, all individuals are statistically equivalent, so we only need to keep track of the number of individuals in each compartment. Let $N_S = N_S(t)$ and $N_I = N_I(t)$ be, respectively, the number of susceptible (S) and infectious (I) individuals at time step t, with $N_S + N_I = N$. Define β as the infection probability, scaled by the average number of contacts between individuals (as described in Section 2.2.1). Also define μ as the individual recovery rate. For each susceptible individual, the chance of *not* being infected by a single infectious individual is $1 - \beta$. The chance of not being infected by anyone is $(1 - \beta)_I^N$. Finally, the infection probability for a single susceptible individual is:

$$q = 1 - (1 - \beta)^{N_I}, \tag{2.47}$$

and the expected number of new infections is given by $q \cdot N_S$. Moreover, the expected number of recoveries (I $\rightarrow$ S) is $\mu \cdot N_I$. Instead of drawing random numbers for each of the N individuals, we can group the events of the same kind, then draw binomial numbers to determine *how many* of them will occur. In our case, we can simply draw $\eta_I = \text{Bin}(N_S, q)$ and $\eta_S = \text{Bin}(N_I, \mu)$, denoting respectively the number of new infections and recovery, where $\text{Bin}(n, p)$ represents a binomial random number with n attempts of probability p. After performing all calculations, we update the number of infectious individuals as $N_I(t+1) = N_I(t) + \eta_I - \eta_S$ (and $N_S = N - N_I$).

For populations defined by a network of contacts, the simplest approach is to keep track of the state of each individual. Let $X_i(t) \in 0, 1$ be an indicator variable of the state of node i, with $X_i(t) = 1$ if i is infectious and 0 otherwise. Redefine β as the probability of disease transmission of each link between S and I nodes and μ, as usual, the recovery probability. The probability of infection for node i, given that it is susceptible, is:

$$q_i = 1 - (1 - \beta)^{N_I^i}, \tag{2.48}$$

where $N_I^i = \sum_j A_{ij} X_j$ is the number of infectious neighbors of node i. One usual approach is to perform a "visit" to each node to determine its state for the next time step. When node i is visited, its state is checked, and then one of the following is performed: (i) if i is susceptible, a Bernoulli event (coin toss) with probability q_i determines whether it should be infected and set as I; (ii) if i is infectious, a Bernoulli event with probability μ determines whether it should be recovered and set as S. Only after all nodes are visited should the node states be updated, preventing that the results of the simulation are affected by the arbitrary sequence of visits.

2.2.6 Continuous-time Monte Carlo - Guillespie algorithm

Continuous-time evolution is a mathematical concept that cannot be executed in a computer, because finite memory imposes discretization of the numbers at some point. However, when the events of a stochastic process have occurrence times that are well defined by continuous functions, this process can be simulated in a computer with a time discretization that

is essentially its numerical precision scale (the so called *machine epsilon*). In particular, if the stochastic process is Markovian (this is, holds no memory of previous states), all events have exponentially distributed occurrence times, and can be simulated with relative ease.

Exploring this idea, Joseph L. Doob and others created an algorithm to simulate chemical or biochemical sets of reactions in 1945, which was presented by Dan Gillespie in 1976.[108,109] Despite being proposed for chemical systems, it can be applied to a very broad variety of stochastic processes, and is now popularly known as Gillespie (or Doob-Gillespie) algorithm. As proposed in the seminal paper, there are two methods for exact simulation: the *direct method* and the *first reaction method*. Here we shall focus on the direct method, which is more efficient when the disease parameters are the same for all hosts. Approximate and more efficient methods were also proposed later.[110]

Let us again use the SIS model in a homogeneously mixed population, exactly as described in Section 2.2.1, to exemplify the method. For a given state of the system, $N_I(t)$ and $N_S(t)$, new infections occur with rate $\beta N_S(t)N_I(t)$, while new recoveries happen with rate $\mu N_I(t)$. The total rate at which *any* event (infection or healing) occurs, is simply given by the sum:

$$a(t) = \beta N_S(t)N_I(t) + \mu N_I(t). \tag{2.49}$$

The method is based on two propositions: (i) the time T to the next reaction (event) is exponentially distributed with rate $a = a(t)$, thus $p(T = \tau) = ae^{-a\tau}$; (ii) the probability that an event α is the next to occur is proportional to its rate a_α. Then, for the well mixed SIS, we can first draw the time τ to the next event from an exponential random number with rate given by Equation 2.49, then choose between performing a new infection (with probability $\beta N_S N_I/a$) or a new healing (with probability $\mu N_I/a$). If an infection (a healing) event is chosen, we increment (decrement) N_I by one unit, and update the current time t to $t + \tau$. By repeating this process, we simulate the continuous-time evolution of the SIS model with feasible computational cost, but a time discretization as small as the precision scale used for τ.

For network-structured populations, it is simple to expand the direct method while keeping its computational efficiency, provided that the disease parameters (β and μ) are the same for all individuals. Even though each S individual has its own rate of infection, we can still group infection events by links between S and I. Let $M_{SI} = M_{SI}(t)$ be the total number of contacts (links) between S and I individuals at time t. The rate at which any event occurs is given by:

$$a(t) = \beta M_{SI}(t) + \mu N_I(t). \tag{2.50}$$

Following the same principle for homogeneous mixing, we draw an exponential time τ with $p(T = \tau) = ae^{-a\tau}$, then choose to perform a new infection with probability $\beta M_{SI}/a$ or a new recovery with probability $\mu N_I/a$. If infection is chosen, we select one of the existing S-I

links at random, then infect the S node. If recovery is chosen, we select a random infectious node and make susceptible again. The current time t is then updated to $t + \tau$ and the iteration is repeated.

During this thesis, we may often refer to SIS-like and SIR-like models. With this, we mean the "cyclic" aspect of the model: if individuals can return to the initial/inactive state and repeat the transitions, we call it SIS-like; if individuals can only run through the sequence of compartments once, we call it SIR-like.

Monte Carlo simulations allow the study of an epidemic model even when no theoretical or mean field formulation is known. This comes at the expense of computational cost, as simulations typically must be repeated many times or for very long periods to produce statistically relevant results. In particular, determining the epidemic threshold can be very tricky, as most epidemic models possess absorbing states and/or subspaces which, once reached by the system, cannot be left (such as the DFE).

For SIS-like models, a rough determination of the epidemic threshold can be made by just plotting the stationary prevalence as a function of β or μ. However, to have a more precise calculation, alternative methods using the distribution of survival times,[111] a small constant source of infection[112] or a reflecting boundary[113] are considered. One particularly efficient method is the simulation of the quasi-stationary state,[114–115] which recovers the system to a previous configuration whenever it falls into an absorbing state.

2.2.6.1 Other models

Up to this point, we described the SIS and SIR models. Due to their simplicity, they are very important for theoretical works, but they lack many details present in real epidemic and information dynamics. Some of these details can be incorporated through simple modifications. We use a homogeneously mixed, continuous-time formulation to explain some other models obtained from the basic SIS and SIR.

In the SIR model, the removed (R) compartment represents individuals that either perished by the disease or acquired lifelong immunity. In reality, however, immunity to many diseases can wane over time, either by pathogen mutation or by reduction in antibody loads. One simple way to incorporate this is to consider an extra transition on the SIR model, from R back to S again. This happens spontaneously, with rate α for each R individual. The resulting model is known as *Susceptible-Infectious-Removed-Susceptible* (SIRS). It has features from both SIS and SIR models: the possibility of an endemic stationary state (as in SIS) and of a transient outbreak peak (as in SIR), depending on the parameters and initial conditions.[84]

Both SIS and SIR models also consider that a host begins to transmit the disease immediately after it is infected. This is not true for real diseases, in which there is a period of pathogen development, since the infection, until the host begins to transmit. This period,

also known as latent period, can be incorporated by the addition of an *exposed* (E) compartment between S and I. This way, once infected, a susceptible host moves to the exposed compartment first, on which it cannot transmit the disease yet. With rate σ, it spontaneously moves to the infectious compartment. By applying this respectively to the SIS and SIR models, we obtain the *Susceptible-Exposed-Infectious-Susceptible* (SEIS) and *Susceptible-Exposed-Infectious-Removed* (SEIR) models.

Finally, and as mentioned in Chapter 1, epidemic models can also be used to describe the spread of information. One way to adapt an epidemic model for this purpose was considered by D. J. Daley and D. G. Kendall[17] in 1965, to what is called a *Daley-Kendal* (DK) rumor model. They considered an SIR-like model, with S interpreted as unaware, I as aware and spreader and R as *stifler* (this is, an individual that already knows the information but does not spread it). Moreover, they proposed a modification to the forgetting ("healing") process. For each contact between a spreader (I) and a stifler (R), with rate α, the spreader can become stifler. Moreover, for each contact between two spreaders, with the same rate, they can both become stiflers. This emulates the fact that, when an informer notices that the people around do already know the information or rumor, he or she may loose interest in propagating it.

A slight variation of the DK model was later proposed in a book by D. P. Maki and M. Thompson.[116] The only difference is that, during the contact between two spreaders (I), each of them become stifler independently with rate σ, instead of both of them. All the other features remain as in the DK model, in which is known as the *Maki-Thompson* (MT) model. In Section 3.2 of Chapter 3, we explore an adapted MT model to explore the interaction between disease and information dynamics.

3 INTERACTION BETWEEN SPREADING PHENOMENA

Dynamic phenomena in nature rarely occur in isolation. The interaction between different dynamics often lead to highly complex outcomes. Cities are great examples of such a complexity. Demographic patterns, job offer and demand, public services, product supply chains, social activities, traffic and transportation are layers of an urban cluster that interact in a complex setup, such that perturbations in one sphere can affect several others in a sensitive way.

Spreading phenomena often interact with each other, as well as with other types of processes. Examples of disease spreading dynamics that interact are common, such as the dynamics of multiple influenza strains,[117] which are subject to cross immunity (i.e., when host immunity to one strain provides total or partial immunity to other), making their dynamics to be dependent on one another. This interaction can give rise to non-trivial phenomena, such as the long-term survival of "unfit" strains.[118] Infection by Human Immunodeficiency Virus (HIV) is known to facilitate infections by other opportunistic diseases,[119–120] especially tuberculosis, but also hepatitis A and B, candidiasis, toxoplasmosis[120] and others. These opportunistic infections can further compromise the immune system,[119] closing a cooperative loop between HIV and other pathogens. Yet less commonly, there are some cases in which co-infected pathogens reduce the replication and/or viral loads of HIV,[121–123] configuring an asymmetric loop of interaction (a "win-loose" scheme).

Epidemic spreading has also strong interaction with host's behavior, especially in human populations.[124–125] Aspects such as host mobility and contact patterns, public mitigation strategies and adoption of self-protective measures strongly influence (and are influenced by) the dynamics of a contagious disease.

In this chapter, we describe our contributions to the dynamics of interacting spreading phenomena. By spreading phenomena, we refer both to diseases and to the "epidemic metaphor", as mentioned in the introduction of the thesis. Our focus was driven to asymmetrically interacting schemes, both in networks and homogeneous populations. In Section 3.1, we review the literature on the topic, with special emphasis to asymmetric coupling. In Section 3.2, we present our first developed work: a study of the disease-information coupling in multiplex networks, with a rumor-like model for the information and a flexible relative time scale. Based on open questions from this work, we follow up with another work in Section 3.3, in which we study asymmetrically interaction spreading processes in a broader sense.

3.1 Literature review

The major topic of interaction between epidemic spreading and other dynamical systems (including epidemics itself) is very extensive in the literature, and a thorough review of the whole topic would go far beyond the scope for this chapter. Instead, we focus on the literature that is most relevant to our works, divided in two subtopics: the interaction between two or more contagion processes (Section 3.1.1), and the coupling between disease and host behavior (Section 3.1.2).

3.1.1 Interacting diseases models

Some early works in epidemic modeling acknowledged the existence of interaction between infectious agents, and mostly focused in the case of competitive interaction. [117,126–129] In 1964, Elveback and others,[126] motivated by a field report of interaction between pathogens,[130] modified the basic Reed-Frost model[79] to consider two pathogens that cause temporary or permanent immunity to one upon infection by the other. They performed Monte Carlo simulations on an IBM 7090 computer, being probably one of the earliest works to evaluate an epidemic model computationally. They conclude that the viral "interference" caused little effect into the outbreak size, but later works have contradicted this result. This model was revisited by Dietz[127] in 1979 who, under a more mathematical approach, analytically calculated the equilibrium points and local stability criteria.

Castillo-Chaves and others[128] later discussed the competition between pathogens in views of the competitive principle, which states that species within the same niche cannot coexist for the long-term. They studied a two-strain SIS mathematical model for gonorrhea, concluding that "in a behaviorally and genetically homogeneous population coexistence is not possible except under very special circumstances". However, they acknowledge that heterogeneity, in its various manifestations, lead to coexistence in ecological systems. This point was later developed after the emergence of complexity science. Indeed, in 2005 Newman[131] studied a competitive two-strain SIR model in graphs with specified degree distribution $p(k)$. Using bond percolation, he deduced that degree heterogeneity may induce a so-called coexistence phase transition (besides the traditional epidemic transition), after which both pathogens invade the population, generalizing what was known from general ecological systems to infectious species.

In 2011, another work by Karrer and Newman[132] further studied the competitive two-strain SIR model. Besides determining conditions for coexistence, they studied the influence of the *relative time scale* between the two diseases, measured by their recovery rates. They show that the relative time scale plays an important role on the behavior of the system, determining for example the existence and size of a coexistence phase, as shown in Figure 5. By coexistence in an SIR-like model, it is understood that both strains infect a macroscopic fraction of the population.

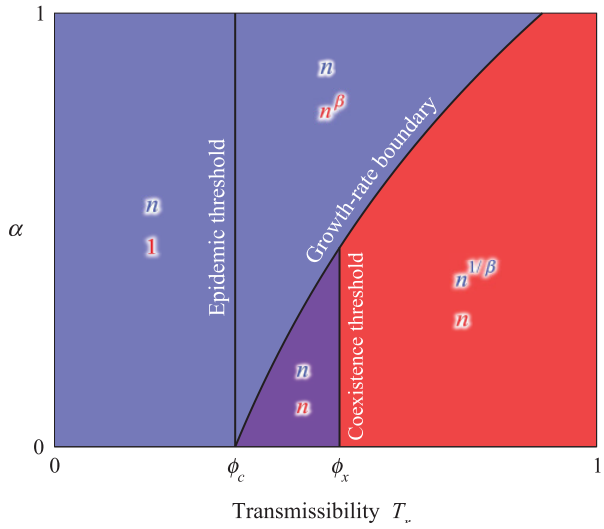

Figure 5 – Phase diagram of Karrer and Newman's two-strain SIR-like competing strains model, with complete mutual cross immunity. The strains are named as red and blue, with T_r representing the transmissibility of the red strain and α its healing rate (the blue strain has fixed parameters). Each region's color represents the dominant strain, while the smaller purple region is the coexistence phase. It is shown to be highly dependent on α, which is a measure of the relative time scale between the two strains.

Source: KARRER; NEWMAN[132]

Other recent works brought the problem of competing diseases into metapopulations[133] and multiplex networks,[134–138] considering that each disease propagates in a separate layer. Funk and Jansen,[134] as well as Marceau and others,[135] independently studied SIR-like competing diseases via cross immunity in two-layer multiplexes (or *overlay* networks, as they call), both showing that inter-layer degree correlations, link overlapping and degree heterogeneity, can influence the outcomes of the process. For example, Funk and Jansen state that positively (negatively) correlated layers increase (decrease) the competition between strains, while heterogeneity enhances the effect in either case. Both works also study the effect of partial cross immunity, which tends to facilitate strain coexistence. Competing SIS-like diseases on multiplexes were studied by Sahneh and Scoglio,[136] who obtained similar conclusions about inter-layer correlation for this family of models. Coexistence for a two-strain SIS-like model means long-term prevalence of both diseases. These works show that the competitive principle for contagious diseases can be challenged by structural features of the population.

Recent research efforts have also focused on cooperative interactions between diseases.[88, 139–144] Chen,[140] Cai[141] and others studied the cooperative version of the SIR-like model for two diseases, in which being formerly infected by one disease increases the chance of being infected by the second. They show that the structure of the underlying network (or lattice), more specifically its capability of generating cascaded mutual infections, determine the existence of a dis-

continuous phase transition. Cui and others[143] also study a similar model for power-law degree distributed networks, using heterogeneous mean-field, reporting also the presence of a discontinuous phase transition.

A few works have also studied cooperative contagion in an SIS scheme. Chen and others[88] studied two SIS diseases in which the presence of one disease in a host increases its susceptibility to the other disease, using both a homogeneously mixed population and a two-dimensional continuous population. They traced the phase diagrams for the homogeneously mixed case, showing how the phase transitions are modified by the cooperation, and also displaying a variety of bistable regions, into which discontinuous phase transitions are observed. Hébert-Dufresne and Althouse[142] studied a similar model on clustered networks. Besides reporting discontinuous phase transitions, they show that, for high enough levels of cooperation, the network clustering can enhance the propagation of the pair of diseases, both by speeding up the transient spread and by reducing the epidemic threshold. This means that collaborative contagion can revert the otherwise hindering effect of network clustering.

Cooperative contagion is a younger research topic compared to the competitive case, yet received some important advances. However, the case of asymmetric interactions between diseases is still much less explored than the other ones. An example of such interaction scheme is the previously mentioned case of HIV and some opportunistic infections that reportedly reduced the HIV load,[121–123] for which the effect over the epidemic dynamics is still unknown.

Noh and others,[145] as well as Ahn and collaborators,[146] used heterogeneous mean field and numerical simulations to study a model with asymmetrical coupling between two types of particles on networks, following a statistical physics workflow. They focused on finding the critical exponents and determining the universality classes, letting aside other details about the model's dynamics itself. Wu and others[147] studied a similar model in a mathematical framework, also using heterogeneous mean field, determining the model's phases and their stability criteria. The model consists of an originally competitive contagion of two SIS diseases, to which a one-way *superinfection* mechanism is added: one of the diseases may superinfect hosts that are infected with the other, replacing it inside the host. This can either configure an asymmetrical or competitive interaction scheme, depending on the rate (or probability) of superinfection. Wu shows that the introduction of the superinfection mechanism can sustain coexistence even in a competitive scheme.

In another context, Zhu and others[148] used a similar model to study the effect of a propagating countermeasure (or antivirus) for computer viruses. Their model is similar to that of Wu and others,[147] yet studied under homogeneous mixing and with demographic dynamics which, in this scenario, represents insertion and removal of computers to/from the web. The idea of spreading "helpful computer worms" to prevent and/or eliminate malware have been considered in practice, such as the Welchia[149] and CodeGreen worms, though this approach can cause more harm than good and poses ethical challenges.

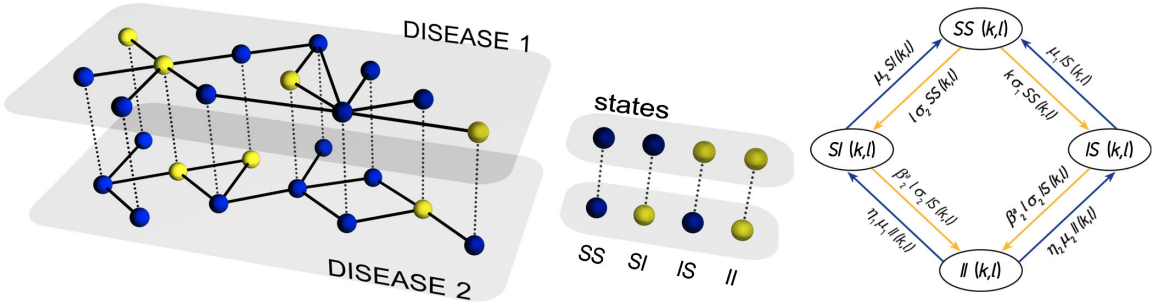

Figure 6 – Schematic representation of the SIS-like interaction scheme from Sanz and others.[1] The model is constructed in a multiplex network (left panel), having one layer fo each disease, and the transitions between the four possible states (SS, SI, IS and II) have arbitrary parameters (right panel), configuring a very general scheme of interactions that can be cooperative, competitive or asymmetrical.

Source: SANZ *et al.*[1]

Asymmetrical coupling between spreading processes have been mostly studied in the context of the interplay between epidemics and information. In human populations, the discovery of an epidemics often causes the spreading of information about it, which in general may work to contain the disease. This scenario has received considerable attention from computational and mathematical models, and we thoroughly describe its literature in Section 3.1.2. However, these works are directed to the problem of epidemics and awareness, while the general understanding about asymmetrically interacting spreading phenomena remains underexplored.

Finally, some works have focused on interacting diseases in a general scheme, which can comprise cooperative, competitive and asymmetric interactions.[1,150–154] Sanz and collaborators[1] propose a model for two diseases that can interact through arbitrary changes to the infection and healing rates due to the presence of a pathogen, so that each transition from any state can have a unique rate. They study both SIS-like (Figure 6) and SIR-like schemes separately, and apply heterogeneous mean-field and numerical simulations in both cases to study their phase diagrams on multiplex networks with known joint degree distribution $P(k,l)$. More recently, this model received a Markov chain approach from Soriano-Paños,[150] as well as Wu and Chen.[152]

The literature on interacting epidemics is very extensive, and is still growing with recently published papers. For a recent review on the topic we refer the reader to Brodka and others.[155]

3.1.2 Coupled disease-behavior models

The interplay between human behavior and epidemic spreading is subject of an intense area of research.[18, 124–125,156] This interplay can happen in several different ways. Mobility patterns determine where and how fast an early epidemic outbreak spreads, and it can also be affected by travel restrictions during this stage. Aspects of human daily habits, such as hygiene,

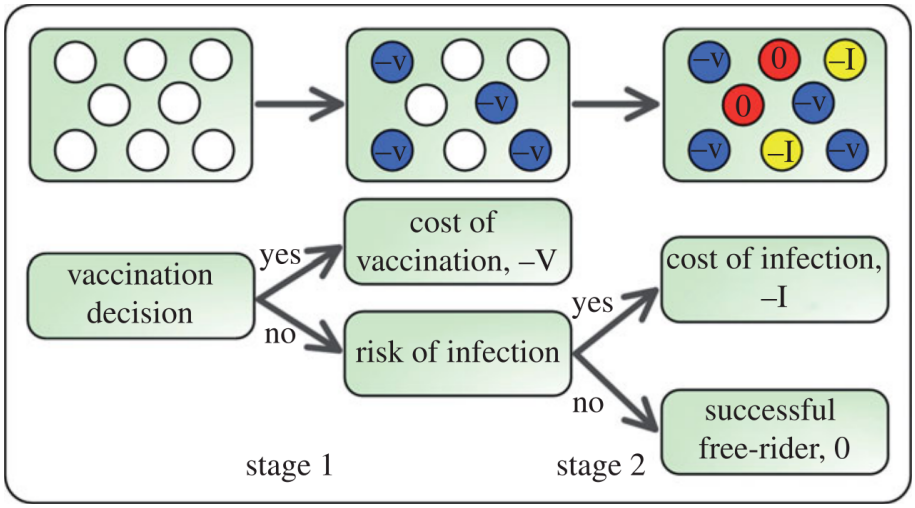

Figure 7 – A model for the vaccination dilemma, as proposed by Fu and others.[2] I a two-step process, the first one is a public goods game, in which individuals may decide to vaccinate at a cost $-V$. The second step is an epidemic SIR-like process, in which vaccinated individuals are completely immune, and infected individuals have a cost $-I$ (greater than that of vaccination).

Source: FU *et al.*[2]

contact patterns and public space activities are decisive for the spread of infectious diseases. Conversely, they can be altered by information spread through mass media, social networks and daily chats, with the aim of containing the spread of diseases. However, the adoption of individual protection measures, such as hand washing, vector elimination and social distancing, are subject to individual opinion and personality traits. Vaccination, in particular, has recently driven considerable attention, due to the rise of anti-vaccine concerns, which may be amplified by opinion bubbles and other phenomena related to social media.[157]

Game-theoretical and opinion-dynamics approaches are often used to account for beliefs, opinion polarization and echo chamber effects.[2,158–161] For example, Fu and others[2] regarded vaccination as a public goods game, coupled with an SIR epidemic model (see Figure 7). They show how, according to their model, the vaccination level drops and the epidemic outbreak size raises as the perceived vaccination cost increases, for well-mixed, lattice-structured and network-structured populations.

Models for opinion dynamics are also used to include behavioral responses to epidemic spread.[162–165] These usually include the idea of *conformity* (that is, the tendency that people have to match the attitudes of their social cycle) and often lead to opinion polarization and/or clustering ("opinion bubbles"). Salathe and Bonhoeffer[162] used a voter model to emulate people's opinion dynamics about vaccination, after which an SIR epidemics was propagated. They found that the probability of outbreaks is greater when the opinion dynamics is more intense, attributing this to clusters of vaccine-rejection opinion. This work was generalized by Eames,[163]

who considered a multilayer network of parents and children. Opinion dynamics is held on the parents' layer, who decide to vaccinate or not their children, while the disease is spread on the children's layer. They show that a high overlap between these two layers (meaning that parents that interact are likely to have children that also interact) can cause unvaccinated clusters and, therefore, higher probabilities of outbreak. These original works were later developed into further situations regarding the interaction between opinion and epidemic spreading.

A simpler approach consists into accounting for individuals' *risk perception*.[166–170] This considers that individuals react to the risk of being infected, which is measured by the number (or fraction) of infectious neighbors. Bagnoli and others[166] developed a simple mean-field approach to study such a model within typical network topologies, such as small-world and scale-free, describing the critical level of awareness (i.e., reduction of individual's susceptibility under risk perception) as a function of other parameters. Wu and others[167] extended this to include individual's number of contacts (degree) and global prevalence, besides infectious neighbors, to account for risk perception. Later on, Massaro and Bagnoli[168] also extended their previous model to a multiplex, evidencing that dissimilarity between the layers would impair the effect of risk perception, because gathering the risk information from a different neighborhood than your contact layer can be "misleading". The individual risk perception approach can be very effective to control a disease, but relies on a feature that is often unpractical: that infectious individuals almost always display clear symptoms.

Another form of behavioral response is the so called *propagating awareness*, consisting into information that is spread from peer to peer ("word-of-mouth") to stimulate individual protection methods. As in the risk perception framework, this method disregards individual beliefs and their influence on the decision to self protect. Nonetheless, by considering awareness as a disease-like spreading phenomena, powerful theoretical insights can be taken from the interaction between two similar dynamical processes.[134, 171–176] Funk and others[171] consider a model for an awareness that is generated from infectious individuals, propagates through their contacts and fades out at each propagation. This is coupled to an SIR epidemic model. Despite not mentioning multiplex networks, their model allow for separate connectivity structures for the disease and information propagation. Among other results, they discuss the effects of network clustering and overlap between the layers, showing that better overlapping provides higher effect of awareness over epidemics.

In a series of two works, Granell and collaborators[172–173] studied the disease-awareness in a different scheme. Their model, which they name UAU-SIS, considers an SIS-like model for both disease and information awareness and a multiplex structure – one layer for the epidemics and another for the information. Each individual can be either susceptible (S) or infectious (I) regarding the disease, and aware (A) or unaware (U) of the information. Aware individuals propagate the information just like infectious individuals spread the disease, but susceptible-aware (SA) individuals are less likely to catch the disease at each contact with an infectious.

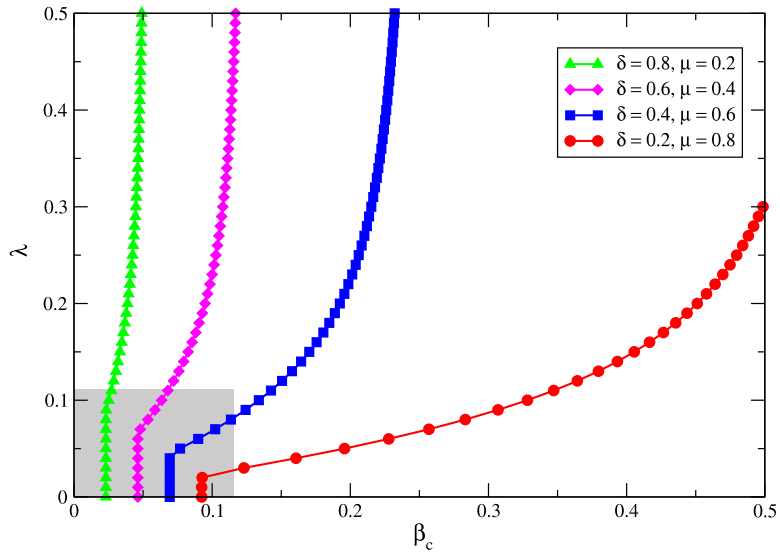

Figure 8 – Critical value of the disease transmission probability β_c as a function of the information transition probability λ, for different combinations of the disease's healing rate μ and the information forgetting rate δ. The corners at each curve are named as metacritical points.

Source: GRANELL *et al.*[172]

In turn, infectious-unaware (IU) individuals can "spontaneously" become aware by noticing their own symptoms, a state change called "self-awareness". This way, the disease-information interplay represents a positive-negative loop, in which awareness impairs the propagation of the disease, which in turn stimulates the propagation of awareness, akin to the asymmetrical case explained in Section 3.1.1. In their second work,[173] the group also considers a "mass media" state change, by which unaware individuals spontaneously become aware regardless of their state (by gathering information from media).

The authors use a microscopic Markov chain approach[107] (as presented here in Section 2.2.4) to describe the model, and show how the parameters influence the prevalence and critical point. They describe what was called a "metacritical point", depicted in Figure 8 and described as a phase transition to the critical point. This is an effect of the phase transition of the information alone, which tells if the awareness is able to be sustained by itself (that is, without the aid from the disease) or not. As a consequence, for example, the metacritical point disappears when the mass media mechanism is introduced. This work was the base for the one that we present in Section 3.2, and understanding the phase diagram of such disease-awareness systems was part of the motivation for the work on Section 3.3.

Back to an SIR basis, Wang and others[174–175] study a multiplex model for epidemics

and awareness with vaccination. Information, as well as a disease, is propagated according to an SIR model, and informed individuals have a probability of vaccinating, becoming permanently immune. Another condition that they pose for vaccination is the presence of at least ϕ infectious neighbors (from the layer of information spreading). With all these ingredients, they found that there is an optimal value of the information transmission probability that minimizes the disease outbreak size. This feature is not present if $\phi = 0$, meaning that the requirement of infectious neighbors for the decision to vaccinate plays a role on this result.

The disease-awareness interplay is still an active area of research, with recent works exploring the diverse aspects of such systems.[177–181]

3.2 Epidemic spreading with awareness on multiplex networks

The content described in this section was published as a paper in Physical Review E.[182]

As we described, most works about epidemics with propagating awareness use an epidemic model for the information. However, information may be more adequately modeled by rumor models, which use a different "recovery" mechanism – in this case, the loss of interest into spreading the information. By considering stiflers into such a model, we can incorporate individuals that hold the information but do not propagate it, and verify if this plays a role in the disease-awareness coupling. Additionally, most works consider that the epidemics and information propagate in the same time scale, in a sense that the healing rates of both processes are similar or equal. As shown in Section 3.1 (for instance, in Figure 5), changing this time scale relationship can sometimes cause a relevant effect in the system's dynamics. In this section, we present our contribution to this research field: an SIS-like disease model coupled with a "cyclic" rumor model for the awareness, with a flexible time scale ratio between the two processes. This work was published in PRE,[182] and chronologically was the first one developing during the author's PhD.

As in previous works,[172–173] our model considers the propagation of a disease in a population, simultaneously to the spreading of information about it, by which individuals become aware of the disease and of prevention methods, reducing their own contagion probabilities. This coupled dynamical system run in a two-layer multiplex network, one layer for the disease spreading and the other for the information awareness to mitigate the disease. We identify each pair of linked nodes from each layer as the same "individual"; the only difference from one layer to the other one lies in the structure of connections inside the layers. The links on the "epidemic layer" represent contacts that can possibly transmit the disease, whereas links on the "informational layer" represent pairs of individuals that share information with each other, like in social online networks.

3.2.1 Model description - Baseline model

The model for the epidemic spreading adopted here is a reactive SIS (susceptible-infected-susceptible) compartmental model in which, at each time step $\Delta t = 1$ of the dynamics, each infectious (I) node tries to transmit the disease to each of its susceptible (S) neighbors on the epidemic layer with probability β, and then tries to recover with probability μ.

For the spreading of information awareness to prevent the transmission we use a cyclic Maki-Thomson rumor model for complex networks,[183] which we call UARU (unaware-aware-stifler-unaware). Notice that we use the letter R here for the stifler compartment to avoid confusion with the susceptible (S) state in the SIS model. A stifler is an informed node who does not propagate the information anymore. When an aware (spreader) node contacts an unaware (ignorant) neighbor in the informational layer, it tries to pass the rumor about the disease. If the contacted neighbor, however, is an aware or stifler node, the node that makes the contact can become stifler. A stifler individual can also forget the information about the disease transmission, becoming ignorant about the disease transmission again. We again use a discrete time approach[107] by considering a reactive formulation in which, at each time step $\Delta t = 1$, each aware (A) node first tries to inform each of its unaware (U) neighbors with probability γ, and then becomes a stifler (R) with probability σ at each contact with an A or R neighbor. Besides, each stifler node becomes ignorant (U) upon forgetting with probability α.

By combining the epidemic and the informational states of each node, we can describe the overall state of each individual. In our model, we have six different states, i.e., SU (susceptible and unaware), SA (susceptible and aware), SR (susceptible and stifler), IU (infected and unaware), IA (infected and aware) and IR (infected and stifler). Using these overall states, we define the interaction between the epidemics and awareness by adding two other features. First, a susceptible node that is informed (aware or stifler) will reduce its contagion probability by a factor Γ (with $0 \leq \Gamma < 1$) for each contact, meaning that it will get the disease from each of its infected neighbors with probability $\Gamma\beta$ (less than β). Such a feature represents the adoption of prevention methods against the disease. Second, an additional transition called *self-awareness* is considered: if not informed by a neighbor, an infected-unaware (IU) node can, during the same time step, become aware with probability κ, by knowing its own condition. This process simulates the case in which an infected subject recognizes the symptoms of the disease and becomes aware of the infection.

The following reaction equations - representing respectively the (3.1) infection of an unaware susceptible, (3.2) infection of an aware susceptible, (3.3) infection of a stifler susceptible and (3.4) healing of an infected node - describe all possible epidemic transitions (where x is used to represent an arbitrary informational state):

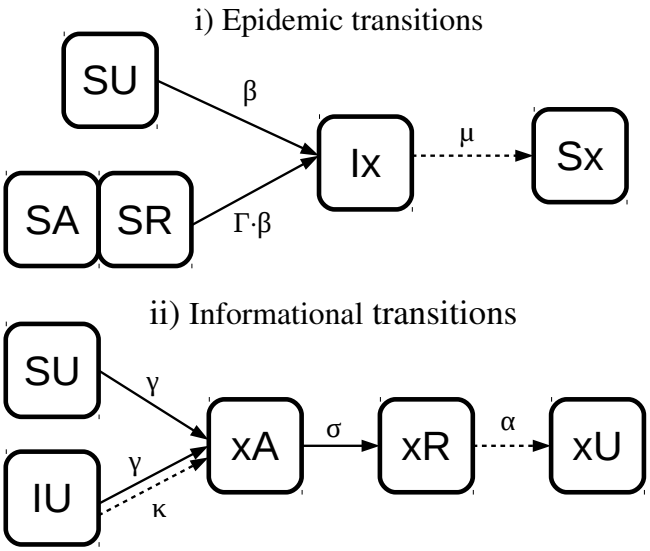

Figure 9 – Schematic illustration showing the states of the nodes in the network and the associated transition probabilities between states, indicated by the Greek letters.

Source: SILVA *et al.*[182]

$$SU + Ix \xrightarrow{\beta} IU + Ix, \tag{3.1}$$
$$SA + Ix \xrightarrow{\Gamma\beta} IA + Ix, \tag{3.2}$$
$$SR + Ix \xrightarrow{\Gamma\beta} IR + Ix, \tag{3.3}$$
$$Ix \xrightarrow{\mu} Sx. \tag{3.4}$$

The informational transitions - respectively (3.5) information of an unaware node, (3.6) self-awareness of an infected unaware, (3.7) “stifling” of an aware node by contacting another aware node, (3.8) “stifling” of an aware via contact with a stifler and (3.9) forgetting of the information - are represented by these equations (x and y represent arbitrary epidemic states):

$$xU + yA \xrightarrow{\gamma} xA + yA, \tag{3.5}$$
$$IU \xrightarrow{\kappa} IA, \tag{3.6}$$
$$xA + yA \xrightarrow{\sigma} xR + yA, \tag{3.7}$$
$$xA + yR \xrightarrow{\sigma} xR + yR, \tag{3.8}$$
$$xR \xrightarrow{\alpha} xU. \tag{3.9}$$

Figure 9 presents the possible transitions between the six states, grouped according to the epidemic and informational dynamics.

The timescale of the model is controlled according to a defined probability. With probability π, only the rumor transitions (awareness, self-awareness, stifling and forgetting) can happen during the current time step. With the complementary probability $(1-\pi)$, the epidemic transitions (infection and recovering) can occur. By setting the value of π, it is possible to emulate different timescales between the two processes. For instance, a value of π close to 1.0 means that the rumor propagates much faster than the infectious agent.

3.2.2 Modified model

Besides the baseline model that we have described, we propose a minor modification that can generate some unexpected behaviors. We extend the idea of self-awareness to stifler nodes, considering that a stifler, which is also infected by the disease, is less likely to forget the information. That is, a node who knows about its own infection does not inform other nodes and also impair the transmission of other nodes, creating additional stiflers around it. This behavior is approximately observed in the case of HIV transmission, in which some infected individuals knows about its own infection but do not voluntarily notify their sexual partners,[184] acting as infected-stiflers. We include this feature by reducing the probability that an infected-stifler node forgets the information by a factor of $(1-\kappa)$ (so that the self-awareness parameter also reduces the rate at which infected-stiflers become infected-unaware). We refer to this version of the model as *modified model*, whereas the version without this modification is referred to as *baseline model*.

In the following section, we describe our results with both baseline and modified models.

3.2.3 Results

We performed extensive Monte Carlo (MC) simulations of our model, where we considered a multiplex network composed by two layers with scale-free organization and $N = 1000$ nodes each. Each layer was generated independently by using the configuration model[185] with power-law exponent $\gamma_{sf} \approx -2.5$ and minimum degree $k_{min} = 4$, with a resulting average degree $\langle k \rangle \approx 7.4$ in each layer. The node correspondence between the two layers is done at random, generating thus no relevant degree correlation for corresponding nodes in each layer. In order to further study the model, we also developed a Markov chain approach that consists of solving a set of fixed point equations that provide the stationary fractions of nodes in each state. The Markov chain method is described in appendix A.

In Figure 10, the stationary density of infected nodes ρ_I^* (prevalence) is plotted against the infection probability β, for different values of the parameters γ (information spreading probability), Γ (immunization factor for informed nodes) and π (relative time scale). For this first analysis, we only used the baseline model. Symbols represent the results from MC simulations of the model, while solid lines correspond to the solution of the Markov chain approach. To

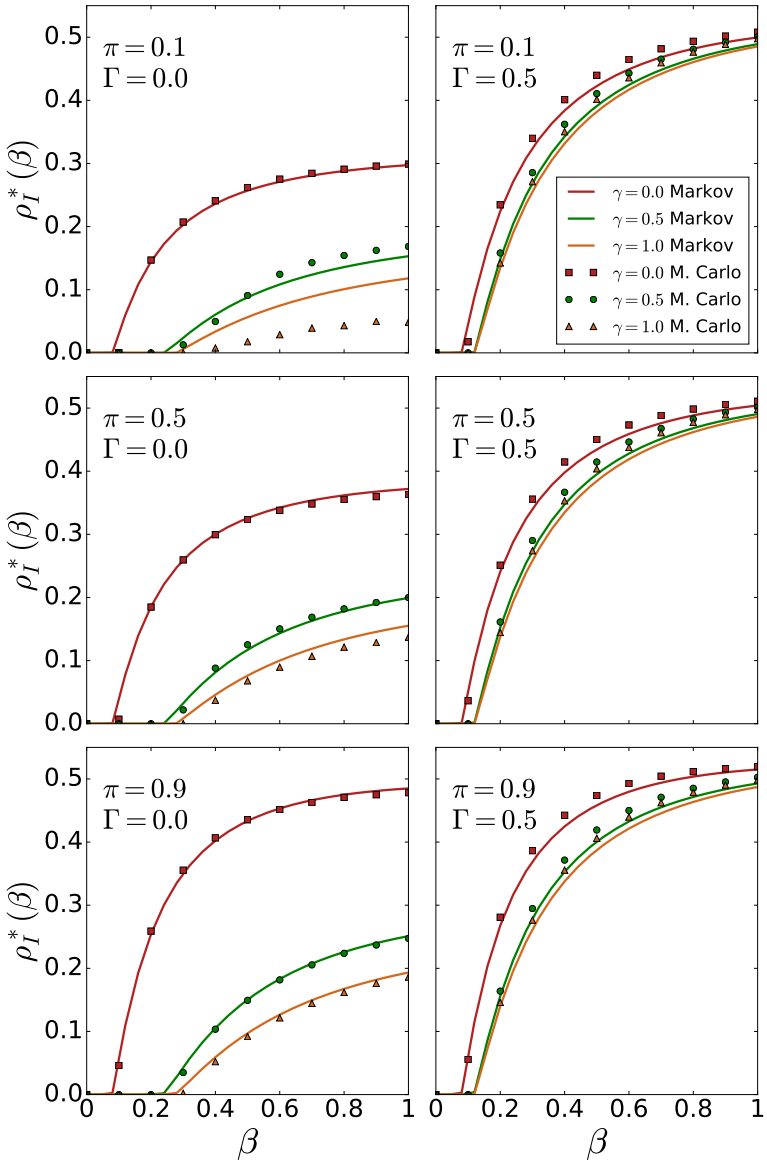

Figure 10 – Stationary density of infected nodes ρ_I^* (disease prevalence) as a function of the disease propagation probability (β), for different values of γ, Γ and π, using the baseline model. For $\pi = 0.5$, the rumor spreading and the epidemic propagation have the same time scale, whereas for $\pi = 0.1$ (0.9) rumor events are slower (faster) than the events of the epidemic process. The solid lines are Markov chain calculations (see appendix A), whereas symbols are results from Monte Carlo simulations. Other parameters of the model are set to: $\mu = 0.9$, $\alpha = 0.6$, $\kappa = 0.5$ and $\sigma = 0.6$.

Source: SILVA *et al.*[182]

calculate stationary densities by MC simulations, we run the dynamics for $T = 1200$ time steps, ignore the first 400 time steps and calculate the average fraction of nodes in the desired state over the remaining 800 steps. Each data point corresponds to an average over 10^3 independent realizations of the dynamics. At the initial state of each realization, 20% of the nodes are randomly chosen and assigned the state IA (infected-aware), whereas the remaining 80%

of nodes are set to the SU state (susceptible unaware).* For the Markov chain calculations, initially each node begins the process with probability $p^i_{IA}(0) = 0.2$ for the infected-aware state and $p^i_{SU}(0) = 0.8$ for the susceptible-unaware state, with the remaining state probabilities being set to zero.

Analyzing Figure 10, we can first check that the information about the disease helps in both reducing the prevalence and increasing the epidemic threshold, by comparing curves with different values for the information spreading probability γ. The prevalence is also decreased when the immunity provided by the awareness is total ($\Gamma = 0.0$) rather than partial ($\Gamma = 0.5$). Additionally, and more difficult to notice from Figure 10, the prevalence is increased if the relative time scale parameter π is greater, i.e., when the transitions of the rumor process are faster than those of the epidemic process. This is an intriguing result as, intuitively, we expect that a faster informational process should be more efficient in preventing the disease spreading. An insight into this counterintuitive effect can be obtained by studying simpler versions of the present model within a mean-field approach or homogeneous mixing, which we did in later works,[90,186] one of which is presented here in Section 3.3.

To investigate in more detail how the variation of the relative timescales between the two processes affects the prevalence, we consider the behavior of the infected, aware, stifler and unaware stationary densities as a function of the parameter κ (probability of self-awareness for an infected-unaware node). Figure 11 shows these stationary densities for two different values of π. Each curve is normalized by its value when there is no self-awareness (i.e., $\kappa = 0$). We notice that, in both cases, the self-awareness is beneficial to the disease prevention, as the densities of aware (A) and stifler (R) nodes increase, thus reducing the density of unaware (U) nodes and the disease prevalence (I). Figure 11 also shows good agreement between Markov chain method and Monte Carlo simulations for these normalized curves.

The picture changes if we consider the modified model, described in Section 3.2.2. Figure 12 shows the same plot as in Figure 11 for the modified model, also with Monte Carlo and Markov chain simulations. For $\pi = 0.1$, as it happens in the baseline model, both densities of aware and stifler nodes increase with κ. However, for $\pi = 0.9$, when the rumor propagates faster than the disease, the fraction of aware (A) nodes decreases with κ, whereas the fraction of stiflers (R) increases very rapidly with κ. This means that the propagation of the information is hindered by the self-awareness of infected stiflers, as they resist to forget the information (unaware) and then become aware (spreaders) again. Notice that, although the stifler population increases in comparison to the aware population, the density of unaware nodes still decreases with κ, meaning that less individuals are unprotected from the disease. Nevertheless, the prevalence (I) increases with κ in this case.

This is another counterintuitive result, because the disease prevalence is greater even

* Even if it is usual to start simulations with a very small fraction of active individuals, we start at 20% to prevent the system from falling into the absorbing (healthy) state while in the active phase.

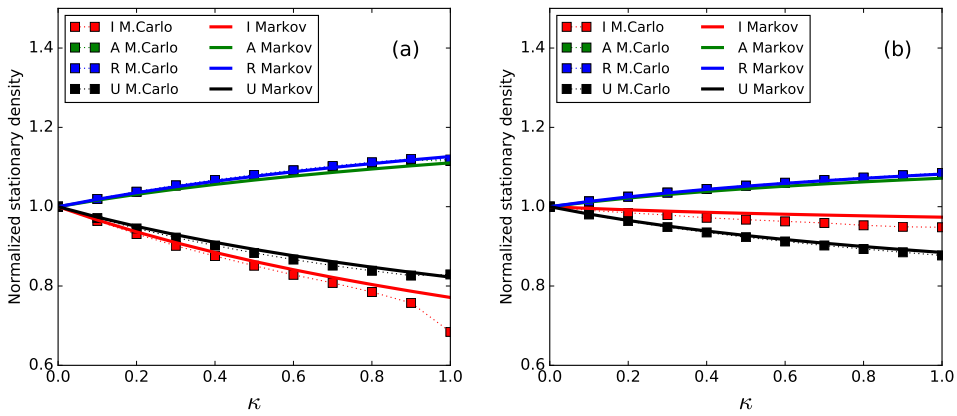

Figure 11 – (*Baseline model*) Stationary densities of nodes in states I (infected), A (aware), R (stifler) and U (unaware) normalized by their non-self-awareness value (at $\kappa = 0$) as a function of κ, for (a) $\pi = 0.1$ (slow rumor spreading) and (b) $\pi = 0.9$ (fast rumor spreading). Squares are the results of Monte Carlo simulations, whereas the solid lines are Markov chain calculations (see the appendix). The dotted lines are guides to the eyes. Other parameters are set to: $\beta = 1.0$, $\mu = 0.9$, $\gamma = 0.5$, $\alpha = 0.6$, $\Gamma = 0.0$, $\sigma = 0.6$.

Source: SILVA *et al.*[182]

though the unaware population is smaller. To understand this, we look at the susceptible population: if most susceptible individuals are unaware of the disease, the information is concentrated at infected nodes and thus is not effective in controlling the disease. In Figure 13, we study the relative distribution of the susceptible population between unaware (SU), aware (SA), stifler (SR) and the combination of the previous two (SA + SR), using the modified model only. For the case of slower information ($\pi = 0.1$), the fraction of informed susceptible nodes (SA, SR) increases with κ, as expected. However, when $\pi = 0.9$, the opposite happens: the fraction of SA and SR decreases and the fraction of susceptible-unaware (SU) nodes increases, meaning that the fraction of susceptible nodes that are protected by the information decreases with κ in this case. Therefore, even if the unaware population is reduced with κ (as reported in Figure 12.b), the information is actually concentrated at infected individuals, making the protection inefficient. In other words, the fraction of informed individuals always increases with κ but, for large π, susceptible individuals become less informed as κ increases, and thus the number of infections increases.

Hence, we conclude that the timescale, controlled by the parameter π, plays a fundamental role on the outbreak size, meaning that the relative timescale between epidemics and information determines if the self-awareness is beneficial or not for the disease prevention. We also study how the parameter π changes the behavior of the prevalence with κ on the modified model, by analyzing the prevalence ρ_I^* vs κ curves for eleven different values of π. Figure 14 shows such curves, normalized by the value of the prevalence when $\kappa = 0$.

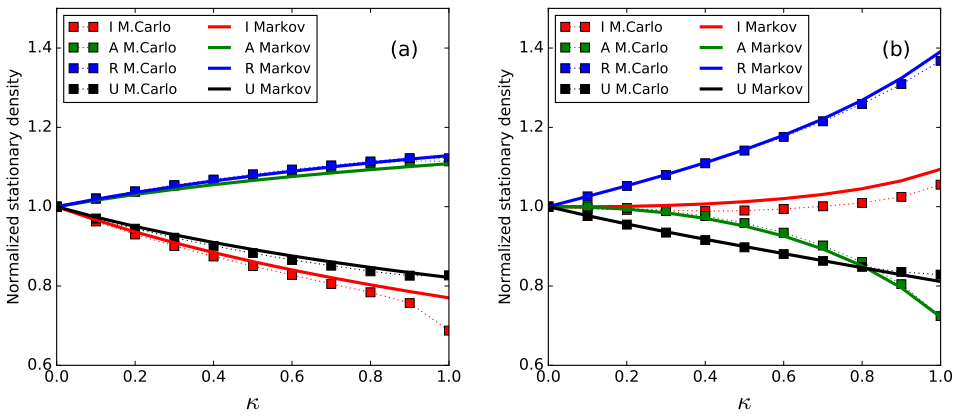

Figure 12 – *(Modified model)* Normalized stationary densities vs κ using the modified model (see text), for (a) $\pi = 0.1$ (fast epidemic spreading) and (b) $\pi = 0.9$ (fast rumor propagation). Squares and solid lines correspond to MC simulations and the Markov chain approach, respectively. Parameter values are the same as those in Fig. 11.

Source: SILVA *et al.*[182]

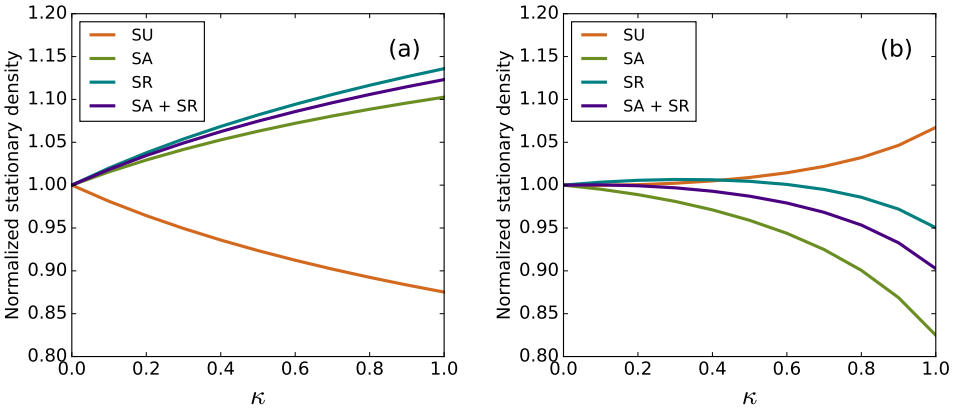

Figure 13 – Stationary densities for the susceptible nodes as a function of the self-awareness probability κ, normalized by their values with $\kappa = 0$, using the modified model, for (a) $\pi = 0.1$ and (b) $\pi = 0.9$. The increasing on SU population with κ for $\pi = 0.9$ helps explaining the behavior in Fig. 12. Other parameters are set to: $\beta = 1.0$, $\mu = 0.9$, $\gamma = 0.5$, $\alpha = 0.6$, $\Gamma = 0.0$ and $\sigma = 0.6$.

Source: SILVA *et al.*[182]

By analyzing the plots in Figure 14, we can conceive the influence of the timescale. For small π (faster epidemics, slower information), the prevalence exhibits its normal decreasing behavior with κ for both baseline and modified models. On the other hand, for larger π (slower epidemics, faster information), the curves for the modified model flip their slope for

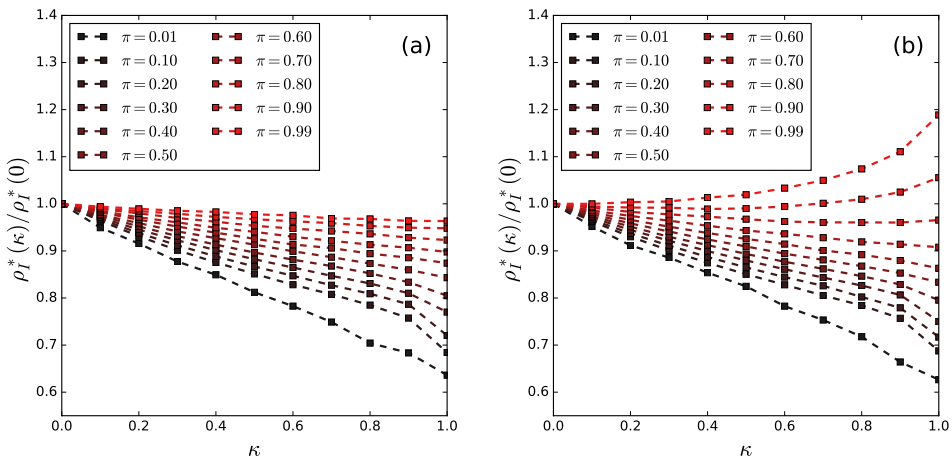

Figure 14 – Normalized disease prevalence $\rho_I^*(\kappa)/\rho_I^*(\kappa = 0)$ vs κ for the (a) baseline and (b) modified models. The values of the timescale parameter π increase from the darker to the brighter color, showing how the curves change their behavior with κ as π increases. Other parameters are set to: $\beta = 1.0$, $\mu = 0.9$, $\gamma = 0.5$, $\alpha = 0.6$, $\Gamma = 0.0$, $\sigma = 0.6$.

Source: SILVA *et al.*[182]

larger κ values, whereas they maintain the same behavior for the baseline model. This means that, when the informational processes are considerably faster than the disease transmission, the self-awareness process can generate too many stiflers and impair the information spreading, increasing the prevalence. For both baseline and modified models, the time scale plays an important role on determining the effectiveness of the information on reducing the disease prevalence.

The results presented so far were taken using a pair of scale-free (SF) networks. One natural question is whether the observed phenomena are due to the particular topology that we used. To answer that, we simulated the (modified) model using combinations of two other topologies: the Watts-Strogatz (WS)[6] and Erdős-Rényi (ER)[41] models. The ER layers were generated with connection probability $p = 0.008$, which produces an average degree of $\langle k \rangle \approx 8$ (for $N = 1000$ nodes). The WS layers were generated with an initial (and average) degree $k = \langle k \rangle = 8$ and rewiring probability $p_r = 0.01$, which produces layers with average clustering coefficient $C \approx 0.47$ and average shortest path length $l \approx 5$. For the simulations, we used the following pairs of epidemic/informational (in this order) layers: ER/ER, ER/SF, ER/WS, WS/WS, SF/WS and the previously used SF/SF pair.

Figure 15 shows the results of Markov chain calculations using other topologies. On the first (left) plot, we show the prevalence as a function of the self-awareness parameter κ, for a high value of the time scale ($\pi = 0.9$, meaning faster informational processes). On the second (right) plot, we show the prevalence as a function of the time scale parameter π for a fixed value

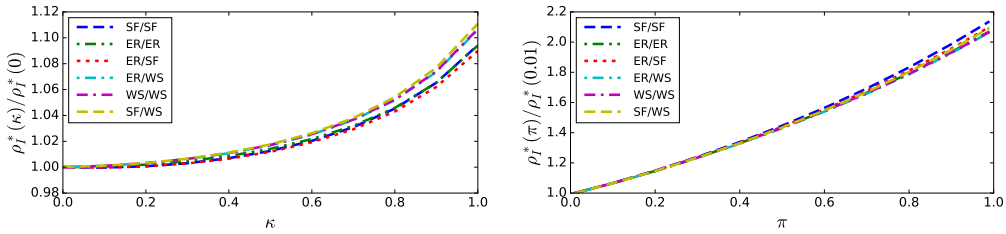

Figure 15 – Markov chain calculations of the normalized prevalence for the modified model, using different pairs of network models between the configurational scale-free (SF), Erdős-Rényi (ER) and Watts-Strogatz (WS) models. On the left panel, the prevalence is shown as a function of the self-awareness parameter (κ) for a fixed value of $\pi = 0.9$ (normalized by the value when $\kappa = 0$), and on the right panel it is shown as a function of π for a fixed value of $\kappa = 0.8$, normalized by prevalence when $\pi = 0.01$. Other parameters are set to the same values as in Figure 14.

Source: SILVA *et al.*[182]

($\kappa = 0.8$) of the self-awareness. All prevalence values are normalized by the first value of the sequence. For all pairs of topologies, the basic results that we presented before - the increasing of the prevalence with π and the reversed behavior with κ for high values of π are consistently preserved.

By noticing that the network topology did not influence the observed behaviors with the SIS/UARU model, we tend to conclude that these are essential characteristics of the model itself. This possibility was part of the motivation for two of our subsequent works.[90,186] one of which is presented in Section 3.3.

3.2.4 Epidemic critical point and phase diagrams

Following the procedure proposed in,[107] we can calculate the epidemic critical point for our model. We show in Section A.2 of appendix A that the phase transition curve between the endemic and the healthy state is, for both baseline and modified models, given by $\beta/\mu = (\Lambda_{\text{max}}(H))^{-1}$, where the elements of matrix H are defined as:

$$H_{ij} = [1 - (p_A^i + p_R^i)(1 - \Gamma)]A_{ij} \tag{3.10}$$

Where A_{ij} is the epidemic layer adjacency matrix and Λ_{max} represents the greatest eigenvalue. This result is the same as in the model from Granell with no mass media,[172] only replacing the probability that node i is simply aware p_A^i by the probability that it is "protected" $p_A^i + p_R^i$, whose value is calculated by solving the Markov chain equations equations without epidemics (that is, null probability of infection for all nodes).

One first notorious fact is that the epidemic critical point does not depend on the relative time scale π, as it does not change the individual "forces" of the epidemic and informational

processes. It also does not depend on κ, as self awareness is irrelevant when the prevalence is very small.

Figure 16 shows the phase transition curves in the β x γ plane, for four different values of the protection factor Γ. At the left of each curve lies the healthy phase (no disease in stationary state), whereas the endemic phase ($\rho_I^* > 0$) is at the right. On the inset, we show how the epidemic critical point depends on the protection factor Γ.

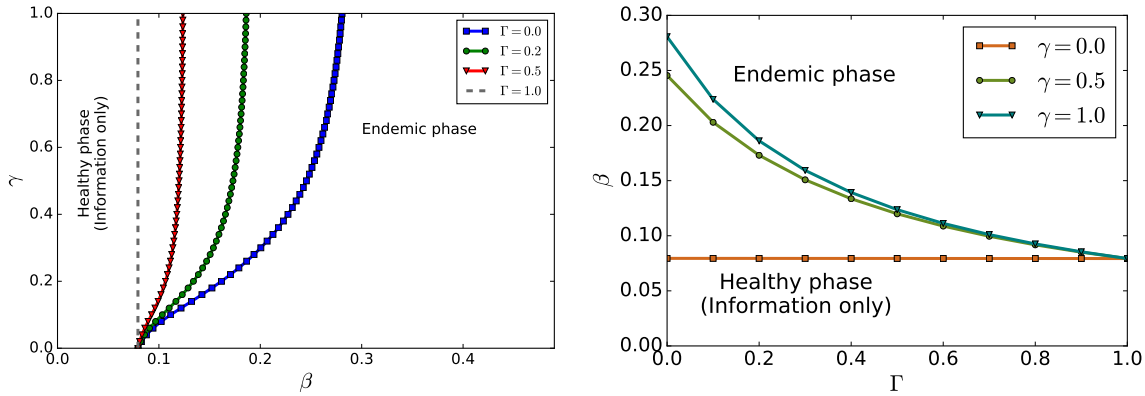

Figure 16 – Phase diagrams of the SIS/UARU calculated via Markov chain approach. The left panel shows the γ (rumor transmission probability) *vs* β (disease transmission probability) phase transition curves between the healthy and endemic phases, for different values of the Γ (protection factor due to awareness). The right plot shows the transition curves for β as a function of Γ, for different values of the information transmission probability γ. The diagram is the same for the modified and baseline models, and does not depend on π and κ. Other parameters are set to: $\mu = 0.9$, $\alpha = 0.6$, $\sigma = 0.6$.

Source: SILVA *et al.*[182]

One of the main differences to the simpler SIS/UAU model presented by Granell and others[172] is that the "metacritical" point is not present, as in the model with mass media[173] from the same authors. This happens because the rumor model UARU is always in the active phase, i.e., there is always a fraction of nodes that is aware, provided that $\gamma > 0$. Therefore, our SIS/UARU model presents only two phases: healthy and endemic, lacking a phase in which both disease and information are extinct. In our model, therefore, the population can be either informed and healthy or informed and endemic. Although information exists even without disease, the density of informed individuals is enhanced by the presence of disease (provided that there is self-awareness), as it can be seen in Figures 11 and 12.

3.2.5 Discussion

In this work, published on Physical Review E in 2019,[182] we studied epidemic spreading with information propagated according to a rumor model. To our knowledge, it was the first work to use a rumor model and a stifler compartment to the spreading of awareness about

a disease. We shown some interesting and non-intuitive phenomena which, apart from their possible consequences to real systems (if applicable), bring some relevant theoretical questions.

First, we report that an aware population is not necessarily more protected against the disease, especially if the information is retained on infectious stiflers (that do not propagate the information). This feature is introduced by the use of stiflers, besides a modification to the baseline model, and thus represents an essential difference from models that use simple epidemic models for the information. Second, we report that the disease prevalence is greater with a "faster" information (i.e., one that evolves in a shorter time scale) than with a "slower" one. We came to know, after publishing, that this result was already reported in a similar model.[187] Despite analogous, their model is not equivalent to ours, which raises an interesting question: what features that such a model must have to display this non-intuitive behavior with the relative time scale? This question is not simple to answer, but it would help understanding to which extend these results should be expected in real systems, where many other factors come into play.

As shown in Figure 15, the behaviors that we reported do not seem to qualitatively depend on the network topology, at least for the number of nodes ($N = 1000$) that we used and the chosen topologies (ER, WS, SF). This motivates the study of such models with no network structure, which reveal the fundamental and intrinsic properties of the dynamical systems (as done in[88]). Besides, the study of an epidemic model without a contact structure to the population often leads to analytically more tractable equations.

This motivated our collaborators, Federico Vazquez and Fátima Velásquez-Rojas (who also participated on the current work), to develop a mean-field analysis of the epidemic with awareness model.[186] They wrote rate equations for the baseline model and without the stifler compartment (SIS/UAU), for more analytical tractability, and used them to find analytical expressions for the fixed point of the system when both the epidemics and the information are active. They also found analytical expressions for the epidemic critical point, which were used to trace the phase diagrams. We observed the same behavior of the prevalence with the relative time scale, both from analytical calculations performed by them and from Monte Carlo simulations made by our group. This provided a relevant advance to the theoretical understanding of these models.

Despite the important advances, we still wanted to better understand some of the points raised by these works with epidemics and awareness. In the next section, we preset a subsequent work that was greatly motivated by the results of our previous ones.

3.3 Asymmetrically interacting contagion

The work presented in this section was published as an open-access paper in Physical Review Research.

The propagation of an epidemics and the concurrent propagation of awareness about it is an example of two spreading phenomena that interact asymmetrically, with strong analogy to a predator-prey system. For the SIS/UARU and SIS/UAU models, as well as for that presented in,[187] the "prey" (i.e., the disease) has its population increased if its intrinsic time scale is slower than that of the "predator" (i.e., the awareness). However, it remained unknown whether this behavior is a general feature of asymmetrically interacting spreading process and, if not, what are the conditions to produce this behavior.

Motivated by this open question, we looked for other models of asymmetric interaction between spreading processes. We found two models that could serve as useful templates to address this question. These models are mostly found in the literature of interacting diseases, not of epidemic with awareness. However, as discussed in Section 3.1.1, the literature on this subject is mostly focused on the symmetrical (competitive and collaborative) cases, with only a few works dealing with asymmetrical interaction. Moreover, many works do not deal with flexible time scale of one process with respect to the other, often assuming that they are equal. We understood this as a research gap, which we could help filling by studying the question raised by our previous work.

We decided to work on models without network structure (homogeneously mixed populations), continuous time and infinite-sized populations – thus a rate equation formulation, as described in Section 2.2.1, allowing for more analytical power and showing the models' intrinsic properties. In the following section, we describe the two models of interacting diseases that we picked to develop this work, showing the main findings. Besides some interesting properties of the dynamics in the asymmetric regime, we found some differences between the two models that helped us to understand the generality of our previous findings.

While the main application for asymmetrically interacting contagion is the interplay between disease and awareness, the already mentioned reports of HIV viral load decrease after infection by other diseases[121–123] open room for applications of our work to the interaction between pathogens.

3.3.1 Description of the models

In what follows, regardless of the model considered, we assume that there are two diseases (I and II) that interact. Moreover, we consider that disease I is the "prey" (it is impaired by the other disease) and disease II is the "predator" (it is benefited from the first disease), in an analogy with the asymmetrical interaction of predator-prey systems. As in our first work (described in Section 3.2), the parameter π controls the relative time scale between the two diseases. Due to the continuous time evolution, however, it is implemented in a different way: the rates of all processes promoted by disease I are multiplied by $1 - \pi$, whereas the rates of disease II processes are multiplied by π. Making π to range between 0 and 1, we sweep through scenarios in which disease I is faster ($\pi < 0.5$) or slower ($\pi > 0.5$) than disease II, as well as

the balanced case ($\pi = 0.5$). Although π does not add a new degree of freedom of the model, the advantages of using this approach are: (i) it allows us to control the relative time scale with a single parameter; (ii) the "overall rate" of the system, which can be regarded as $\sim (1-\pi)+\pi$, is kept constant when varying π; (iii) plotting variables as a function of π is simple because it is limited between 0 and 1; and (iv) it simplifies the comparison of results with our previous work.[182] Let us now describe each of the models scrutinized in the rest of the section.

3.3.1.1 Model A: interacting diseases through susceptibility change

In this variant, we consider that the presence of one disease impairs the spreading of the second one by changing the individual's susceptibility to catch the other disease. It has been used to describe the dynamics of competing pathogens with partial cross immunity[117] and for collaborative contagion,[1,88] but its asymmetrical version is still largely unexplored. The latter regime is a good prototype to describe the interplay between epidemics and awareness, due to its mathematical similarity to models used for this purpose.

In this model, each individual can either be susceptible to both diseases (S_1S_2), infected by one disease and susceptible to the second one (I_1S_2 and S_1I_2), or infected by both diseases (I_1I_2). We denote as I_1 and I_2 individuals that are, respectively, infected by disease I and II, regardless of their state with respect to the other disease. For completely susceptible individuals S_1S_2, the baseline contagion rate of disease I (II) when in contact with an individual infected by disease I (II) is β_1 (β_2). For individuals already infected by disease I but susceptible to disease II (I_1S_2), the contagion rate for disease II is $\Gamma_2 \cdot \beta_2$, i.e., it is multiplied by a factor Γ_2. The same holds for S_1I_2 individuals, for which the contagion rate by disease I is changed to $\Gamma_1 \cdot \beta_1$. The healing rates from disease I and II are respectively μ_1 and μ_2, and are not affected by the other disease. We also define $\lambda_1 = \beta_1/\mu_1$ and $\lambda_2 = \beta_2/\mu_2$, which are the basic reproduction numbers of each disease as if they were independent. Figure 17 represents all the possible transitions for this model, with their respective time scale factors as explained before.

The asymmetrical interaction between the two diseases can be obtained by setting $0 \leq \Gamma_1 < 1$ and $\Gamma_2 > 1$. This means that individuals that hold disease II are less susceptible to catch disease I in comparison to fully susceptible individuals. On the other hand, individuals infected by disease I are more likely to catch disease II. Therefore, disease I enhances the propagation of disease II, whereas disease II impairs the propagation of disease I. We represent the density of individuals in a given state X by ρ_x, with X being either a composite state (like I_1S_2) or a simple state (like I_2). Based on the diagram from Figure 17, the time evolution of the composite state densities is given by the following equations:

$$\frac{d\rho_{s_1s_2}}{dt} = -(1-\pi)\beta_1\rho_{s_1s_2}\rho_{i_1} - \pi\beta_2\rho_{s_1s_2}\rho_{i_2} + (1-\pi)\mu_1\rho_{i_1s_2} + \pi\mu_2\rho_{s_1i_2} \quad (3.11)$$

$$\frac{d\rho_{s_1i_2}}{dt} = -(1-\pi)\Gamma_1\beta_1\rho_{s_1i_2}\rho_{i_1} + \pi\beta_2\rho_{s_1s_2}\rho_{i_2} + (1-\pi)\mu_1\rho_{i_1i_2} - \pi\mu_2\rho_{s_1i_2} \quad (3.12)$$

$$\frac{d\rho_{i_1s_2}}{dt} = +(1-\pi)\beta_1\rho_{s_1s_2}\rho_{i_1} - \pi\Gamma_2\beta_2\rho_{i_1s_2}\rho_{i_2} - (1-\pi)\mu_1\rho_{i_1s_2} + \pi\mu_2\rho_{i_1i_2} \quad (3.13)$$

$$\frac{d\rho_{i_1i_2}}{dt} = +(1-\pi)\Gamma_1\beta_1\rho_{s_1i_2}\rho_{i_1} + \pi\Gamma_2\beta_2\rho_{i_1s_2}\rho_{i_2} - (1-\pi)\mu_1\rho_{i_1i_2} - \pi\mu_2\rho_{i_1i_2}. \quad (3.14)$$

The densities are yet subject to the normalization constraint $\rho_{s_1s_2}+\rho_{s_1i_2}+\rho_{i_1s_2}+\rho_{i_1i_2} = 1$. This constraint makes the system effectively three-dimensional. One can reduce the number of equations and simplify the notation by using the following variable change (as done in[88]):

$$\begin{cases} u = \rho_{i_1} = \rho_{i_1s_2} + \rho_{i_1i_2}, \\ v = \rho_{i_2} = \rho_{s_1i_2} + \rho_{i_1i_2}, \\ w = \rho_{i_1i_2}. \end{cases} \quad (3.15)$$

For which the dynamical equations are:

$$\dot{u} = (1-\pi)\left[\beta_1(1-u) + (\Gamma_1 - 1)\beta_1(v-w) - \right. \\ \left. -\mu_1\right] u \quad (3.16)$$

$$\dot{v} = \pi\left[\beta_2(1-v) + (\Gamma_2 - 1)\beta_2(u-w) - \mu_2\right] v \quad (3.17)$$

$$\dot{w} = (1-\pi)\left[\Gamma_1\beta_1(v-w)u - \mu_1 w\right] + \\ +\pi\left[\Gamma_2\beta_2(u-w)v - \mu_2 w\right]. \quad (3.18)$$

3.3.1.2 Model B: competing diseases with superinfection

Model B constitutes a modification of models of competing strains, in which a host cannot have the two diseases at the same time. This could be achieved from model A by setting $\Gamma_1 = \Gamma_2 = 0$. However, we also allow the in-host disease replacement via superinfection: if an individual infected by disease I contacts another one infected by disease II, the first can also become infected by disease II, which immediately replaces disease I in the host. The other way around, from disease II to I, is not possible. Superinfection is a phenomenon that is claimed to occur for some diseases such as HIV[188–190] and bacterial pathogens,[191] although it does not necessarily leads to in-host replacement of the first infection. There is a considerable amount of works about epidemic models with superinfection, both with homogeneous populations[192–195] and complex networks[145–147] and including other realistic aspects such as demography. Beyond epidemiological examples, the present model could abstract the interaction between computer viruses and the spreading of anti-malware, or the dynamics of fake news and fact-checking

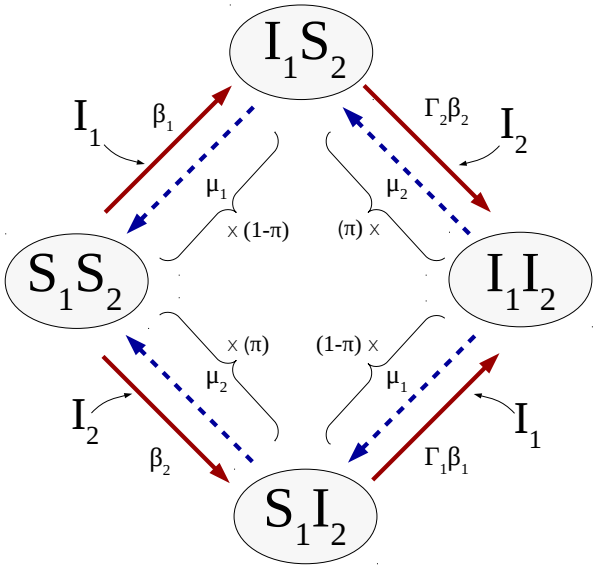

Figure 17 – State transitions allowed in model A. The baseline infection and healing rates of disease I (II) are respectively β_1 (β_2) and μ_1 (μ_2). Γ_1 (Γ_2) represents the modification to the baseline transmission rate of of disease I (II) due to the presence of the other disease in the host. Besides, each rate is multiplied by its corresponding time scale factor: $1 - \pi$ for processes of disease I and π for disease II.

Source: VENTURA *et al.*[90]

messages. In such scenarios, either the anti-malware or the fact-checked message replaces the previous "infectious agent". We also note that our model is a particular case of the model discussed in,[147] and can also be interpreted as a generalized predator-prey model.[196]

Specifically, in model B, we represent susceptible individuals simply by S, and infected individuals of diseases I and II, respectively, by I_1 and I_2. The transmission rates are β_1 and β_2, the healing rates are μ_1 and μ_2, and the rate at which I_1 individuals are “superinfected” by disease II when exposed to I_2 individuals is given by a modified term $\alpha \cdot \beta_2$. As in model A, each term is also multiplied by the corresponding time scale factor ($(1 - \pi)$ for disease I and π for disease II), and also $\lambda_1 = \beta_1/\mu_1$ and $\lambda_2 = \beta_2/\mu_2$ are the basic reproduction numbers of the independent diseases. The transitions are schematically represented in Figure 18. Despite the competitive aspect of the model, one can generate an asymmetrical interaction by setting $\alpha > 1$. This is because I_1 individuals, in this case, are more easily infected by disease II than susceptible ones, meaning that the spreading of disease II is enhanced by the presence of disease I, which in turn is in disadvantage due to the competition with disease II.

Using the same notation as before, ρ_x, for the density of individuals in state X, we write the dynamical equations:

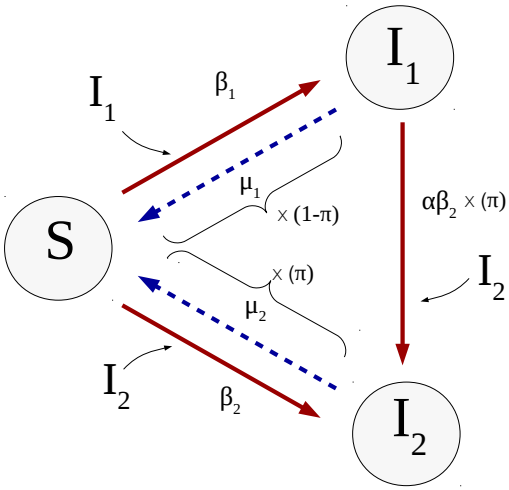

Figure 18 – State transitions of model B. Infection and healing rates of disease I (II) are respectively β_1 (β_2) and μ_1 (μ_2). I_1 individuals can be (super)infected by disease II with rate $\alpha\beta_2$. Each rate is multiplied by its corresponding time scale factor: $1-\pi$ for disease I processes and π for disease II processes.

Source: VENTURA *et al.*[90]

$$\frac{d\rho_s}{dt} = -(1-\pi)\beta_1\rho_s\rho_{i_1} - \pi\beta_2\rho_s\rho_{i_2} + (1-\pi)\mu_1\rho_{i_1} + \pi\mu_2\rho_s r \tag{3.19}$$

$$\frac{d\rho_{i_1}}{dt} = (1-\pi)\beta_1\rho_s\rho_{i_1} - \pi\alpha\beta_2\rho_{i_1}\rho_{i_2} - (1-\pi)\mu_1\rho_{i_1} \tag{3.20}$$

$$\frac{d\rho_{i_2}}{dt} = \pi\beta_2\rho_s\rho_{i_2} + \pi\alpha\beta_2\rho_{i_1}\rho_{i_2} - \pi\mu_2\rho_{i_2}, \tag{3.21}$$

where the normalization constraint is $\rho_s + \rho_{i_1} + \rho_{i_2} = 1$. As in model A, we make the change of variables $u = \rho_{i_1}$, $v = \rho_{i_2}$ to obtain the reduced set of dynamical equations:

$$\dot{u} = (1-\pi)\,[\beta_1(1-u-v) - \mu_1]u - \pi\alpha\beta_2 uv \tag{3.22}$$

$$\dot{v} = \pi[\,\beta_2(1-u-v) - \mu_2]v + \pi\alpha\beta_2 u\,v. \tag{3.23}$$

3.3.2 Results

3.3.2.1 Phase diagrams

In the asymmetrically interacting regime, models A and B share a common feature: for any given set of parameters, there is exactly one stable fixed point within the region of the phase portrait that corresponds to physically possible solutions. Therefore, unlike what has

been reported for mutually competitive or cooperative scenarios,[88,192] our models do not present bistability [†]. This in intrinsic to the positive-negative feedback of the asymmetric interaction between the diseases. Both models A and B present four phases, separated by transcritical bifurcations: (P1) no disease, (P2) disease I only, (P3) disease II only and (P4) coexistence of both diseases. Here, we investigate the $\lambda_1 \times \lambda_2$ phase diagrams, setting the other parameters to fixed values. Figure 19 shows the phase diagrams for both models.

Through a stability analysis, described in Section B.1 of appendix B, we can obtain the phase transition curves of both models. The boundary between phases (P2) and (P4) in model A is expressed as:

$$\frac{1}{\lambda_2} = 1 + (\Gamma_2 - 1)\left(1 - \frac{1}{\lambda_1}\right), \quad \lambda_1 > 1, \tag{3.24}$$

whereas, by the symmetry of the model, the boundary between phases (P3) and (P4) is given by:

$$\frac{1}{\lambda_1} = 1 - (1 - \Gamma_1)\left(1 - \frac{1}{\lambda_2}\right), \quad \lambda_2 > 1. \tag{3.25}$$

From the Equation 3.25, we can check that, when $\Gamma_1 = 1$ (i.e., no interaction), the boundary between phases (P3) and (P4) are separated by a vertical line. On the other limit, for $\Gamma_1 = 0$, the boundary becomes the identity line $\lambda_1 = \lambda_2$.

The other two bifurcations are trivial and are given by $\lambda_2 = 1$ for $0 \leq \lambda_1 \leq 1$ (boundary between (P1) and (P3)) and $\lambda_1 = 1$ for $0 \leq \lambda_2 \leq 1$ ((P1) and (P2)). It is worth noticing that, for model A, none of the phase transition curves depends on the time scale parameter π.

The phase transition curves have similar shapes to those reported in other works using single layer[150] and multiplex[1] networks, which shows that such feature is essential to the model itself. It can also be shown that the transition curves between (P1) and (P2) and between (P3) and (P4) are equivalent to the curve between healthy and endemic phases in a model for epidemics with awareness.[172]

For model B, the boundary between (P2) and (P4) is given by:

$$\frac{1}{\lambda_2} = 1 + (\alpha - 1)\left(1 - \frac{1}{\lambda_1}\right), \quad \lambda_1 > 1, \tag{3.26}$$

which is similar to that in Equation 3.24, only replacing Γ_2 by α. The boundary between (P3) and (P4) is expressed as:

$$\lambda_1 = [\alpha\chi(\lambda_2 - 1) + 1]\,\lambda_2, \quad \lambda_2 > 1, \tag{3.27}$$

[†] For model B, it can be shown that the bistability condition given by Wu and collaborators in[147] cannot be met when $\alpha > 1$, which is our case.

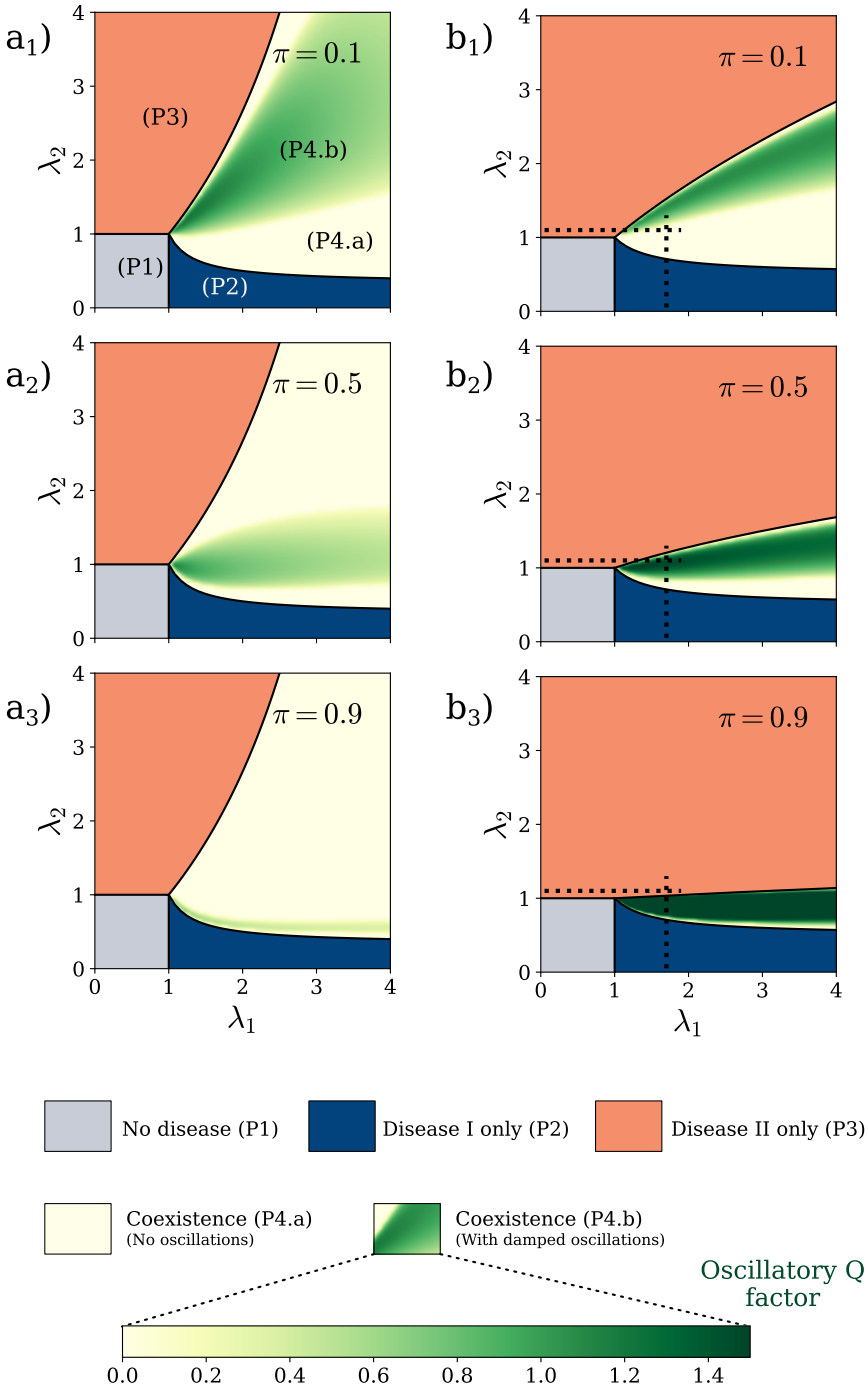

Figure 19 – Phase diagrams of models A (a_1 to a_3) and B (b_1 to b_3), for three different values of the time scale parameter π. The phases are (P1) no disease, (P2) disease I only, (P3) disease II only and (P4) coexistence. For model B, the dotted lines indicate the (λ_1, λ_2) values used in Figure 20. Inside the coexistence region, there is also the possibility of damped oscillations, quantified by the Q factor defined in Equation 3.28 and exhibited here as a green scale. The points of the oscillatory region mesh are calculated in steps of ≈ 0.033 units in λ_1 and λ_2, then smoothed with bicubic interpolation. Other parameters are set to: $\Gamma_1 = 0.20$, $\Gamma_2 = 3.0$ and $\alpha = 2.0$.

Source: VENTURA *et al.*[90]

where we define χ (interpreted as the time scale ratio between diseases II and I) as:

$$\chi = \frac{\pi\mu_2}{(1-\pi)\mu_1}.$$

The trivial boundaries of region (P1) with regions (P2) and (P3) are the same as in model A. Notice, however, that the parameter χ depends increasingly on the time scale parameter π, and so does the critical λ_1 value from Equation 3.27. This means that, as π increases (i.e., when disease II propagates on shorter time scales), the phase transition between (P3) and (P4) moves to lower values of λ_2, contracting the region of coexistence and approaching the horizontal line $\lambda_2 = 1$ as $\pi \to 1$ (notice that χ diverges). Therefore, in this model, a faster clock for disease II makes it more effective to suppress disease I. This is an interesting result that might be used to control the prevalence of disease (or any other "infectious agent") in the host population. In the limit of $\pi \to 0$, the transition between (P3) and (P4) becomes the identity line $\lambda_1 = \lambda_2$. The π-dependence of the phase diagrams of model B constitutes an important difference with respect to model A, and was already reported by Wu and collaborators[147] as a dependency on the recovery rate when keeping the ratios β/μ constant.

The reason for such difference in model B is the existence of superinfection, which is a process of disease II that modifies the state of an individual for both diseases. In contrast, for model A, the processes of a given disease can only change its own states, making the relative time scale irrelevant near the phase transitions.

3.3.2.2 Behavior of the stationary prevalence

We now discuss how the stationary prevalence behaves with some of the parameters of the models, including the relative time scale π, which will allow us to do a comparison with the results from Section 3.2.

In the phase of coexistence (region (P4) of the phase diagrams), both models present a single stable fixed point, for which $u, v \neq 0$. One can use the dynamical equations (Equations 3.16 to 3.18 for model A and 3.22 and 3.23 for model B) to derive analytical expressions for the prevalences at the coexistence fixed point. The derivation and the final expressions are shown in Section B.2 of Appendix B. As expected, the stationary prevalence of each disease is a non-decreasing function of its reproduction ratio $\lambda = \beta/\mu$, when considering other parameters as fixed. However, the dependence of the prevalences with the relative time scale parameter π is not trivial, and is different in each model.

Figure 20 shows the basic behavior of the fixed point prevalences with π for models A and B. While the prevalence v of disease II decreases with π for both models, the prevalence u of disease I has opposite behaviors in each of them. In model A, the prevalence w of coinfection increases with π. This variant shows the same behavior (if equating disease II with the information) as reported in our works with epidemics and awareness[182,186] and by Wang and collaborators[187] in complex networks, namely, a faster relative clock of the information induces

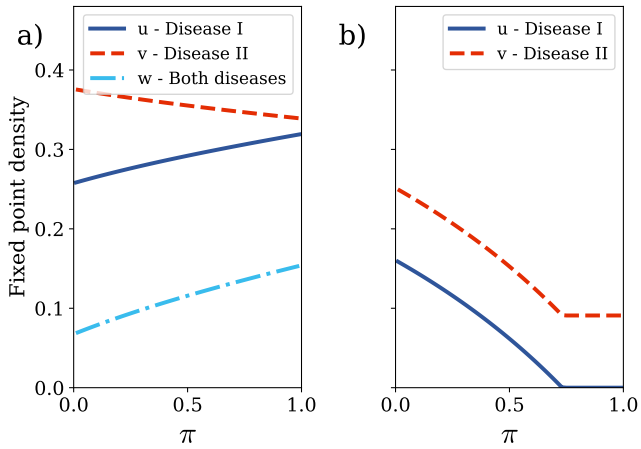

Figure 20 – Stationary values of the prevalences as a function of π for (a) model A and (b) model B. For both models, λ_1 and λ_2 are respectively set to 1.7 and 1.1. Other parameters are set to $\Gamma_1 = 0.5$, $\Gamma_2 = 2.5$ in (a) and $\alpha = 2.0$ in (b).

Source: VENTURA *et al.*[90]

an increase on the disease prevalence. For model B, however, the behavior is the opposite: the prevalence of disease I decreases with π. Considering also how the time scale parameter distorts the phase diagram of model B (see Figure 19, where the (λ_1, λ_2) values used in Figure 20 are indicated by dotted lines), we see that a faster clock of the "predator" process (disease II) effectively decreases the spreading of the "prey" process, leading to its extinction if $\lambda_2 > 1$ and for sufficiently large π. Therefore, the relationship between the prevalences and the relative time scale in asymmetrically interacting spreading phenomena is a feature that depends on the specific shape of the considered model.

In Figures 21 and 22, we further analyze the behavior of the prevalences with π and the parameters that control the interactions: Γ_1, Γ_2 for model A and α for model B. We first notice that the increasing or decreasing trends with respect to π, as observed in Figure 20, are not changed for different values of the interaction parameters: disease I increases while disease II decreases with π for model A (Figure 21), whereas both prevalences decrease with π for model B (Figure 22). To rule out the possibility that there is a region of the parameter space in which the reported behaviors with respect to π might be different, we show in Section B.3 of Appendix B that this is not possible, i.e., that the behavior with π is always the same for each model in the coexistence region.

We can also analyze how the prevalences vary with changes in the interaction parameters. For model A (Figure 21), we see that an increase in Γ_1 increases both the prevalences of disease I (a) and II (b). This is expected, as a greater Γ_1 value means a weaker impairing to the propagation of disease I, which is beneficial for both diseases (as disease II benefits from disease I). On the other hand, an increase in Γ_2 causes a decrease in disease I (c) and an increase

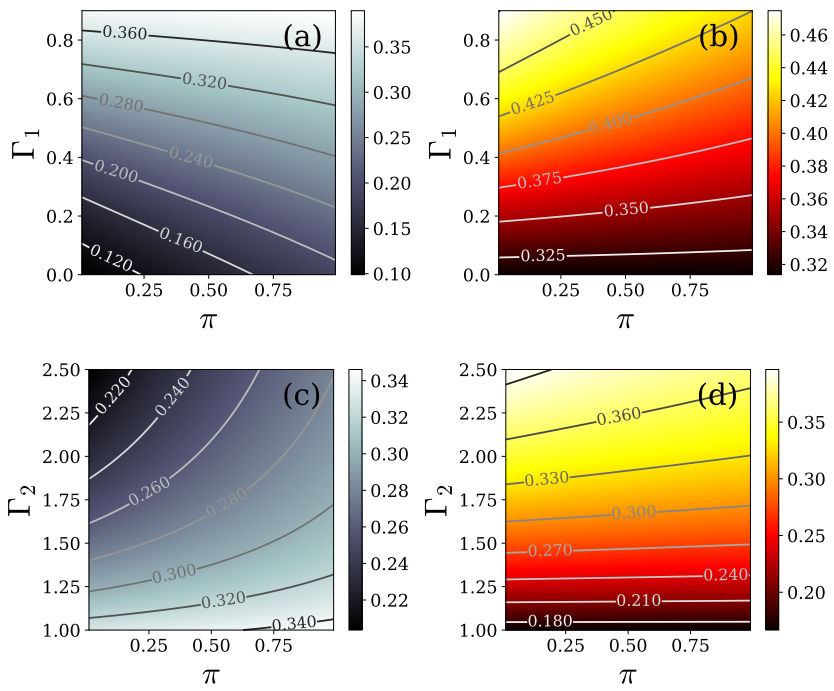

Figure 21 – Values of the stationary prevalences of disease I ((a) and (c)) and disease II ((b) and (d)) for model A, plotted as functions of π, Γ_1 and Γ_2. In (a) and (b), Γ_2 is fixed to 2.5, whereas in (c) and (d) Γ_1 is fixed to 0.4. The reproduction ratios are set to $\lambda_1 = 1.70$ and $\lambda_2 = 1.2$.

Source: VENTURA *et al.*[90]

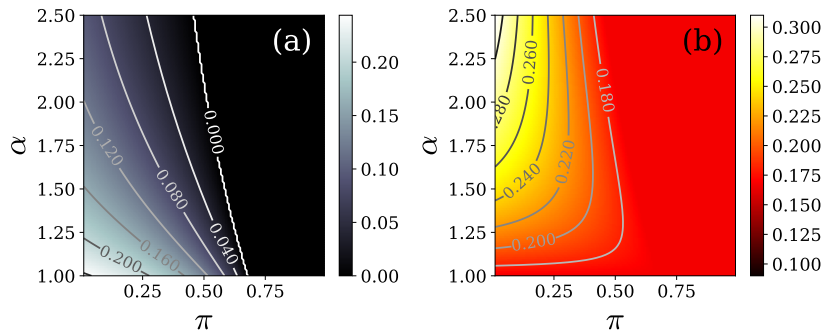

Figure 22 – Stationary prevalences of (a) disease I and (b) disease II for model B, plotted as functions of π and α. The dashed line shows the position of the prevalence peaks. The reproduction ratios are set to $\lambda_1 = 1.7$ and $\lambda_2 = 1.2$.

Source: VENTURA *et al.*[90]

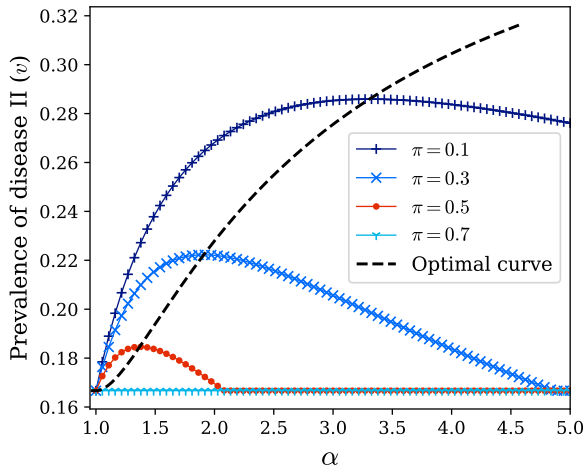

Figure 23 – Stationary prevalences of disease II for model B, plotted as a function of and α and for different values of π. The dashed line represents the optimal value of α and its corresponding v as π is continuously changed. The other parameters are set to $\beta_1 = 1.7$, $\beta_2 = 1.2$ and $\mu_1 = \mu_2 = 1$.

Source: VENTURA *et al.*[90]

in disease II (d). This is also expected, as a larger value of Γ_2 means a greater benefit to disease II, which in turn is detrimental to disease I. Therefore, for model A, the effect of the two interaction parameters in each disease's prevalence is intuitive and predictable. The effects are also numerically influenced by the time scale π, yet not qualitatively changed.

However, for model B, which has a single interaction parameter α, the behavior of the prevalence is not trivial. From Figure 22, we see that, while disease I prevalence (a) is always reduced with an increase in α, the behavior of the prevalence of disease II (b) with α is not uniform, and may have an optimal value that depends on π. This happens because the superinfection transition, controlled by α, is simultaneously beneficial to disease II and detrimental to disease I. Thus, as seen from model A, an increase in α certainly reduces the prevalence of disease I, but has a "conflicting" effect to the prevalence of disease II. While a value of α close to 1 means almost no benefit to disease II from disease I, a large value $\alpha \gg 1$ means an excessive "predation" from disease II, therefore existing an optimal intensity of the interaction α. This is further illustrated in Figure 23, where we show the prevalence of disease II in model B as a function of α, for different values of π. As it can be seen, there is an optimal value of α that maximizes the prevalence, for fixed values of the other parameters.

3.3.3 Damped oscillations: node *vs* spiral point

Some predator-prey systems, which naturally have an asymmetrical relationship between two processes, are known to present stable closed orbits (i.e., sustained oscillations).[196] For both epidemic models addressed in our work, there are no closed orbits in the physical re-

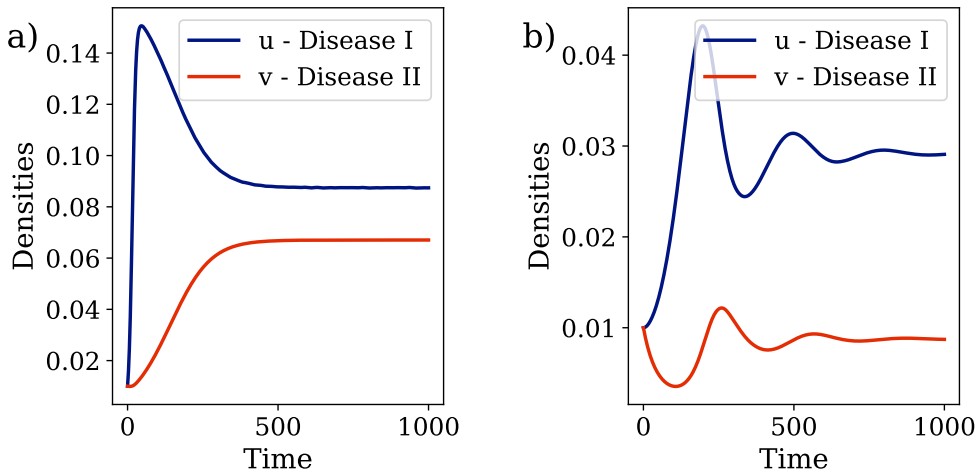

Figure 24 – Time evolution of model B prevalences for two different conditions: (left) $\pi = 0.1$, for which $Q = 0$, meaning that there are no local oscillations around the fixed point, and (right) $\pi = 0.9$, for which $Q = 3.65$ and the system oscillates before converging to the steady state. Other parameters are set to: $\beta_1 = 1.20$, $\beta_2 = 0.98$, $\mu_1 = \mu_2 = 1.0$ and $\alpha = 2.0$. The initial fraction of infected individuals is set to 0.01 for both diseases.

Source: VENTURA *et al.*[90]

gion of the phase portrait [‡]. However, in the coexistence phase (region (P4) of Figure 19), the stable fixed point can be either a node or a spiral point. In the second case, the transient dynamics of the system towards the fixed point may present some damped oscillations. The presence of such local oscillations is determined by the imaginary part of the eigenvalues of the model's Jacobian matrix, calculated at the stable fixed point. For model B, which is two-dimensional, the Jacobian's eigenvalues σ_1, σ_2 can either be both real or complex conjugate to each other. For model A, which is three-dimensional, the 3x3 Jacobian matrix can either have none or two non-real conjugate eigenvalues. For both models A and B, one can use the quantity:

$$Q = \max_{i=1,\,\ldots,d} \left(\left| \frac{\mathrm{Im}(\sigma_i)}{\mathrm{Re}(\sigma_i)} \right| \right), \tag{3.28}$$

to measure the "quality factor" of the oscillations when $\mathrm{Re}(\sigma_i) \neq 0$ ($\{\sigma_i\}$ are the eigenvalues of the Jacobian at the fixed point, d is the dimensionality of the system). This is because the imaginary part is responsible for the oscillations, and the real part for the damping, thus the imaginary-to-real part ratio measures the propensity of the system to oscillate around the fixed point.

In Figure 19, together with the regular phases of the model, we show in (color-coded) green the numerically calculated values of Q. The coexistence phase can thus be subdivided ac-

‡ This can be proven, for model B, using Dulac's criterion, as done in.[196]

cording to the existence of a non-real Jacobian eigenvalue: within the white regions, the eigenvalues are real and the fixed point is a node whereas in the green areas, the fixed point is a spiral point and there may occur oscillations around it. Notice that, for both models A and B, the shape of the spiral point region depends considerably on the time scale parameter π. Greater values of π seem to shrink the oscillatory region and reduce the values of Q for model A, but the opposite appears to happen with model B. Furthermore, we show the difference between a node and a spiral point in Figure 24, in which the time evolution of the prevalences of model B is shown for two situations: one with $Q = 0$ (hence no local oscillations (left)), and another with $Q = 3.65$ (thus there are damped oscillations before reaching the steady state). Interestingly, we only had to change the relative time scale parameter π to switch between the two situations.

An important fact is that damped oscillations can only occur when the interaction between the diseases is asymmetrical, for both models A and B. For model A, we numerically check this by observing that the oscillatory region of the phase diagram shrinks and disappears as Γ_1 or Γ_2 leaves the region for which interactions are asymmetric. For model B, it can be shown that the Jacobian's eigenvalue equation (which is quadratic) can only assume non-real solutions if $\alpha > 1$. Finally, we note that despite that our deterministic formulation predicts that the oscillations are always damped, stochasticity - which is intrinsic to real-world systems, and are inherent when performing Monte Carlo simulations - could cause such oscillations to last for the long term, as small perturbations to the prevalences could recover the oscillatory pattern.

3.3.4 Discussion

In the work presented in this section, we have studied two minimalist models for interacting diseases in the asymmetrical regime, for homogeneously mixed populations and with continuous-time evolution. We focus on the influence of the relative time scale between the two diseases. The simplicity of our framework not only provides us with analytical tractability, but also reveals the fundamental properties of asymmetrically interacting contagion. The models are simple enough to be applied to different situations, and the choice for two models is justified by our goal of achieving a more general understanding about interacting processes.

In their asymmetrical interacting regime, Model A is a mathematical prototype for epidemic with awareness, as well as the possibly asymmetrical interaction between HIV and some specific diseases,[121–123] while Model B is inspired in situations such as computer viruses and spreading countermeasures[148, 197–199] or fake *vs* fact-checked news.

We have unveiled some interesting dynamical features of these models: their phase diagrams with respect to the disease transmission rates, the behavior of the stationary prevalences upon changes in the interaction strength and the relative time scale, and the transient oscillatory behavior, which interestingly appears only in a sub-region of the coexistence phase. Moreover for Model B, which has a single parameter (α) that controls the intensity of the interaction, we show that the prevalence of disease II reaches a maximum for a given value of the interac-

tion strength. This value depends on the relative time scale (here controlled by π), and so does the oscillatory region, the stationary prevalences and the shape of Model B's phase diagram. This leaves a message for current and future works on interacting diseases: the time scale ratio between the process can play an important role, and should not always be set to 1.

In the context of our research, this work clarified some important points. The increase on the prevalence when the time scale of the information spreading was shorter, reported in Section 3.2, was reproduced in Model A, which has a similar mathematical structure, and with an unstructured population (homogeneously mixed). Despite not being a conclusive evidence, this suggests that such behavior is expected when the asymmetric interaction occurs by making individuals infected with one disease to change their susceptibility to the other. Also in this case, the phase boundaries do not depend on the time scale, as seen from Figure 19. However, Model B did not reproduce this behavior, as both prevalences decrease when the predator process spreads in a shorter time scale. This seems to rely on the shape of the interaction, which occurs by directly transferring I1 individuals into the I2 compartment, though we still do not fully understand the reason behind this. Nonetheless, this leaves an important message with respect to our first work: before extrapolating its conclusions to real systems, we should check if real world interaction between disease and information happens via change in susceptibility – which seems a good assumption – and, moreover, if the interference of other aspects of reality would not break this behavior.

4 EPIDEMIC SPREADING WITH HOST MOBILITY

Starting in the year of 1346, an unprecedentedly lethal pandemic of bubonic plague took place in Afro-Eurasia. Known as the *Black Death*, it is attributed to the bacterium *Yersinia pestis*, transmitted primarily by fleas that live on black rats. With an estimated toll of 75 to 200 millions of deaths, it was the first in a series of events known as the "Second plague pandemic", with recurrent outbreaks from the 14th to the 18th centuries.

The Black Death is thought to have originated in Asia and spread to Europe and Africa by ships, which were frequently infested by rats. Although black rats and the rat flea, carried inside ships, were the main source of primary infections in Europe, it could not explain the rapid continental spread of the plague, due to the considerably slow movement of the rats, as well as the low activity of fleas during the winter in northern regions. As explained in ,[200] contemporary evidence shows that the strain responsible to the black death has a strong tendency to produce a pneumonic manifestation of the plague, by which patients with compromised lungs cause person-to-person transmission via droplets, enabling the spread by terrestrial travel. It is also considered that human flea, besides the rat flea, could have driven the pandemics inland.[201] Therefore, human mobility flows by terrestrial paths are the only explanation for the fast continental spread. Figure 25 shows a map of the year in which the first outbreak was reported in each region of Europe, northern Africa and western Asia. Black arrows show the possible routes of primary infections via ships. We see that, despite the early cases were concentrated on cities reached by marine routes, there was a rapid continental spread of the plague.

The Black Death is an example of how the knowledge about human and animal mobility can be crucial to understand the dynamics of an epidemics. The mechanisms of the Black Death pandemic can be further studied with the use of modern methodology, such as network theory and data about pilgrimage and commercial routes from the 14th century.[203]

While the spread of the Black Death was considered fast for that age, reaching the whole European continent during five years, contemporary epidemics can reach worldwide dimensions in a much shorter time. Demographic and mobility patterns substantially changed since the Middle Age, with travels between diametrically opposed points of the globe being possible within less then a 24 hours period, and urban settlements reaching tenths of million inhabitants. Availability of massive data is also a reality,[204] especially during the digital revolution of the 21st century. The currently fast socioeconomic evolution drives constant changes in human mobility patterns that cannot be neglected.[205]

In this chapter, we discuss the relationship between mobility and epidemic spread through the eyes of contemporary scientific methods. In the literature review (Section 4.1), we show how computational and mathematical tools can be used to model and understand patterns of

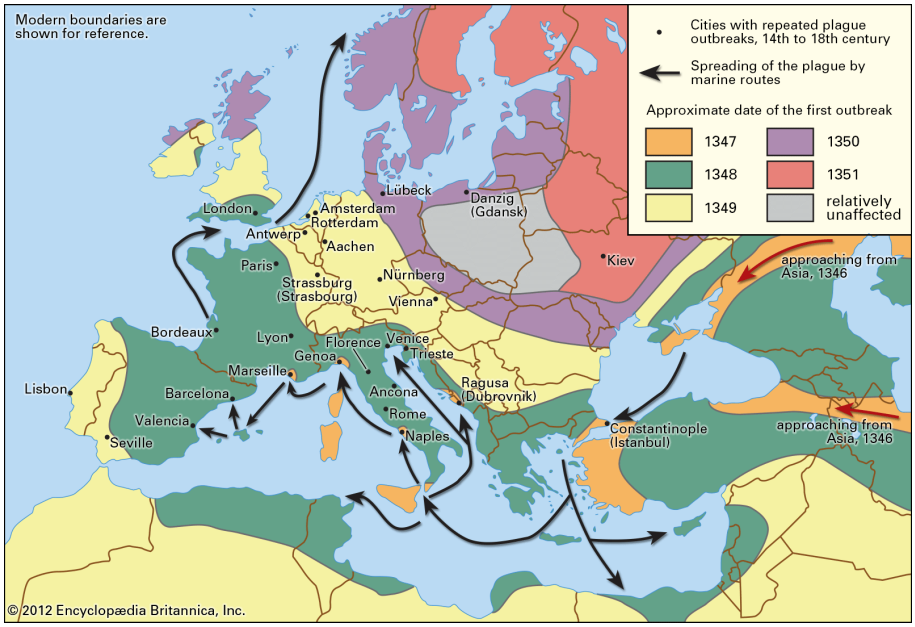

Figure 25 – Spreading of the Black Death in Europe between 1347 and 1351, which took a proportionately greater toll of life than any other known epidemic or war up to that time. The Black Death is widely thought to have been the result of a plague, caused by infection with the bacterium *Yersinia pestis*. The color of each region represents the approximate year in which the first outbreak was registered, while arrows indicate possible routes of the plague by marine navigation.

Source: ENCYCLOPEDIA BRITANNICA[202]

human and animal mobility, and present applications to epidemic modeling on metapopulations and agent-based mobility models. In the following sections (4.2 and 4.3), we present two of our contributions to the topic. A model that incorporates social distancing behaviors into an agent-based random walk model is presented in Section 4.2. Collective behavioral responses (including but not restricted to social distancing) are incorporated into an epidemic model for metapopulations, which we describe in Section 4.3.

4.1 Literature review

4.1.1 Mobility models and data

Early attempts to describe human mobility, or more specifically migration flows, date back to the end of the 19th century, when the German-English geographer Ernst Georg Ravenstein stated some laws to describe the intensity of human migration between geographic regions depending on their distances, as well as social aspects of the migrating population.[206] His laws were purely observational and defined by sentences, thus not consisting a mathematical formulation. A simple attempt to give a quantitative description of human mobility was made by Zipf in 1946,[207] who tested the hypothesis that the number of people that move between two connected cities is directly proportional to their populations and inversely proportional to the

distance between them. This hypotheses is known as the *gravity model*, due to its similarity with Newton's gravitation law.[208–209] It became a standard framework to fit real data on traffic, daily commuting migration and overall mobility between cities,[210–211] as well as trade flows.[212–214] Among these applications, it is common to use more general expressions for the gravity model, in the shape[215]:

$$T_{ij} = \frac{m_i m_j}{f(r_{ij})}, \tag{4.1}$$

Where T_{ij} is the flow (traffic, trade, etc.) between communities i and j, m_i and m_j are respectively the populations of i and j, and $f(r_{ij})$ is some increasing function of the distance r_{ij} between i and j.

Despite its popularity, the gravity model has several limitations, being unable to explain some large discrepancies on the flows between similar pairs of cities (regarding population and physical distance). It also has analytical issues, for example allowing the flow between two cities to be greater than the population of the smaller one, besides lacking a derivation from empirical principles. In 2012, Simini and others[215] proposed an alternative to the gravity model, based on the case of daily commuting between locations. They start from a stochastic process, in which workers choose jobs with a preference to those that are closer to their home, to derive an expression for the flux T_{ij} from location i to j:

$$T_{ij} = T_i \frac{m_i m_j}{(m_i + s_{ij})(m_i + m_j + s_{ij})}, \tag{4.2}$$

Where T_i is the total outbound flux from i, m_i and m_j are the populations of i and j respectively, and s_{ij} is the total population in the circle that is centered at community i and has a radius r_{ij} (the distance between the communities), excluding the populations of i and j. The term s_{ij} comes from the process of choosing jobs, thus being more well founded in an empirical feature than the gravity model. As it is designed for the commuting between locations, T_{ij} is not necessarily equals to T_{ji}. The authors named this as the *radiation model*, which has been widely used since its proposal.[216–217]

Another fundamental model, created by Stouffer[218] but more well known as the version made by Schneider,[219] considers that human displacements are proportional to the *intervening opportunities* between the origin and destination. In Schneider's formulation, the probability that a trip ends in a given location is equal to the probability that this location has an acceptable opportunity times the probability that an opportunity in another location closer to the origin of the trips has not been chosen yet. The meaning of "opportunities" is chosen according to the type of mobility in question, but is often assumed to be proportional to the population of the region.

A different approach to describe human mobility between cities is to use machine learn-

ing and statistical methods instead of phenomenological models. Spadon and others[220] propose such an approach by using machine learning and link prediction algorithms to reconstruct the network of daily commuters between cities, using data from the *Brazilian Institute of Geography and Statistics* (IBGE). To feed the model, they use not only the population of each city and the distances between them, but also other 21 urban indicators such as *Gross Domestic Product* (GDP), sanitation and criminality. They show that, besides distance and population, GDP and unemployment rate play a central role on determining the human daily flows between cities, and reconstruct the real network with 90.40% of accuracy.

For some applications, it is necessary to describe not just the net flows of individuals between locations, but also the actual mobility of each individual. This can be accomplished with agent-based mobility models, often in the form of modified random walks.[221] These can be classified regarding the discreteness of time, space and the spatial steps, as well as the existence of correlations between consecutive steps and directional biases.[216]

Uncorrelated and unbiased random walks are simple to implement, and somehow plausible to analytical description.[222] They have been used for the dispersal of species in synthetic ecosystems, and more recently for epidemic spreading.[4] One such random walk can be constructed as follows: at each of a series of discrete time steps, an agent performs a spatial step in a two-dimensional continuous space (a subregion of $\mathbb{R}^2$) with fixed length d, and a uniformly random angle $\theta \in [0, 2\pi)$. Another example is the simple diffusion process, which is a version of the simple random walk with continuous time and space, and has been used for epidemic spreading models too (reaction-diffusion process).[223–224] Due to the simple implementation, these random walks are suitable for fundamental applications that need to incorporate individual mobility in some form. However, it is known that both human and animal mobility have features that are far from those produced by a simple uncorrelated random walk.[225]

One simple and very popular extension to the simple uncorrelated random walk is known as the *Levy flights*. A Levy flight consists of an unbiased random walk with random step sizes, whose distribution is given by a negative-exponent power law. This long-tailed distribution implies that most steps will be short, but a few ones will be long-ranged, displacing the agent from the surroundings in which it was before. This still configures an uncorrelated random walk, in the sense that consecutive steps are statistically independent. Levy flights were used to fit real mobility data of animal motion for several different species,[226–229] as well as for humans when foraging for resources.[230] Indeed, there is a hypothesis stating that Levy flights optimize the search for resources in space,[231] thus species naturally develop Levy flight patterns.[232]

However, more recently and with larger availability of data, the validity of the Levy flight hypothesis was questioned. In a revisit of animal motion patterns with higher quality data, Edwards and others[233] argue that the flight times are gamma-distributed with an exponential cutoff for very long times. By revisiting the original data on albatross flights[226] (which originally triggered further works on Levy flights), they also argue that the long-distance jumps

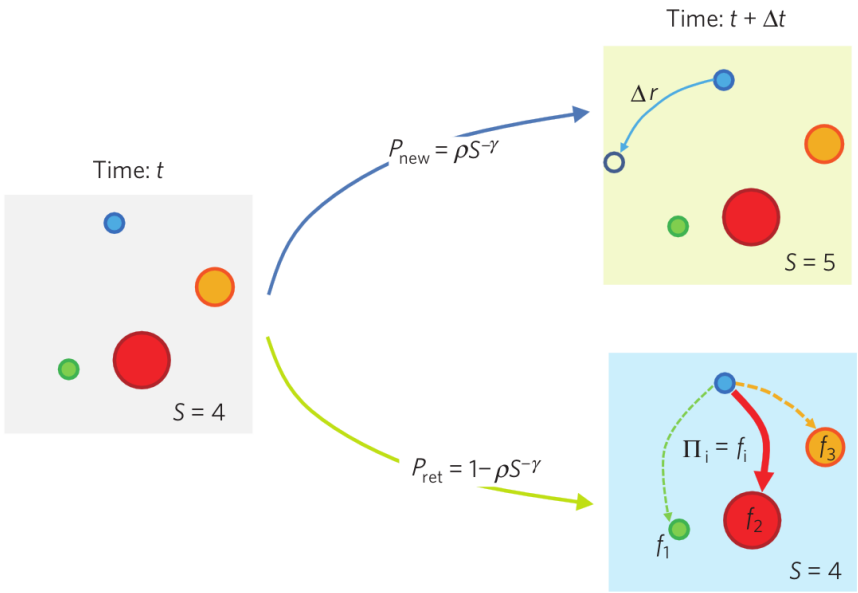

Figure 26 – The exploration and preferential return mobility model, proposed by Song and others[3] In the left, an agent has visited S=4 different locations up to time t, with frequencies given by the sizes of the circles. For time $t + \Delta t$, the agent may either choose to visit a new location (upper square) at a random distance Δr drawn from a fat-tailed distribution, or to move to a previously visited location (lower square), chosen proportionally to the current frequency of visits.

Source: SONG *et al.*[3]

were spurious. Other recent works[234–236] claim that the optimal foraging has no relationship with Levy flights, including an analytical study[236] showing that Levy flights are typically not the optimal strategies for spatial dimensions $d > 2$. Nonetheless, other recent works show supportive evidence for the Levy flights in nature and human behavior,[237–238] thus making Levy flights and their applications a current topic of controversy between researchers.

Enhancements to the basic random walk models are often proposed by the community, specially as real mobility data becomes more available. Song and others[3] considered the fact that humans tend to revisit common locations (such as home, workplaces, etc.) instead of simply wandering at random, a claim that is backed up by mobile-phone users' data. They propose a correlated and biased random walk model, with two main features: (a) *preferential return*, meaning that agents have a chance to return to previously visited locations at each move, and (b) *exploration*, by which agents can forage new locations, with probability complementary to the preferential return. The distance distribution during an exploration step has a fat-tailed distribution, akin to Levy flights. Their model is represented in Figure 26. Within this framework, they could not only reproduce scaling laws from the empirical data, but also analytically derive most of the scaling exponents.

Another enhanced random walk mobility model was proposed by Starnini and others[70]

They had access to multiple datasets of the SocioPatterns collaboration,[71] which collected time resolved proximity data between human individuals in different contexts such a school, a hospital and a scientific conference. Their model accounts for the fact that people's interactions are heterogeneous, and that individuals do not interact with others all the time. Each agent of their model has a *social attractiveness* score ($0 \leq a \leq 1$), which influences other's mobility around them. An agent may temporarily stop its motion around other agents, with probability proportional to the most "attractive" of its neighbors. Each agent also has an *activity* score, meaning that lower scored agents spend less time engaged on the mobility and interaction activities. Otherwise, spatial steps are performed as a simple two-dimensional random walk. The authors successfully reproduced scaling laws for the duration of peer interactions and the time interval between consecutive interactions, showing also that the simple unbiased random walk fails to reproduce these laws.

4.1.2 Epidemic spreading with agent-based mobility models

From the works reviewed in Section 4.1.1, we should be convinced that important features can be obtained from random walk-based mobility models. Although the basic random walk must be adapted to produce realistic results, it is still a good starting point to study epidemic spreading on temporal networks driven by agents. In this section, we review works on this topic, paving the way to later explain our contribution.

Agent-based mobility models were not popular for epidemic modeling up to the 21st century. An early example was presented by Gonzales and Herrmann,[239] who described a simple SIS disease spreading among agents that move with molecular dynamics. The particles (agents) move in a 2D square space with periodic bounds, following Newtonian motion and interacting with a Lennard-Jones potential. The authors show the time series of disease prevalence as a function of different parameters, such as particle density and temperature (which determines the average speed). They also compare their model with a simple mean field formulation, showing some scaling laws. The framework proposed in this work was not much recurrent over the following years, but it can be considered as a precursor for agent-based epidemic modeling with mobility.

A pioneer reference of a random walk-based epidemic model was published by Frasca and others[4] in 2006. The authors propose an SIR disease that spreads over agents performing a discrete-step random walk in a 2D square space. Besides the basic random walk, each agent has a probability p_{jump} of being reallocated, at each time step, to a new position on space, chosen uniformly at random. Using only Monte Carlo simulations, they show that, as expected, higher agent density and probability p_{jump} of the so called long-range jumps implies on higher disease prevalence. They also describe the time evolution of some metrics of the instantaneous network of contacts. Buscarino and others[5,240] continued the work, now comparing the simulations with a homogeneously mixed formulation, and showing that $p_{\text{jump}} > 0.1$ is enough to make the

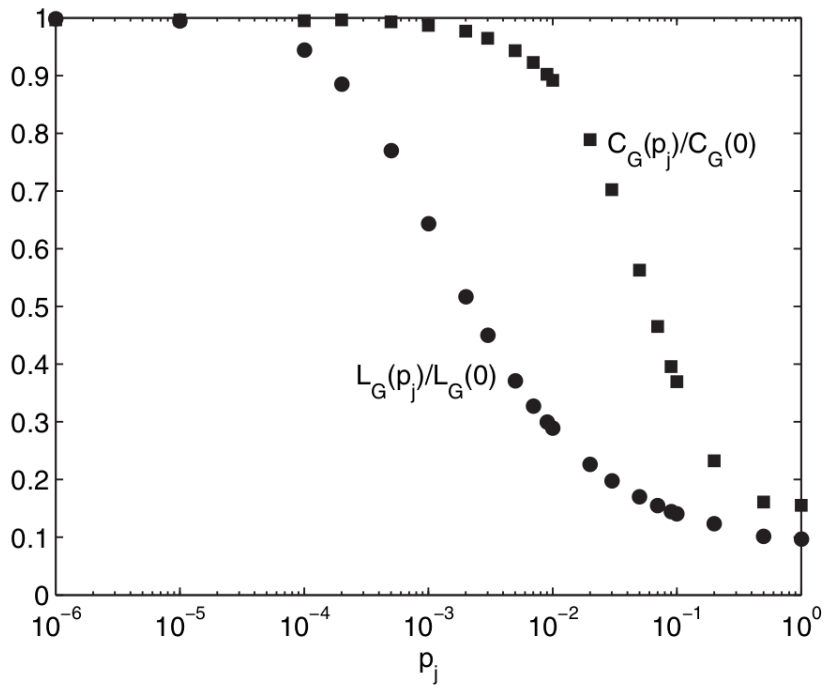

Figure 27 – Normalized average clustering coefficient ($C_G(p_j)$) and shortest path lengths ($L_G(p_j)$) of the instantaneous networks of mobile agents, as a function of the long-range jump probability (p_j or p_{jump} as in[4]), for the random walk epidemic model described by Buscarino and others.[5] The curves behave as in the small-world transition on Watts-Strogatz networks.[6]

Source: BUSCARINO *et al.*[5]

population behave as if it was homogeneously mixed. This occurs because the long-range jumps break the otherwise strong spatial correlation imposed by the smaller random walk steps (this is also verifiable in a work by Xia and others[241]). They also show, for a logarithmic range of p_{jump} values, how these correlations are broken (by measuring average clustering coefficients and shortest path lengths), in an effect that is very similar to the small-world phenomena observed on Watts-Strogatz networks.[6] Buscarino further studied the model with Levy walkers instead of random walkers with jumps, this time tracing an analogy with the behavior of scale-free networks.

The strong spatial correlations of the pure random walk, as described by Buscarino and coauthors, make it difficult to analytically describe the epidemic dynamics on this type of population, except when some other process (like the random jumps) breaks these correlations. This was somehow exploited by Zhou and Liu,[242] who proposed an SIS model with simple random walkers that could jump between square spaces of different sizes, emulating cities of different densities. In the case of two or three square regions, one with half the lateral size of the others, they study the disease prevalence in each region as a function of the jumping probability between regions, the area of the greater regions and the radius of interaction.

Zhou also compare their stochastic simulations with an analytical formulation that does not consider the strong spatial correlations present in populations of random walkers. This makes their formulation essentially homogeneously mixed, and the notable agreement with simulations can be explained by two factors: (i) the typically high probability of jump between regions, which randomizes the agents' positions and destroys the correlations, and (ii) the typically high densities of agents, which bring the system closer to a homogeneous mixing behavior. Zhou and other authors[243] employ a similar formulation for the case of a separate region that represents public transportation, with the agreement explained by the same factors.

Buscarino and others[244] also explored the topic of spatial heterogeneity, by setting a sub-region of the square space to have different transmission probability than the reast of the space. With an SIR model, they report the occurrence of both local outbreaks, driven by the sub-region, and global outbreaks in the whole space, depending on the transmission probabilities of each region. They again show that the model becomes homogeneously mixed for high jumping probabilities.

Huang and others[245] study the case of heterogeneous interaction radius in an SIS model, where each agent has its own radius around which it can catch the disease. They show that a greater variance on the distribution of radii decreases the epidemic threshold, as expected, but interestingly also decreases the stationary prevalence. Feng and others[246] also approaches the case of heterogeneous radii, but in terms of control theory, showing that there is an optimal distribution of radii to minimize the epidemic spreading. Ichinose and others[247] employed a biased random walk, in which all agents have a net tendency to move towards a given direction, and infectious ones (of an SIR model) move slower than others. While the effect of the direction bias is unclear, they show that lower mobility of infectious reduces the outbreak size and delays the peak of infectious prevalence. Finally, Peng and others[248] incorporate vaccination into the SIS model with heterogeneous radii, showing that an optimal vaccination strategy always exists regardless of the radii distribution.

The works covered so far in this section represent most of the research on random-walk-based epidemic models for mobile agents. Thus, although some significant results were reported, big improvements are yet to be done regarding this topic because, as shown in Section 4.1.1, animal and specially human motion can be constructed upon random walk models, but heavily deviates from the basic unbiased/uncorrelated case. In Section 4.2, we present our contribution to the topic, including a form of behavioral response to a disease into a random walk epidemic model.

4.1.3 Epidemic spreading in metapopulations

For the description of larger scale spreading of diseases, agent-based models may be not ideal, as the big numbers of individuals involved could easily make computational simulations unfeasible. Instead, the use of net human flows between places, either from real data or from

synthetic models (as presented in Section 4.1.1), may be more well suited. One particularly popular way of doing this is to use *metapopulations*,[249] which can be simply defined as populations composed of other subpopulations.

For modeling purposes, metapopulations were first used in the context of computational ecology, where they were usually called "patchy environments",[250–251] and each subpopulation was called a patch. For epidemic models, there were some works in the late 20th century,[252–254] but metapopulation epidemic spreading became considerably more popular in mid 2000s, when network science had already emerged as a field. In this context, Colizza and others[255–256] adapted the heterogeneous mean field approach (described in Section 2.2.2) for metapopulations, and used it to derive an epidemic threshold for uncorrelated networks. In this simple context, as well as in many other works, the metapopulation is simply a network in which each node (subpopulation) is a homogeneously mixed population, and individuals travel between subpopulations by the links of the network.

For SIR-like models, besides the traditional (called local) epidemic threshold, we also need to consider the so called *invasion threshold*[256] for metapopulations. Put into words, this threshold is reached when the mobility between subpopulations is low enough that an outbreak in one is likely to not propagate to its neighboring subpopulations. Mathematically, it is found from the so-called R_*, a reproduction number for the disease transmission between subpopulations (and not between individuals). If $R_* < 1$, the outbreaks are most likely to remain in a finite fraction of the subpopulations (even if the regular reproduction number R_0 is greater than 1 and local outbreaks occur).

The metapopulation approach can also consider recurrent travel patterns instead of a simple Markovian random walk (e.g., when the individuals have home places and frequent destinations).[257–259] Models for human migration (as explained in Section 4.1.1) can be employed to determine the net flows between subpopulations and, ultimately, real mobility data can be incorporated.[252,260] This last possibility led to the use of metapopulations for a variety of realistic epidemic simulators, such as the Global Epidemic and Mobility Model (GLEaM).[261] This model incorporates global mobility data based on flights, and divides the global territory by distance to important airports. Along with a demographic layer and a compartmental epidemic model, GLEaM was used during the 2009 H1N1 pandemics to assess the risk and disease attack times in multiple countries, as well as the effects of travel restrictions.[82,262] More recently, metapopulation models were important to address the spreading of COVID-19.[263–267] In particular, Aleta and others[267] used detailed data from the city of Boston–US to model the impact of contact tracing, a strategy that became more powerful than in any preceding pandemics due to the use of mobile device trackers.

Despite the notorious progress of metapopulation models for epidemic spreading, most models still do not include host behavioral changes due to an ongoing outbreak. Realistic simulators need to be constantly calibrated with real data to account for human decisions and be-

havioral responses, which are indeed complex and somehow unpredictable. However, some patterns of the human behavior can be incorporated into epidemic models (as the ones presented in Section 3.2), potentially making simulations more resilient through time. Therefore, as already justified, it is of great interest to develop epidemic models that include behavioral responses.

We contribute to the literature on this topic by expanding a proposed model for social distancing and other containment measures in general, applying it to metapopulations. This model can be applied either locally (at subpopulation level) or globally (for the whole metapopulation). We address the question of which of these formulations is better in different scenarios, and study other aspects of the proposed model. This work is described in Section 4.3.

4.2 Mobile agents with behavioral responses to epidemics

The work presented in this section was published in the journal *Chaos, Solitons and Fractals* in 2022.[268]

As we discussed in section 4.1.2, agent-based mobility models are abundant, but relatively few ones have been employed for epidemic modeling. Among these works, most deal with a simple unbiased random walk with random long-range jumps, but real mobility is shown to be far from unbiased.[70] In this section, we present our contribution to the topic, by studying epidemic spread among agents that perform a modified random walk. In particular, considering that human behavioral responses are highly demanded for computational epidemiology (see section 3.1.2), we modify the basic random walk to make susceptible agents avoid contacts with infectious ones.

The idea of avoiding contacts with infectious individuals resembles works on a more well studied type of system, called *adaptive network*. It was initiated by Gross and others,[269,270] who proposed a simple model in which susceptible individuals (represented as nodes of a network) can randomly change links that point to infectious nodes, redirecting them to other susceptibles. This generates a dynamic network that evolves simultaneously to the disease spreading, with susceptible nodes forming highly connected clusters between themselves to exclude infected ones. This behavior produces rich dynamical phenomena such as bistability, oscillations and hysteresis. The model later received refined analytical treatments[271–272] and motivated a series of subsequent studies.[273–276] In particular, Zhou and others[275] proposed a variant of the adaptive rewiring model that considers network growth and isolation avoidance, showing that the combination of these two factors can produce multiple epidemic bursts in an SIS model before the disease is eradicated.

In the present work, we merge the richness of adaptive behavioral responses with the modeling potential of mobile agents. As the model itself considers a very simple adaptive mechanism, in which susceptibles are fully and instantaneously aware of the epidemic state of their neighbors, the aim of this work is not to provide results that are directly applicable to the real

world. Instead, our goal is to study its basic dynamical properties, proposing the merge between mobility models and adaptive responses.

We also use a simple semi-analytical approach for the case in which the disease dynamics is slow compared to the agents' mobility. While it still relies on computational simulations, it allows to easily extract, among other results, the stationary prevalences and the phase diagrams, including the transcritical and saddle-node bifurcations that our model presents. Ultimately, it also provides an interpolated functional form for the reduction of contacts due to the adaptive mechanism. This can be applied into the local/regional dynamics of more complex models, such as those with metapopulations,[253–254,277–280] to include behavioral responses to epidemic spreading.

4.2.1 The model

4.2.1.1 Epidemic model

The epidemic model employed in this work is the reactive Susceptible-Infected-Susceptible (SIS) with discrete time evolution. Each agent can either be susceptible (S) to the disease or infected (I). At each time step, an infected agent that interacts with a susceptible one can transmit the disease with probability β. In addition, an infected agent can also be healed with probability μ. Infection and healing events are only applied in the next time step, so the order of agent visits does not matter, and reinfection after healing in a single time step is not allowed.

4.2.1.2 Basic mechanism of motion and interaction

For the baseline population dynamics, we use the simple random walk with hard interaction circles, as in references,[4,5,240] but with no long-range jumps. A population of N agents is initially distributed at random in a square space of length L with periodic boundary conditions. At each time step, each agent can perform a *random move* of fixed length v and uniformly random direction θ. Thus, the horizontal (x) and vertical (y) coordinates of the position of the agent at time $t+1$ after a random move are given by:

$$\begin{cases} x(t+1) = x(t) + v\cos(\theta) \\ y(t+1) = y(t) + v\sin(\theta) \end{cases} \tag{4.3}$$

Each agent has an interaction radius r, meaning that if two agents have a spatial distance smaller than r they interact reciprocally. With this interaction scheme, one can construct a snapshot network at each time step of the model.

To avoid any dependency on the implementation, both epidemic and positional state changes are calculated at each time step, but they are only applied after all changes were calculated.

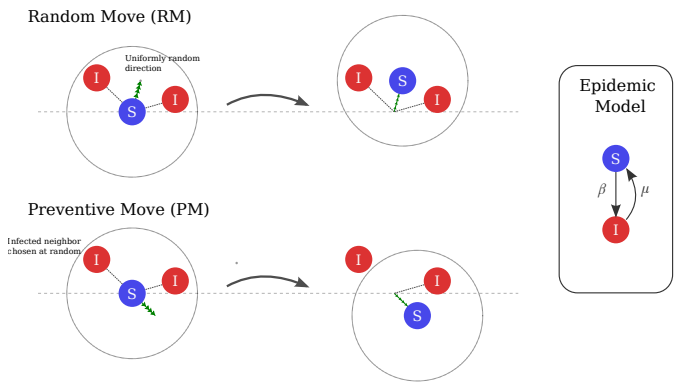

Figure 28 – Schematic representation of the possible mobility steps and the epidemic model. A susceptible (S) agent can either perform a random move (RM) to a direction chosen at random, or a preventive move (PM), in which it chooses one of its infected neighbors (if more than one is present) and move away from it.

Source: Adapted from VENTURA *et al.*[268]

We incorporate an adaptive reaction to the local presence of infected individuals, represented in Figure 28. At each time step, each susceptible (S) individual chooses, with probability p_a, to flee from an infected neighbor by moving in its opposite direction, using the following algorithm: (i) if there is exactly one infected neighbor, the susceptible agent moves in its opposite direction with step size v, which we call a *preventive move*. Here opposite direction means that the displacement vector makes an angle of π with the relative position vector that goes from the S to the I agent (see Figure 28). (ii) If there are two or more infected neighbors, the susceptible chooses one of them at random and promotes a preventive move away from it. (iii) If there are no infected neighbors, it simply promotes a random move to a uniformly random direction, as already described. Also, with probability $1 - p_a$, the susceptible promotes a random move regardless of its infected neighborhood. Therefore, in this model, infected agents do not react by the local mechanism, i.e., they do not perform preventive moves.

Notice that, for simplicity, the "awareness radius" of the agents is the same as their interaction radius r. Another simplification is that every infected individual is immediately perceived as such, which can be interpreted, for example, as if the disease symptoms are clear and display immediately after infection. The diagram in Figure 29 illustrates the decision algorithm for the motion of an agent, based on its own state. Table 1 displays all the symbols and acronyms that are used in the work of this section.

We perform Monte Carlo simulations of the SIS model under two different motion schemes for the mobile agents: (i) simple random walk (RW), for which no reaction mechanism is considered (i.e., $p_a = 0$) and (ii) random walk with local reactions (LR), for which we use $p_a = 1$, except where explicitly mentioned. We also compare our model with a homogeneously mixed population (HM) with an average number of contacts per unit time given

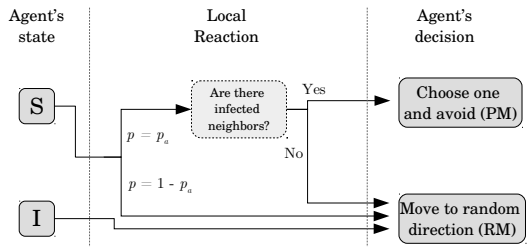

Figure 29 – Scheme of the decision algorithm for the motion of each agent, at each time step. With the local reaction mechanism, susceptible agents may decide to move away from an infected neighbor, if there is one, with probability p_a.

Source: Adapted from VENTURA *et al.*[268]

Table 1 – List of symbols used in section 4.2.

Symbol	**Meaning**
N	Number of agents
N_I	Number of infected agents
L	Size of the square space
r	Interaction radius of the agents
v	Size of spatial step
p_a	Probability of avoiding infected neighbors
t_{tr}	Simulation transient period
t_{av}	Simulation stationary period (data collection)
n_{ex}	Number of independent executions
β	Infection probability
μ	Healing probability
λ	$= \beta/\mu$ Infection-to-healing ratio
k_H	$= (N/L^2)\pi r^2$ Homogeneous degree
R_H	$= \lambda\ k_H$ Homogeneous reproduction number
ρ_I	$= N_I/N$ Disease prevalence
ρ_I^*	Steady state disease prevalence
HM	Homogeneously mixed population
RW	Random walker agents
LR	Random walk + local reaction agents

Source: VENTURA *et al.*[268]

by:

$$k_H = \frac{N}{L^2} \cdot \pi r^2 \tag{4.4}$$

Which is the expected average degree of the population if agents were uniformly distributed in space. We call k_H the *homogeneous degree*. We can also name:

$$R_H = \lambda k_H \tag{4.5}$$

The *homogeneous reproduction number* (i.e., the epidemic reproduction number if the nodes were homogeneously mixed with k_H contacts per time step in average), where $\lambda = \beta/\mu$ is the infection-to-healing ratio of probabilities.

4.2.2 Basic results

We start the analysis by studying the stationary state prevalence ρ_I^* of the system under a fixed initial infected fraction $\rho_I(0)$. We perform simulations under four different regimes with respect to the density of agents and the relative time scale between epidemic and motion dynamics.

In Figure 30, we show the stationary prevalence as a function of the homogeneous reproduction number R_H, for $\rho_I(0) = 0.30$. In each execution, the model is first simulated for a transient period of t_{tr} time steps, and then for t_{av} additional steps during which the data is collected and averaged. Each point is also an average of a number n_{ex} of such independent executions. In the regime in which the epidemics is slow compared to the motion dynamics ($\mu = 0.005$ - panels (a) and (c) of Figure 30), we use $n_{ex} = 50$, $t_{av} = 10000$ and t_{tr} from 1000 to 10000 depending on the point, ensuring it is enough to skip the transient stage. For the regime in which epidemics and motion have similar time scales ($\mu = 0.1$ - panels (b) and (d)), we use $n_{ex} = 500$, $t_{av} = 1000$ and t_{tr} from 200 to 2000.

First analyzing the low density regime (panels (a) and (b)), we notice that the local reaction mechanism (LR) considerably raises the epidemic threshold, both with respect to homogeneously mixed (HM) and random walking (RW) populations. In the high density regime (panels (c) and (d)), we notice an abrupt phase transition from healthy to endemic stationary states with the LR population, which is not observed within the other models. Such phenomenon was already reported for SIS-like models on adaptive networks,[269,273,274] and is actually a fingerprint of another important feature: a bistable phase caused by a saddle-node bifurcation.

Yet from Figure 30, we notice that our LR model deviates from homogeneous mixing even in the condition of slow epidemics (panels (a) and (c)), while the simple random walk (RW) can be reasonably described by HM in this regime, as observed in previous works.[242–243]

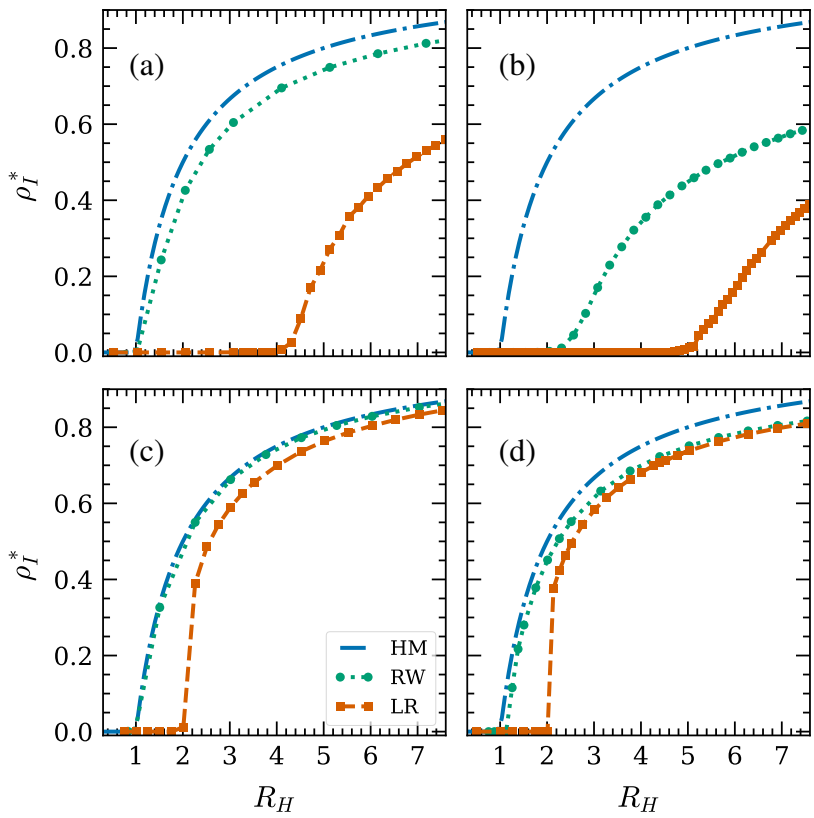

Figure 30 – Stationary prevalence as a function of the homogeneous reproduction number R_H, for different models of population (HM, RW and LR), under four different regimes: (a) low density, slow epidemics; (b) low density, similar time scale; (c) high density, slow epidemics; (d) high density, similar time scale. High (low) density is obtained by setting the $L = 10\,(35)$, for which the homogeneous degree is $k_H = 12.57\,(1.03)$. The slow epidemics is performed with $\mu = 0.005$, while the similar time scale regime uses $\mu = 0.1$. Other parameters are: $N = 400$, $r = 1.0$, $v = 0.3$. Different values of R_H are obtained by varying the infection probability β.

Source: Adapted from VENTURA *et al.*[268]

We evaluate the effect of the probability of avoiding infectious contacts p_a in Figure 31, which shows the prevalence curves at the low density and similar time scale regime for different values of p_a. For intermediate values of the parameter, the curves monotonically fill the range between full avoiding mechanism (LR $p_a = 1$) and simple random walk (RW, equivalent to LR with $p_a = 0$).

To show that our model presents bistability in the high density regime, we plot in Figure 32 time series of the LR model for different initial infected fractions $\rho_I(0)$, averaged over $n_{ex} = 50$ executions each, and observe the basins of attraction. The system can converge to two different stationary states, depending on the initial conditions. For this figure, we use $N = 1600$ individuals in the population to reduce stochasticity effects. Yet, the gray-shaded region repre-

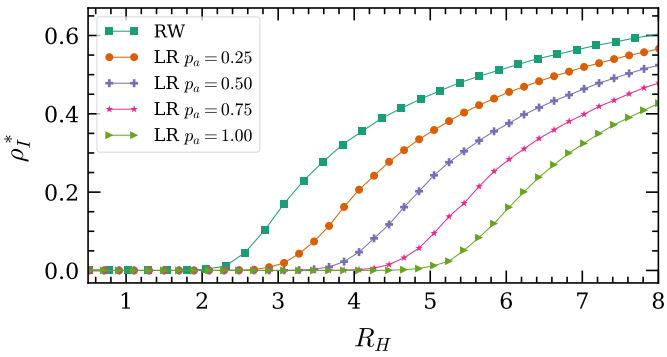

Figure 31 – Stationary prevalence ρ_I^* as a function of the homogeneous reproduction number R_H in the low density and similar time scale regime (as in Figure 30.b), for different values of the avoidance probability p_a. Parameters are: $\mu = 0.1$, $r = 1$, $v = 0.3$, $L = 35$, $N = 400$ (thus $k_H = 1.03$). Each curve is an average over $n_{ex} = 500$ executions.

Source: Adapted from VENTURA *et al.*[268]

sents the approximate location of an unstable fixed point where, due to stochastic fluctuations, each execution of the simulation can take different courses.

As reported in previous works with adaptive networks,[73,75,281] susceptible individuals can form highly connected clusters due to the behavioral response mechanism. We report such feature in our model by noticing that, during transient stages of simulations under high density regime, susceptible agents form spatial clusters that are densely connected due to proximity. Figure 33 shows a "snapshot" network of the population during transient stage of a typical execution, clearly showing the presence of clusters of susceptibles (blue circles), which we call *S-clusters*. The time evolution of this transient behavior can be captured by the average degrees (normalized by k_H) among susceptible and infected agents, as shown in Figure 34 (a), along with the prevalence (b) for a single execution starting with $\rho_I(0) = 0.13$. The simulation starts with $\langle k_S \rangle = \langle k_I \rangle = k_H$, but the degree of susceptible agents (blue curve) quickly raises as the S-clusters are formed, whereas the degree of infected agents drops. For this particular execution, the avoidance mechanism was able to reduce and eventually eliminate the disease, but the initial prevalence falls into the shaded region in Figure 32, meaning that the destiny of the system could have been different.

The formation of S-clusters is related to the spatial gaps that are left by the infected agents performing simple random walks. Susceptible agents tend to move into such gaps and form the observed clusters, which move and change throughout the time.

For some of the models of adaptive networks,[269,272] susceptibles follow rules that explicitly make them prefer connections between each other, which easily explains the formation of strong S clusters. However, Gusmán-Risau and Zanette[274] have shown that susceptibles can

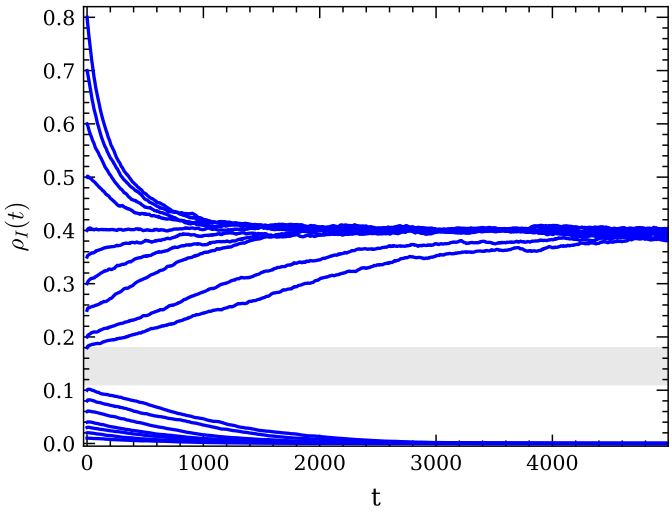

Figure 32 – Time evolution of the prevalence, starting from different initial conditions. This shows the bistability. The light gray stripe shows the region at which stochasticity allows the system to go both directions, causing the average curve to lay in between them. Parameters are: $\beta = 0.0009$, $\mu = 0.005$, $r = 1$, $v = 0.3$, $N = 1600$ and $L = 20$ (thus $k_H = 12.57$). Each curve is an average over $n_{ex} = 50$ executions.

Source: Adapted from VENTURA *et al.*[268]

increase their connectivity only with an avoiding mechanism, which is the case in our model.

In other works, clusters of susceptibles were observed both when S individuals actively seek connections to other susceptibles[269,272] and when they simply avoid infectious contacts.[274] Our model is an example of the latter, reinforcing that the S-clusters can occur without explicit preference to susceptibles in the rewiring mechanism.

The S-clusters are transient. If the prevalence at a given time and the disease transmissibility are not high enough, the lack of infectious contacts causes the disease to disappear, along with the S-clusters. However, if the prevalence and/or transmissibility are high enough, the infected agents eventually break the S-clusters and the disease takes over the population, which reaches a steady unclustered regime. The break of the susceptible clusters is similar to that observed by Zhou and others[75] during the epidemic bursts present in their model.

Due to this ambiguity of trajectories from the clustered regime, it is clear that such clusters are closely related to our model's bistability. In the next section, we develop a semi-analytical approach that corroborates this hypothesis.

4.2.3 A semi-analytic approach for slow epidemics

For slow epidemic evolution, achieved by sufficiently low values of β and μ, we can not only approximate the discrete time dynamics of the disease to a continuous one, but also assume that any metrics related to the population of agents is a function of the prevalence, as

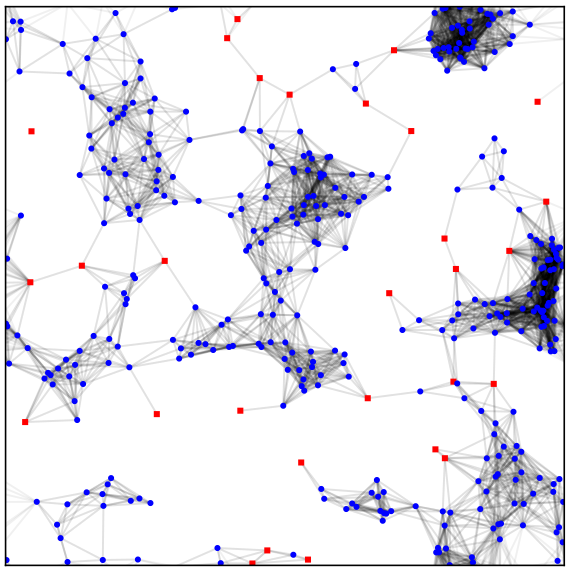

Figure 33 – Snapshot network of the population with 400 agents after $t = 180$ steps of a simulation with $\beta = 0.001$, $\mu = 0.005$, $r = 1$, $v = 0.3$ and $k_H = 12.57$. Red squares represent infected agents, while blue circles are susceptible. The average degree of susceptible agents is $\langle k_S \rangle = 21.5$ and of infected agents is $\langle k_I \rangle = 9.4$. The prevalence is around 7%.

Source: Adapted from VENTURA *et al.*[268]

the population quickly responds to the slow changes in epidemic states. With this in mind, the SIS dynamics is given by the following rate equation for the overall prevalence ρ_I:

$$\dot{\rho}_I = \beta l_{SI} - \mu \rho_I \tag{4.6}$$

Where $l_{SI} = L_{SI}/N$ is the number of links L_{SI} that connect susceptible to infected agents normalized by the population size N, and is a function of the prevalence ρ_I. Effectively, this approximation promotes a time scale decoupling of the epidemic and motion dynamics.

We know no analytical method to estimate the functional form of $l_{SI} = l_{SI}(\rho_I)$ for mobile agents, but we can directly sample it from Monte Carlo simulations of the population with no epidemic dynamics ($\mu = \beta = 0$), this is: each agent receives a given state at the beginning, S or I, and holds it during the whole simulation. This way, we can manually set the number of infected agents N_I to achieve a desired value of the prevalence $\rho_I = N_I/N$. We calculate l_{SI} at each time step in the stationary state, then average its value over time and over independent executions. This process is repeated for different values of ρ_I, enough to have a precise shape of the $l_{SI}(\rho_I)$ curve, which is then interpolated to obtain a continuous approximation. For this work, we apply a spline interpolation of third order. Figure 35 shows the data acquired by this method. In the a) panel, we see how the LR model deviates from the

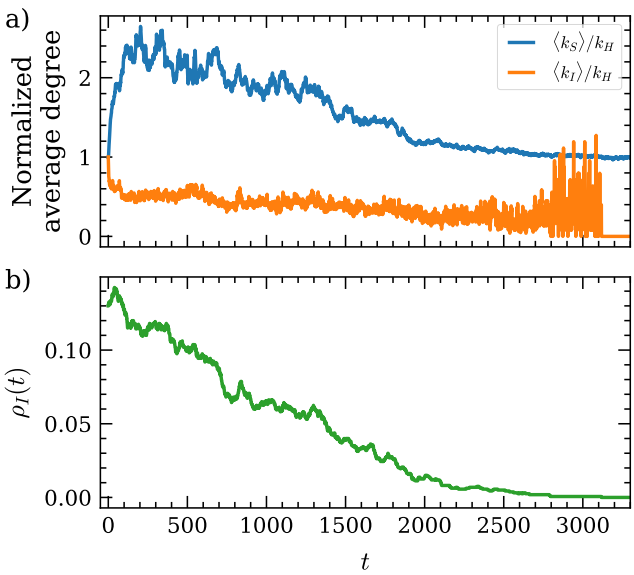

Figure 34 – Time evolution of the average degree of susceptible (blue) and infected (orange) agents for a single execution, shown in panel a), along with the prevalence in panel b). The degrees are normalized by the homogeneous degree k_H. Parameters are the same as in Figure 32, with $\rho_I(0) = 0.13$ and a single $n_{ex} = 1$ execution.

Source: Adapted from VENTURA *et al.*[268]

mass-action law used for homogeneous mixing.[282]

Once obtained, the function $l_{SI}(\rho_I)$ can be used to determine the epidemic dynamics in the slow regime. For instance, the fixed points are the values ρ_I^* for which $\dot{\rho}_I = 0$ in Equation 4.6. This is equivalent to solve the equation:

$$\rho_I^* = \lambda l_{SI}(\rho_I^*) \tag{4.7}$$

Where $\lambda = \beta/\mu$ is the infection-to-healing probability ratio. In Figure 35.b), the fixed points can be found as the crossings between $\lambda l_{SI}(\rho_I)$ and the identity line (gray dashed line). Also according to Equation 4.6, the stability of the solution is given by the slope of $\lambda l_{SI}(\rho_I)$ at the fixed point: if greater than 1 (i.e., the slope of the identity line), the solution is unstable, and if less than 1 it is stable.

Notice from Figure 35.b) that each curve represents a different phase of the LR model. For $\lambda = 0.1$, the only solution is the trivial $\rho_I = 0$, i.e., the healthy state. For $\lambda = 0.2$, the system presents two more solutions, of which one is stable (the one with greater ρ_I), while the healthy state remains stable. This characterizes the bistable phase, obtained after a saddle node bifurcation. Finally, for $\lambda = 0.4$, the healthy solution is unstable (as the initial slope of $\lambda l_{SI}(\rho_I)$ is greater than 1), characterizing the regular epidemic phase. This phase is reached after a transcritical bifurcation.

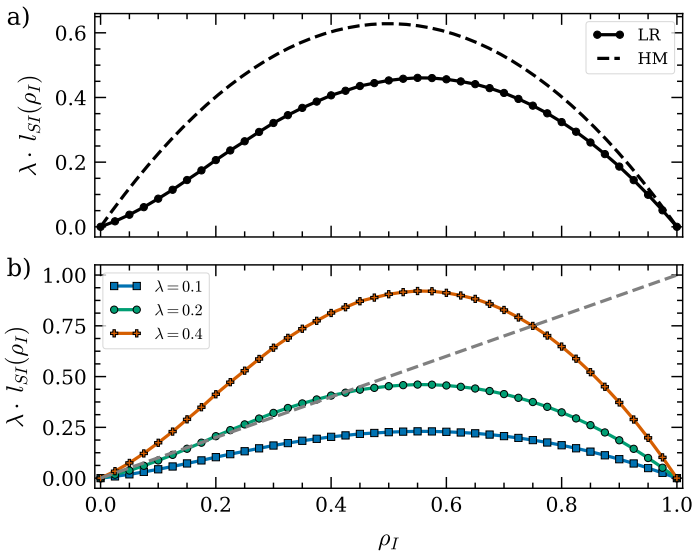

Figure 35 – Panel a): $\lambda \cdot l_{SI}$ as a function of the (static) prevalence ρ_I, for the local reaction agents (LR) and for homogeneous mixed populations (HM). Panel b): $\lambda \cdot l_{SI}$ curve of LR model for three values of the infection-to-healing probability ratio λ, along with the identity line (gray dashed). We use $N = 400$, $r = 1$, $v = 0.25$, and $k_H = 12.57$.

Source: Adapted from VENTURA *et al.*[268]

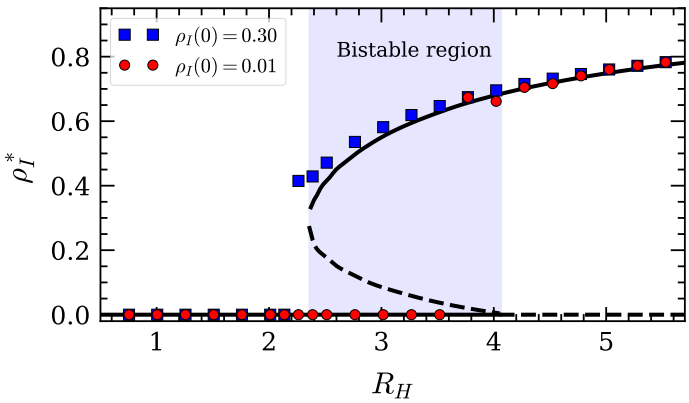

Figure 36 – Comparison between the fixed points of $\lambda \cdot l_{SI}$ using the semi-analytical approach (solid lines are stable solutions, dashed ones are unstable) and the results of Monte Carlo simulations, using $\rho_I(0) = 0.3$ (blue squares) and 0.01 (red circles) as the initial prevalence. We use $N = 400$ for the l_{SI} curves and $N = 1600$ for the Monte Carlo simulations, $r = 1$, $v = 0.25$, $k_H = 12.57$ and $\mu = 0.005$. Each point is an average over $n_{ex} = 50$ executions with $t_{tr} = 5000$ and $t_{av} = 10000$. Different values of R_H are obtained by varying the infection probability β.

Source: Adapted from VENTURA *et al.*[268]

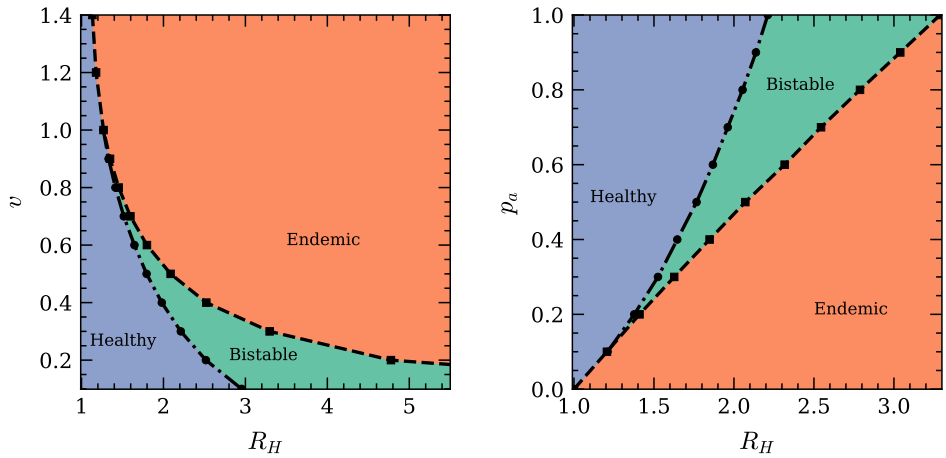

Figure 37 – Phase diagrams of the mobile agents model with local reaction (LR) mechanism, using the semi-analytical approach. The y axis parameter is the agent's step size v in the upper panel, and the local reaction probability p_a in the lower panel, while different values of R_H are obtained by varying the transmission probability β. A dashed line with squares represents a transcritical bifurcation, while a dash-dotted line with circles is a saddle-node bifurcation. Other parameters are: $N = 400$, $r = 1$, $v = 0.3$ (lower panel) and $p_a = 1$ (lower panel).

Source: Adapted from VENTURA *et al.*[268]

To compare the semi-analytical approach with Monte Carlo simulations of the epidemic dynamics, we plot the fixed points (both stable and unstable) obtained from the $l_{SI}(\rho_I)$ curves as a function of the disease transmission rate β, rescaled as the homogeneous reproduction number $R_H = \beta k_H/\mu$. The results are in Figure 36, where fixed points of the semi-analytical approach are represented as solid (stable) and dashed (unstable) lines, and the stationary prevalences obtained from Monte Carlo simulations are represented as squares (starting from $\rho_I(0) = 0.30$) and circles (starting from $\rho_I(0) = 0.01$). The region where both the healthy and endemic solutions are stable (according to the semi-analytical approach) is shaded on the plot.

We first notice the good agreement between the semi-analytical and Monte Carlo formulations in Figure 36. Notice that, in the bistable region, the stationary prevalence of the Monte Carlo simulations depends on the initial conditions, although there is some disagreement at the edges of the bistable region, which may be attributed to stochasticity and population's finite size.

Using the sampled and interpolated approximation for $l_{SI}(\rho_I)$, we can numerically calculate the critical points. In Figure 37, we show two phase diagrams: one for the agents' step size v (upper panel) and another for the local reaction parameter p_a, both as a function of the homogeneous reproduction number R_H.

Notice that, as the step size v increases, the bistable region shrinks and disappears, as the fast motion prevents the agents from forming S-clusters. For greater velocities, the critical

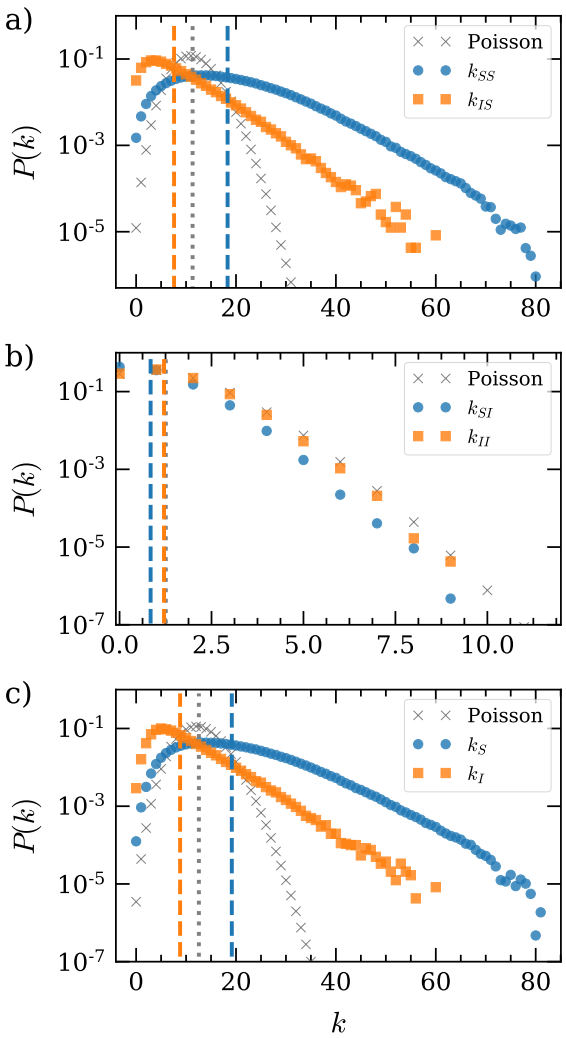

Figure 38 – Degree distributions for snapshots of the dynamic network, averaged over time steps and executions, using simulations of the local reaction (LR) model with no epidemic dynamics ($\beta = \mu = 0$). We group the degrees according to the state of target nodes: susceptibles (a), infecteds (b) and both (c). Each dashed line is the average of the distribution with the same color. As a null model, we show a Poisson distribution ("x" symbols) that represents homogeneously random interactions in each situation, as explained in text. Other parameters are: $N = 400$, $r = 1$, $v = 0.3$, $p_a = 1$, $k_H = 12.57$ and a fixed prevalence $\rho_I = 0.2$. Also $t_{av} = t_{tr} = 1000$, and $n_{ex} = 60$.

Source: Adapted from VENTURA *et al.*[268]

value of R_H approaches that of a homogeneously mixed population (i.e., $R_H = 1$). From the p_a phase diagram (lower panel), we infer that the size of the bistable region grows with the parameter p_a that controls the intensity of the local reaction, as expected.

4.2.4 Characterization of the dynamic network

We can further study the structure of the networks that are formed by this model in the clustered regime by looking at the degree distributions. To simplify the execution, we also remove the epidemic dynamics for this measurement, so the S and I agent states are static. We consider the connectivity between different classes of agents, so for example k_{SS} is the number of links of a susceptible agent that point to other susceptibles, k_{SI} is the number of links of a susceptible that point to infected agents, and so on. Also k_S and k_I are the total degrees of susceptibles and infecteds, respectively. Figure 38 shows each of these degree distributions, grouped by the state of the link targets. As a reference, we also plot a Poisson distribution (gray *x* symbols) $f(k; s) = e^{-s}s^k/k!$ with $s = k_H(1 - \rho_I)$ (a), $s = k_H\rho_I$ (b) and $s = k_H$ (c). These are, in each case, the expected degree distributions if the agents were homogeneously distributed at random in the space. Each vertical line also shows the average of each distribution of the corresponding color.

From Figure 38.a), we can see how susceptibles are highly connected to each other, but weakly connected to infected agents, as the k_{SS} distribution spans over higher values than the k_{IS}. In panel b), we see that k_{II} is well described by the equivalent Poisson distribution because infected agents perform simple random walks, whereas k_{SI} is slightly reduced due to the local reaction mechanism. Finally, panel c) shows how the overall degree distributions are distorted and broadened from the basic Poisson curve, similar to the effect observed by Gross and others[269] in adaptive networks. It also shows that, in average, susceptible agents are more connected than infected ones.

Yet under the same framework that considers static disease states, we can analyze how the average degrees, as well as some other network metrics, vary with the prevalence, in order to determine where the S-clustering regime occurs. Figure 39 (b) shows the average degrees of susceptible ($\langle k_S \rangle$), infected ($\langle k_I \rangle$) and ($\langle k \rangle$) agents of the snapshot network, normalized by the homogeneous degree k_H, as a function of the prevalence. The peak on the $\langle k_S \rangle$ curve is a consequence of the S-clusters, and it is also visible in the total average degree $\langle k \rangle$. The average degree of infected agents $\langle k_I \rangle$, on the other hand, is always smaller than k_H, as a consequence of the local reaction mechanism itself, which reduces the contacts with infected agents.

In Figure 39.b), we show the average clustering coefficient C and the degree assortativity r_{deg} of the snapshot networks also as a function of the prevalence. The value of C, which is naturally high on dense random geometric networks, is enhanced at the range in which the S-clusters occur, having a good correlation with the $\langle k_S \rangle$ curve. The assortativity r_{deg} is also enhanced by the avoidance mechanism, displaying a broader peak, which means that the effect of the mechanism into the assortativity prevails even when the S-clusters are not very expressive. As also reported in,[269] the increase in degree correlations may be an effect of the segregation between S and I agents, as reported in the degree distributions in Figure 38.

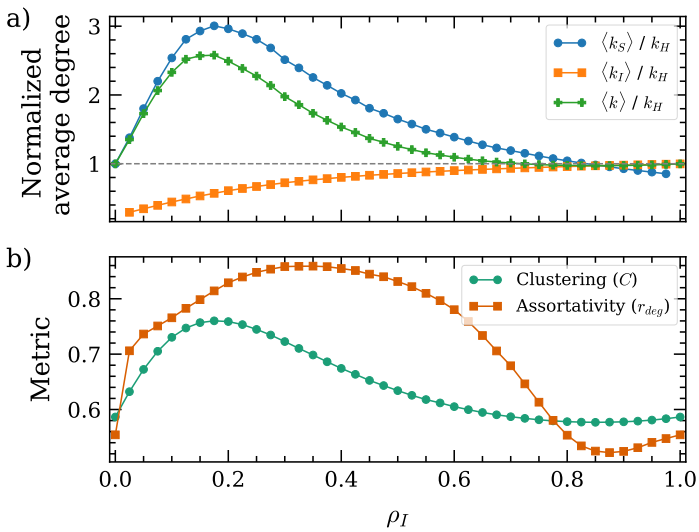

Figure 39 – Average degrees normalized by the homogeneous degree k_H (a) and other metrics (b) as a function of the (static) prevalence ρ_I, for snapshot networks of the LR model with no epidemic dynamics ($\beta = \mu = 0$). Other parameters are: $N = 400$, $r = 1$, $v = 0.25$, $p_a = 1$, $k_H = 12.57$. Moreover $t_{tr} = 1000$, $t_{av} = 10000$, and $n_{ex} = 40$.

Source: Adapted from VENTURA *et al.*[268]

We finally notice that the range of unstable prevalences in Figure 35.b) is compatible with the region at which $\langle k_S \rangle$ and C have their peaks in the plots of Figure 39 meaning that, as observed, the S-clusters are unstable when the epidemic dynamics is active, causing the disease to either spread globally by breaking the S-clusters or be eradicated, as explained in section 4.2.2. This reinforces the relationship between the S-clusters and the model's bistability.

4.2.5 Discussion

We propose a simple mechanism to incorporate behavioral responses to epidemics in a population of mobile agents, based on the avoidance of contacts with infectious individuals. We show that, with such mechanism, we can merge the rich dynamical features of adaptive contacts, initially studied on networks, with the potential of mobile agents for epidemic modeling.

For the low density regime, which is often used to reproduce empirical data,[70] the local reaction mechanism considerably suppresses the disease propagation. This is because, when the agents are spatially sparse, the susceptibles easily find the direction to avoid infected agents. In the high density regime, the stationary prevalence is not strongly reduced from the homogeneous mixing scenario, but new dynamical features are introduced: the bistability and the clusters of susceptibles.

In the bistable regime, the transient S-clusters can either succeed to eradicate the disease or permit it to spread, depending on the initial prevalence. The bistability is inherited from the

adaptive contact changes, but the collective motion of susceptibles between the gaps left by infected agents is an interesting feature that is exclusive of our spatial model.

We also apply a simple semi-analytic approach to describe the dynamic features of the LR model in the slow epidemics regime, based on simulating the population with static epidemic conditions. This framework can be generalized to a variety of other dynamic population models, provided that the epidemic dynamics is slow, and a functional form of the behavioral reduction of contacts can be extracted from it.

Finally, we characterize the networks obtained by snapshots of the population with static epidemics in the steady state. We show how the local reaction mechanism deviates the behavior from the simple random walk, pointing to how the infective contacts are avoided while susceptibles are joint into highly connected clusters. In a practical point of view, this represents a situation in which space is limited and infected individuals do not change their behavior, and is not realistic due to several aspects. However, and as our main goal, we seed merging between adaptive reactions and mobile agent models, calling for further works in the topic.

4.3 Behavioral responses on metapopulations

The work presented in this section was published in the journal *Epidemics* in 2022.

In section 4.1.3, we presented a quick literature review on the subject of epidemic models over metapopulations. This framework is one of the most frequently used for more realistic works with epidemic spreading, as it allows for a reasonable and tractable representation of populations from a city to worldwide level.[283] Despite the topic of behavioral responses to epidemics has been widely studied lately, it has been focused on homogeneously mixed populations and simple networks/multiplexes of contacts, while most works on metapopulations still use overly simple assumptions for behavioral responses.

In the work covered by this section, we address this by proposing a dynamic model of behavioral responses to epidemics in a metapopulation. By dynamic, we mean that the responses are incorporated into the system as extra dynamical variables, coupled to the epidemic spreading variables.

The spreading of COVID-19 has clearly demonstrated the variety of ways in which humans react to an epidemic. For instance, without forceful government intervention, traffic in Seoul's subway declined sharply following the first deaths in South Korea.[284] Conversely, several communities in other regions of the world defied social distancing measures.[285–286] Especially in the events of emerging diseases, such as COVID-19, public health authorities base many decisions on the forecasts produced by epidemic models. Therefore, it is of paramount importance to include the effect of behavioral changes as something inherently attached to the spreading of the epidemic.

Our model is based on a recently proposed model[89] for the effects of social distancing on

homogeneously mixed populations, which we adapted to metapopulations. Besides the proposal and study of the dynamics, we also aim to understand the role that social distancing and other contention measures can play in the spread of emerging diseases, and shed some light on the scenario in which the response is heterogeneous across regions.

4.3.1 Model description

We implement a discrete and stochastic SIR metapopulation model composed by V subpopulations.[249,287–288] In each subpopulation, individuals can interact with each other and spread the disease following the classical SIR model. These subpopulations are connected through a certain network, so that an individual may travel to another subpopulation only if it exists a direct link between the source and target subpopulations.

To include the effect of contention measures, either policy-driven or as a consequence of fear of infection, we consider an additional coefficient that modifies the transmissibility of individuals. This coefficient mimics the behavioral responses of the population, and evolves according to the densities of infectious and recovered individuals.[89] In section 4.3.2, we study this model in an homogeneously mixed population. For the remaining sections, we apply the model to a metapopulation system.

4.3.1.1 Epidemic spreading

For the SIR compartmental model, individuals are assigned compartments according to their infectious status: susceptible (S) if they do not have the disease and can catch it; infectious (I) when they have the disease and can transmit it to susceptibles, and removed (R) when they no longer transmit the disease after being infectious (either by recovery or deceasing). At each model's epidemic update, the following rules determine the transitions between compartments:

- **S** $\rightarrow$ **I**: a susceptible individual in subpopulation i can become infectious with probability $P_i(S \rightarrow I) = 1-(1-a_i\beta/N_i)^{I_i}$, where β is the individual transmission probability, N_i is the number of individuals in subpopulation i and I_i is the number of infectious individuals in the same subpopulation. The term a_i is called the *coefficient of contact reduction*, and depends on the considered scenario as we describe later on.

- **I** $\rightarrow$ **R**: an infectious individual is moved to the R (removed) compartment with probability μ, which is the inverse of the average infectious period. After this event, the individual no longer participates on the epidemic dynamics.

Throughout this section, we set μ to $1/4$ and the basic reproductive number $R_0 = \beta/\mu$ to 1.5, which is compatible with the parameters of an influenza-like disease. We define $N_S = \sum_{i=1}^{V} S_i$ as the total number of susceptible individuals in the whole population and, analogously, N_I and N_R for the infectious and removed compartments. The coefficient of contact reduction

Table 2 – List of symbols used for the work with metapopulations with behavioral responses.

Description	Symbol
Individual infection probability	β
Recovery probability/rate	μ
Basic reproduction number	$R_0 = \beta/\mu$
Contact reduction coefficient	a_i
Response strength exponent	k
Long-term coefficient	l
Mobility coefficient	τ
Threshold for infectious fraction	ε_I
Individual counts in each state in subpopulation i	S_i, I_i, R_i
Global individual counts in each state	N_S, N_I, N_R
Global fractions in each state	ρ_S, ρ_I, ρ_R
Number of nodes (subpopulations) on network	V
Number of links on network	M
Number of individuals in subpopulation i	N_i
Total number of individuals in population	N_{pop}
Maximum distance for connection on RGN	d
Link weight between subpopulations i and j	T_{ij}
Long-term scenario	LT
Short-term scenario	ST
network	RGN

Source: VENTURA *et al.*[289]

a_i is what determines the behavioral responses to the epidemics, and we consider different strategies for such a response, each one with a different definition of a_i:

1. **Social distancing based on global information**

   This scenario is based on the one proposed by Eksin and others in,[89] which here we extend to metapopulations. The coefficient of contact reduction emulates the social response to an increase in the number of infections, and it is a function of the total (global) number of infected and recovered individuals, given by:

$$a_i = \left(1 - \frac{(N_I + l \cdot N_R)}{N}\right)^k \tag{4.8}$$

   Since a_i only depends on global quantities, its value is the same for all subpopulations. The parameter k is the *response strength*, an adjustable exponent that calibrates the intensity of the response against the number of cases. The coefficient l is called *coefficient of long-term*, and determines the importance of the R compartment to the behavioral response. Following,[89] $l = 0$ represents the *short-term scenario* (ST), where the response

weakens when the incidence drops. The case $l = 1$ is the *long-term scenario* (LT), in which the awareness is proportional to the total accumulated number of cases. These two limiting cases differ in many aspects, which we describe throughout the rest of the section.

2. **Social distancing based on local information**

   In this variant of the previous setup, we consider that each subpopulation (node) responds individually, according to its own number of cases. The expression for the coefficient of contact reduction is:

$$a_i = \left(1 - \frac{(I_i + l \cdot R_i)}{N_i}\right)^k \tag{4.9}$$

3. **Constant response after threshold**

   For comparison, we also implement a more traditional scenario in which the transmissibility is reduced by a constant factor a_0 once the overall number of cases $N_I + N_R$ overcomes a given threshold $N \cdot \varepsilon_I$ (with $0 \leq \varepsilon_I < 1$). Here we use only the global and cumulative information, thus a_i is defined as:

$$a_i = \begin{cases} 1 & N_I + N_R < N\varepsilon_I \\ a_0 & N_I + N_R \geq N\varepsilon_I \end{cases} \tag{4.10}$$

   and is the same for all subpopulations. This scenario can be considered as a baseline in which social distancing (or governments policies) is constant and independent of the state of the system, and it is a benchmark that is often assumed as the behavioral response in metapopulation epidemics.[124,263,265,290]

4.3.1.2 Mobility model

Following a standard metapopulation framework, the mobility between subpopulations is modeled as a random walk through the links of a graph of V nodes and M links. It is controlled by a master parameter τ called the *mobility coefficient*, as well as the weights T_{ij} of existing links between subpopulations (nodes) i and j. During a mobility update, each individual in subpopulation i travels to subpopulation j with probability $p_{ij} = \tau \cdot T_{ij}/N_i(0)$, where $N_i(0)$ is the number of individuals attributed to subpopulation i at the initial time step. Within this scheme, we have the following features:

- If all links are reciprocal and symmetric (i.e., $T_{ji} = T_{ij}$ for all connected pairs of subpopulations i, j), then the net fluxes between the subpopulations are balanced and the population of each one remains approximately constant, fluctuating around $N_i(0)$. We use this configuration throughout this work.

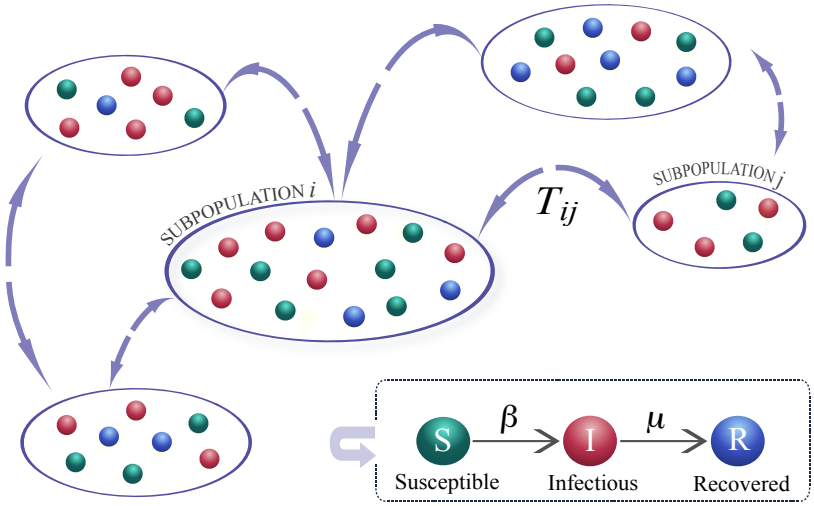

Figure 40 – Scheme of the epidemic and mobility models in a metapopulation. The SIR epidemic dynamics occur inside each subpopulation, where homogeneous mixing is assumed. Also at each time step, individuals move between neighboring subpopulations i and j according to a mobility matrix T_{ij}.

Source: VENTURA *et al.*[289]

- The average number of individuals expected to travel from i to j is $\tau \cdot T_{ij}$, with small variations due to fluctuations of $N_i(t)$ around $N_i(0)$.
- The probability that an individual in subpopulation i travels anywhere is $p_i = \tau \sum_j T_{ij}/N_i(0)$, and may vary for each subpopulation. We always set τ to be small enough so that $p_i < 1$ for every subpopulation i.

During a single time step, we first perform the epidemic interactions in each subpopulation, then update the number of individuals that are in each state. After this, we apply the mobility rules to determine how many individuals move through each link, and update the actual numbers of individuals in each site only after all fluxes have been calculated. This way, the results do not depend on the order at which we "visit" the subpopulations to perform the calculations. The mobility and epidemic models are schematically represented in Figure 40. Table 2 shows the meaning of each symbol and acronym used during this work.

4.3.2 Analytical insights for homogeneously mixed populations

For sufficiently low mobility between subpopulations, the local dynamics can be well described by an isolated homogeneously mixed system. Also for sufficiently high number of individuals, we can use rate equations for the expected fractions of the population in each compartment, substituting S/N, I/N and R/N by ρ_S, ρ_I and ρ_R, respectively. The chosen expression for the behavioral response mechanism is simple enough to allow for analytical ma-

nipulation. Particularly, in the long-term (LT) scenario (i.e., with $l = 1$ in Equations 4.8 and 4.9), these rate equations can be integrated to find the trajectory of the dynamical system. In this section, we explore this tractability to extract some insights from the model.

4.3.2.1 Long-term scenario

Considering the dynamics of a single isolated subpopulation, the dynamical equations for the average fractions ρ_S, ρ_I and ρ_R of susceptible, infectious and removed individuals can be written as:

$$\dot{\rho_S} = -\mu R_0 \, \rho_S \rho_I \cdot \, a(\rho_I, \rho_R) \tag{4.11}$$

$$\dot{\rho_I} = \mu R_0 \, \rho_S \rho_I \cdot \, a(\rho_I, \rho_R) - \mu \rho_I \tag{4.12}$$

$$\dot{\rho_R} = \mu \rho_I, \tag{4.13}$$

where $R_0 = \beta/\mu$ is the basic reproduction number and μ is now interpreted as the recovery rate (instead of probability). For the long-term scenario, $a(\rho_I, \rho_R) = (1-(\rho_I+\rho_R))^k = \rho_S^k$, given that $\rho_S + \rho_I + \rho_R = 1$. As described in[89] and similarly to what we presented in section 2.2.1 for SIR, we can divide Equation 4.11 by Equation 4.13 to obtain a separable differential equation:

$$\frac{\mathrm{d}\rho_S}{\mathrm{d}\rho_R} = -R_0 \rho_S^{k+1} \tag{4.14}$$

For $k > 0$ and assuming that $\rho_R(0) = \rho_0 \geq 0$ and $\rho_I(0) = \delta \to 0$, its solution is given by:

$$\rho_S = \left[\frac{1}{(1-\rho_0)^k} + kR_0(\rho_R - \rho_0) \right]^{-\frac{1}{k}} \tag{4.15}$$

Alternatively, writing ρ_I as a function of ρ_R:

$$\rho_I = 1 - \rho_R - \left[\frac{1}{(1-\rho_0)^k} + kR_0(\rho_R - \rho_0) \right]^{-\frac{1}{k}} \tag{4.16}$$

Equation 4.16 represents the trajectory of the system in a ρ_I *vs* ρ_R diagram, showing how the fraction of infectious individuals peaks as the fraction of removed increases in the LT scenario. The solid lines in Figure 41 show such trajectories for different values of the response strength k, $\rho_0 = 0$ and $R_0 = 1.5$. Also, the final ρ_R prevalence at the end of the outbreak can be found by solving Equation 4.16 for $\rho_I = 0$ besides the trivial solution $\rho_R = \rho_0$.

For $k = 0$, Equation 4.14 solves as a simple SIR model which, for $\rho_R(0) = \rho_0$ and $\rho_I(0) = \delta \to 0$, leads to a ρ_I *vs* ρ_R trajectory given by:

$$\rho_I = 1 - \rho_R - (1 - \rho_0)e^{-R_0(\rho_R - \rho_0)} \tag{4.17}$$

In the long-term scenario with $k > 0$, the contact reduction coefficient $a(\rho_I, \rho_R)$ is a decreasing function of $\rho_R + \rho_I$, which in turn can only increase over time. This means that $a(\rho_I, \rho_R)$ will also always decrease as if the disease contention measures are held forever. This is not reasonable to assume for the long term behavior of a real situation and, for this reason, we can consider that at some point after the main outbreak, $a(\rho_I, \rho_R)$ is set to 1 again, which we call henceforth a *system release* (representing a *release* of the contention measures).

For instance, consider that a system release occurs when the fraction of infectious individuals reaches a small value $\delta > 0$ after the main outbreak initiated. This comprises the fact that, during the time evolution given by Equations 4.11 to 4.13, $\rho_I(t)$ tends to but never actually reaches zero. For the calculation of the ρ_I *vs* ρ_R trajectories though, we can consider $\delta \to 0$. After the system is released, the trajectory follows Eq. 4.17 with ρ_0 set to the final size of the first outbreak. In Figure 41, the dashed lines represent the secondary outbreaks produced after the system's release.

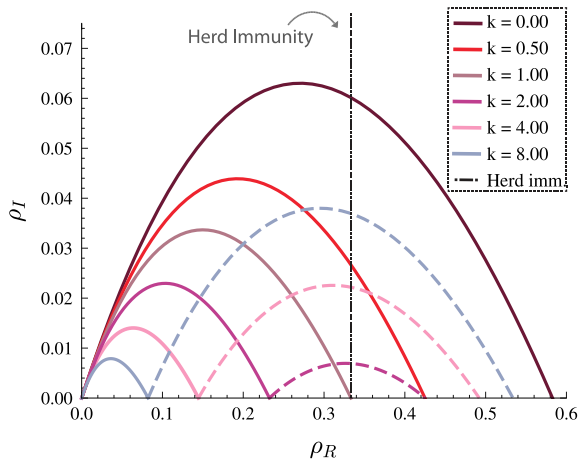

Figure 41 – Analytical trajectories of the homogeneously mixed long-term (LT) scenario with system release after the first outbreak (i.e., complete lift of the contention measures). The trajectories are combinations of Equations 4.16 (solid lines) and 4.17 (dashed lines) with ρ_0 set to the size of the first outbreak. R_0 is set to 1.5.

Source: VENTURA *et al.*[289]

As observed in the figure, a system release can generate a second outbreak which, for higher values of k, can be greater than the first one. This happens because, although the long-term scenario effectively reduces the size of the first outbreak (both in ρ_R and ρ_I), it may leave the system under its herd immunity threshold, and thus vulnerable to new outbreaks.[291] In this homogeneous model, the threshold for herd immunity is given by $\rho_{herd} = 1 - R_0^{-1}$, meaning that for $\rho_R \geq \rho_{herd}$ the fraction of infectious individuals can no longer increase. If the disease dies

out before the prevalence reaches that value, the system will experience a new outbreak if the social distancing measures are relaxed and the disease is reintroduced in the population. Note that the critical value of k for reaching herd immunity at the first outbreak is $k = 1$, for which the final outbreak size is exactly solved as $\rho_R^* = 1 - R_0^{-1}$, as noticed by Eksin and others.[89]

4.3.2.2 System resets

Besides *releasing* the system after the first outbreak, we propose another way to work with multiple outbreaks in the LT scenario. What makes the $a(\rho_I, \rho_R)$ coefficient to be by default strictly decreasing is its dependence on ρ_R, which holds a "long-term memory". We can modify such memory by subtracting a constant ρ_0 from the prevalence that's considered for the contact reduction coefficient $a(\rho_I, \rho_R)$. If we do this right after the main outbreak and set ρ_0 to the recovered fraction at that time, then $a(\rho_I, \rho_R)$ is momentarily reset to 1 (i.e., no contention measures), but the system will still react in the event of another outbreak. We call this a *system reset* (the memory of the population is reset, but the contention measures still apply), in contrast with the simpler system release described in the previous section (in which the contention measures are completely removed). We are again assuming that ρ_I is arbitrarily small at the end of an outbreak.

During this new round of the dynamics, Equation 4.11 divided by Equation 4.13 yields the following differential equation:

$$\frac{\mathrm{d}\rho_S}{\mathrm{d}\rho_R} = -R_0 \cdot (\rho_S - \rho_0)^k \rho_S \tag{4.18}$$

which is still separable, but for $\rho_0 > 0$ solves into a less insightful expression:

$$R_0 \cdot (\rho_R - \rho_0) = P_{\rho_0,k}(\rho_S) \tag{4.19}$$

where we define:

$$\begin{aligned} P_{\rho_0,k}(\rho_S) &= \int_{\rho_S}^{1-\rho_0} \frac{\mathrm{d}u}{u(u+\rho_0)^k} = \\ &= -\frac{1}{k(u+\rho_0)^k} \left(1 + \frac{\rho_0}{u}\right)^k {}_2F_1\left(k, k; k+1, -\frac{\rho_0}{u}\right)\Bigg|_{\rho_S}^{1-\rho_0} \end{aligned} \tag{4.20}$$

where ${}_2F_1$ is the Gaussian hypergeometric function. Equations 4.19 and 4.20 provide ρ_R for any given ρ_S. For each of these values, ρ_I is calculated as $\rho_I = 1 - \rho_S - \rho_R$, which finally allows the construction of a ρ_I *vs* ρ_R trajectory.

Figure 42 shows the trajectories of the model with system resets, for different values of k. The first outbreak of each execution is represented by solid lines, and are traced using

Equation 4.16. For the executions that did not achieve the herd immunity threshold (which is shown as a black dot-dashed line), subsequent outbreaks are represented by dashed lines and traced using Equations 4.19 and 4.20. In this scenario, stricter contention measures (that is, higher k) always cause smaller infectious peaks, but can generate more secondary outbreaks, making it more difficult to comply with the measures. The inset of Figure 42 shows in more detail the secondary outbreaks for $k = 2, 4$ and 8, where we can see that there are multiple outbreaks with decreasing peak size.

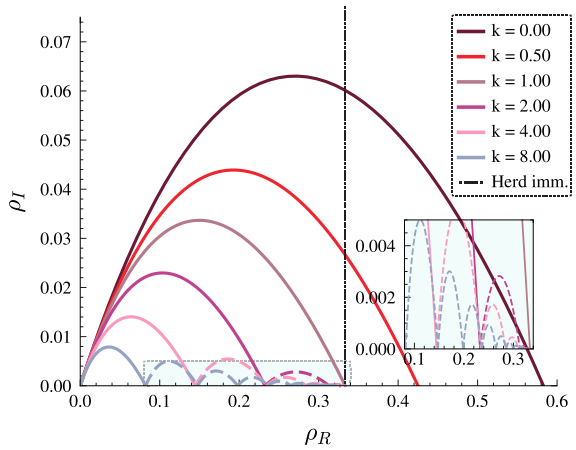

Figure 42 – Analytical trajectories of the homogeneously mixed long-term (LT) scenario with system resets. The first outbreak (solid lines) follows Equation 4.16, while subsequent outbreaks (dashed lines) are traced using Equations 4.19 and 4.20. The inset shows a sub-region of the main plot (indicated by a blue dotted rectangle) where secondary outbreaks are more easily visible, showing how there may be multiple and successively smaller peaks. R_0 is set to 1.5.

Source: VENTURA *et al.*[289]

4.3.2.3 Short-term scenario

For the short-term (ST) scenario, the coefficient of contact reduction depends only on ρ_I, being written as $a(\rho_I) = (1 - \rho_I)^k = (\rho_R + \rho_S)^k$. This breaks the separability of the differential equation obtained by dividing Equations 4.11 and 4.13, leaving no simple method to solve it for arbitrary values of k. We can still use a classic Runge-Kutta[100] of order 4(5) to integrate the equations in time, and plot the ρ_I *vs* ρ_R trajectories.

Figure 43 shows the numerically solved trajectories of the system for different values of k. The main difference with respect to the LT scenario is that the system eventually reaches the herd immunity condition within the first and only outbreak. Higher values of k reduce the size of the peak in ρ_I, at the expense of larger time-span in which the contention measures have to be sustained. This cannot be visualized in Figure 43 as the time parameter is implicit, but we further explore the interplay between peak size and time span in section 4.3.4.1. Note also

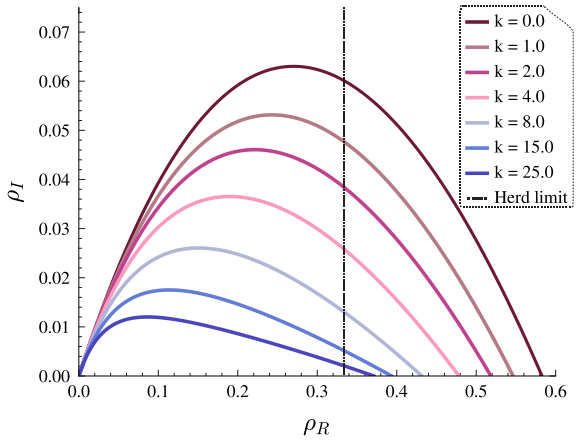

Figure 43 – Numerical trajectories of the homogeneously mixed short-term (ST) scenario, obtained from Runge-Kutta integration of Equations 4.11 to 4.13 starting with $\rho_I(0) = 1 \cdot 10^{-5}$ and $\rho_R(0) = 0$. R_0 is set to 1.5. Unlike the LT scenario, the system always reaches the herd immunity condition in a single outbreak, without considering any modification to the baseline model.

Source: VENTURA *et al.*[289]

that even for very large values of k the final fraction of removed individuals is beyond the herd immunity threshold.

4.3.3 Global strategies and the heterogeneity of local features

The previous analysis has shown that, even if local disease extinction might be achievable with social distancing, it renders the system vulnerable to further reintroductions of the pathogen. Thus, if mobility between subpopulations is allowed, there could be spill overs from those with still ongoing outbreaks to those which contained the epidemic. To study this type of events, we now focus on the proposed model in a metapopulation using Monte Carlo simulations, with the algorithm described in section 4.3.1. For the metapopulation, we use a typical sample of a random geometric network (RGN) of $V = 50$ subpopulations, constructed in a square space of length 1 and connecting subpopulations that are closer than $d = 0.25$. At this initial point, all links are unweighted and reciprocal. This gives an expected average degree of $V\pi d^2 \approx 9.82$, though the specific realization we used through this section has an average degree of 7.2. We choose such a network topology because it emulates the spatial distribution of cities in small to mid scale, where size hierarchy and long-range links are not very present.

Once this unweighted graph is constructed, we set the initial population of each subpopulation i proportional to its degree k_i, according to $N_i(0) = \lfloor N_{pop} k_i/(2M) \rfloor$, where we set $N_{pop} = 10^7$. This makes the overall population to be not exactly equal but very close to N_{pop}, only deviated due to truncation. Then we set the weights of existing links between subpopulations i and j as $T_{ij} = N_i(0)N_j(0)/N_{pop} = T_{ji}$. Within this scheme, the local population sizes

fluctuate around $N(0)$ over time, as explained before. Moreover, the most connected subpopulations are also most populous ones, though the RGN is reasonably homogeneous in this sense. For consistency of the results, we also use a fixed subpopulation as the seed of the disease, seeding 10 infectious individuals at the beginning of the simulations, with all other subpopulations starting with susceptibles only. The seeded subpopulation was chosen to be around the center of the square space.

4.3.3.1 Long-term (LT) global scenario

For the long-term (LT) scenario with global information, we can compare the outcomes of the simulations with those of a constant response after a threshold (explained in section 4.3.1.1). Figure 44 shows the outbreak size (total number of infected individuals) in each subpopulation for the two strategies, each one averaged over 1000 independent executions. The constant coefficient of contact reduction $a_0 = 0.78$ was chosen to yield a global outbreak size of ~ 0.20, approximately equal to that obtained with the LT global scenario with $k = 2$. We notice that the LT scenario provides more heterogeneous outcomes between subpopulations compared to the constant response. Specially, as it can be seen in Figure 45, subpopulations that are farther from the seed tend to have smaller outbreak sizes. This happens because, in the global LT scenario, the intensity of contention measures due to public awareness is the same for all subpopulations and increases with time, thus subpopulations that are seeded later have smaller effective reproduction numbers.

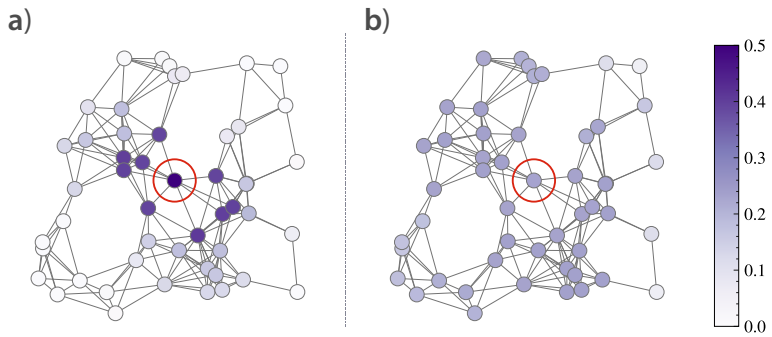

Figure 44 – Comparison of the average outbreak size in each subpopulation between a) global LT scenario and b) global constant response with threshold. For the LT scenario, a response strength $k = 2$ was used, while the constant response uses $a_0 = 0.78$ and a threshold of $\varepsilon_I = 10^{-3}$, meaning that the contact reduction is triggered after 10^4 overall infections (out of $N_{pop} = 10^7$ individuals) are registered. Both simulations use $\tau = 1 \cdot 10^{-3}$ as the travel parameter.

Source: VENTURA *et al.*[289]

The fact that our proposed model for behavioral responses with global strategy produces more heterogeneous outbreak sizes is notorious, as this is generally observed after outbreaks of

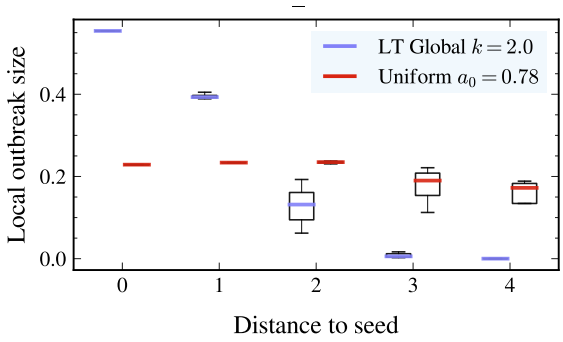

Figure 45 – Local outbreak size (given by the maximum of R_i/N_i over time) in each subpopulation as a function of its shortest path length to the seed, for global LT scenario with response strength $k = 2$ (circles) and for constant response with factor $a_0 = 0.78$ (squares). The y-axis values represent averages over 1000 independent executions. The boxes show the inner quartiles of each set. The mobility coefficient is set to $\tau = 1 \cdot 10^{-3}$.

Source: VENTURA *et al.*[289]

real diseases. In particular, this situation is compatible with the one observed in 2020 during the COVID-19 pandemic in those countries that imposed strict global lockdowns even if only part of the country was severely affected.[292–294]

4.3.4 The efficiency of local and global strategies

We now describe a framework to compare local and global strategies in terms of their efficiency, characterized by the costs and benefits of each strategy in each scenario. Direct comparison of simulations with global and local strategies using the same response strength k is inappropriate, as global strategies require greater values of k to yield similar effects. We therefore define two metrics, one for the cost and another for the effectiveness, and compare local and global strategies in parametric plots of such metrics (with k as an implicit parameter). As long-term and short-term strategies are qualitatively different, we apply different metrics to characterize each one.

4.3.4.1 Short-term (ST) scenario

The short-term scenario, in which the contact reduction coefficient only responds to the (either local or global) density of infectious individuals, is characterized by a slow progression of the system towards its herd immunity. A higher value of the response strength k represents a more effective response, which reflects into a smaller prevalence peak (i.e., the maximum ρ_I) yet longer outbreak duration. The outbreak size (i.e., maximum of ρ_R) however does not vary much with k, as it essentially depends on the herd immunity limit of the system. Therefore, the infectious peak size $\rho_I^{\max}$ is a reasonable measure of effectiveness in this case, with smaller peaks attributed to more effective strategies.

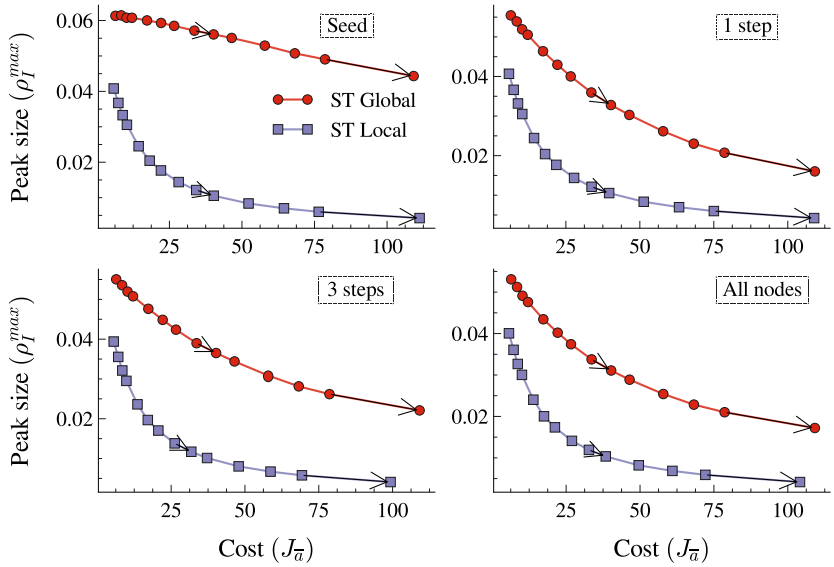

Figure 46 – Parametric curves for the effectiveness and cost of local and global ST scenario, for values of k ranging from 3 to 90. The first plot is for the seeded subpopulation, whereas other plots are arithmetic averages over sets of subpopulations according to their shortest path length to the seeded subpopulation. The last (lower right) plot is an arithmetic average over all subpopulations. The arrows indicate the direction towards which k increases. The mobility factor is set to $\tau = 1 \cdot 10^{-3}$. The metric $\rho_I^{\max}$ is the maximum over time of the local infection prevalence ρ_I, while J is given by Equation 4.21.

Source: VENTURA *et al.*[289]

Higher values of k also imply more time in which contention measures are active to control disease propagation. This translates into a_i being smaller than 1 during longer times. We can quantify "how much and for how long" the contention measures are applied with the quantity:

$$J_i = \sum_{t=0}^{\infty} (1 - a_i(t)) \tag{4.21}$$

which accounts for the intensity and time span of the contact reduction. This provides, in a broad sense, a metric for the cost of the short term scenario, considering that contention measures typically bring social and economical costs to the population. Notice that these metrics must be calculated for each subpopulation.

For the same population and RGN structure described in section 4.3.3, we compare local and global strategies with respect to $\rho_I^{\max}$ and J for simulations with different values of k. Figure 46 shows the plots of these metrics against each other, grouped by sets of subpopulations according to their distance to the seeded subpopulation. The metric values are averaged over 1000 independent executions.

From the plots, it is clear that local strategies outperform global ones for all subpopulations, as the former produces much smaller peaks sizes for similar values of J in the considered range. This means that, for the ST scenario, the use of local information about contagions is more efficient than using a unified, global strategy. This happens because using global information may not be well suited for the epidemic situation of a given subpopulation. For instance, subpopulations that are far from the seed effectively apply the contention measures before the epidemic arrives, but as these measures are relaxed at some moment (when the global prevalence decreases), these subpopulations will still undergo an intense outbreak, given that they were only subject to minor outbreaks and the majority of the individuals in these subpopulations are susceptible.

Although we only display the results for a single value of the mobility coefficient $\tau = 10^{-3}$, the same conclusions are obtained for $\tau = 10^{-2}$ and 10^{-4}, but the advantage of local strategies over global ones is more pronounced with lower mobility rates. This is expected, because with lower τ values, the dynamics of each subpopulation is less coupled by mobility, making local strategies more practical.

4.3.4.2 Long-term (LT) scenario

In the long-term scenario, the overall intensity of contention measures increases with time (though it can locally decrease due to migration), as they are proportional to both I and R densities. As shown in section 4.3.2 for homogeneous mixing, for sufficiently high k, the epidemic spreading is halted before herd immunity is achieved, leaving the system vulnerable to secondary waves in case of a system release without other immunization policies. We can still characterize the effectiveness of the strategy in this first wave, either by its outbreak size ($\rho_R^{\max}$) or by the peak size ($\rho_I^{\max}$). For consistency with section 4.3.4.1, we chose to work with $\rho_I^{\max}$ as well.

For the cost of the strategy, J (given by Equation 4.21) does not provide a reliable measure, as in this case a_i does not tend to 1 again at the end of the main outbreak, making J overly sensitive to the time taken until the epidemic vanishes. We choose instead to simply work with $\overline{a}_{\max} = 1 - \min a(t)$, which is the maximum level of contact reduction adopted by the subpopulation during the simulation. This metric disregards the temporal evolution of a_i, but still provides a number that is proportional to the social costs of contention measures adopted.

Using the same RGN setup, we find that the cost *vs* effectiveness curves are more complex for the LT scenario than for the ST one. Figure 47 shows the $\rho_R^{\max}$ x $\overline{a}_{\max}$ parametric curves for local and global strategies, and for three values of the mobility master parameter $\tau = 10^{-2}$, 10^{-3} and 10^{-4}. In this case, there is not a clear advantage of local strategies over global ones, and this depends both on mobility levels and the distance to the seed. For instance, when $\tau = 10^{-2}$ (Figure 47.a)), a local strategy is better for the seed, while it is generally worse for more distant subpopulations. For immediate neighbors of the seed (one step away), the curves cross each

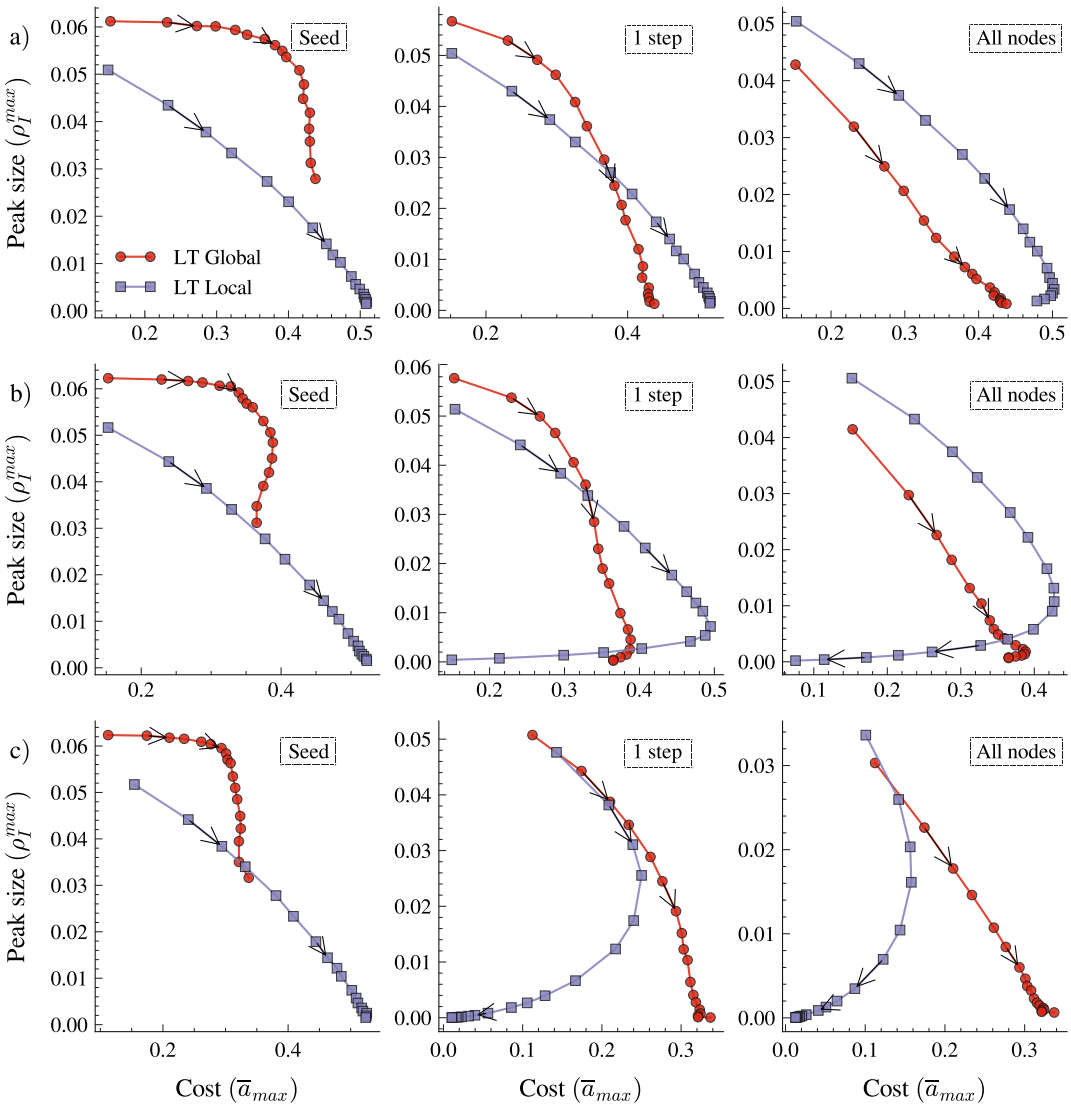

Figure 47 – Parametric curves for the effectiveness and cost of local and global LT strategy, for the mobility parameter (a) $\tau = 10^{-2}$, (b) $\tau = 10^{-3}$ and (c) $\tau = 10^{-4}$. The k values range from 0.25 to 50. The leftmost panels represent the seeded subpopulation, the middle panels represent an arithmetic average over its immediate neighbors, and the rightmost panels show the averages over all subpopulations. The arrows indicate the direction towards which k increases. The cost $\overline{a}_{\text{max}}$ is the maximum value of $1 - a_i$ reached during the simulation.

Source: VENTURA *et al.*[289]

other, making the optimal strategy to depend on the value of k.

For lower mobility values (Figure 47.b) and c)), another interesting feature is evident: the curves for the local strategies are not monotonic with the cost, meaning that two strategies (given by two different values of k) may have the same cost but notably different effectiveness. This happens because the LT strategy can affect the invasion threshold and attack rate of the system,[256] preventing some subpopulations from being reached by the disease for sufficiently high k. In this case, as the strategy is based on local prevalences, these subpopulations will not have to implement contention measures, which explains the decrease in the strategy cost.

4.3.5 Local and global strategies on real topologies

The results from the previous section are highly relevant from a theoretical perspective. They unveil interesting behaviors for when the system is close or not much above its invasion threshold, a theoretical value of mobility in which the disease no longer propagates between subpopulations. However, human mobility flows in almost any realistic scenario puts the system far above its invasion threshold, even when considerable travel restrictions are employed. Therefore, we still need to study our model in a more realistic setup.

Instead of simply adjusting the travel coefficient τ of our RGN to match that of some real system, we decided to directly simulate our model in metapopulations created from real mobility data. For this, we successfully gathered data from two countries that are significant different in scale and demographics: Spain and Brazil.

The Spanish metapopulation was reused from a recent work from our collaborators, Alberto Aleta and Yamir Moreno.[265] The mobility was retained from a pilot project of the country's Ministry of Development, built using mobile phone data from 16 million users (from a total estimated population of ~ 47 millions inhabitants). The used data was acquired during the last two weeks of October 2017, then averaged and symmetrized to be used as a metapopulation. Each subpopulation represents one of the 47 mainland provinces, 3 island provinces and 2 autonomous cities, in a total of 52 subpopulations, for which the number of inhabitants was provided by the Spanish Statistical Office.

The Spanish mobility matrices consider all transportation means, and the flows are renormalized for a very confident overall picture of the country's mobility. For Brazil, however, we could not access a publicly available dataset as complete as that from Spain. Instead, we aggregated mobility data from three different datasets: (i) passenger and cargo flights from the *National Agency of Civil Aviation* (ANAC); (ii) interstate passenger buses from the *National Agency of Terrestrial Transport* (ANTT); (iii) daily commuters, from a survey of pendular migration promoted by the Brazilian Institute of Geography and Statistics (IBGE) as part of its national census of 2010. The mobility data from sources (i) and (ii) were averaged during the whole year of 2019, then renormalized to daily flows and symmetrized to weight the links of the metapopulation. The subpopulations, in this case, represent the 27 federative units of the

country, of which population data was also provided by IBGE.

Even though the Brazilian dataset does not represent the totality of the country's mobility, we believe that it still represents well the relative flows. We repeated our simulations with a 150% multiplier on the travel fluxes, but observed no qualitative changes in results.

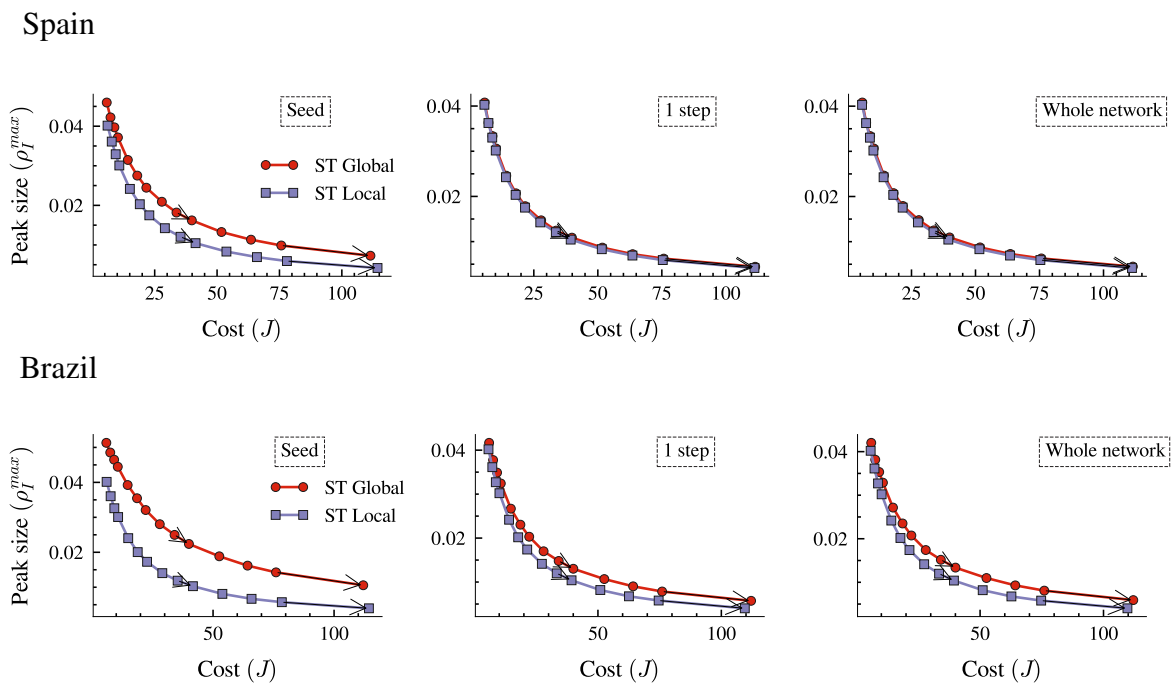

Figure 48 – Parametric effectiveness/cost curves of local and global strategies with ST scenario, using metapopulations from real data (upper plot: Spain; lower plot: Brazil). As every subpopulation is connected by at least one traveler, they are all one step far from the seed. Each point is an average over 1000 executions.

Source: VENTURA *et al.*[289]

Once the real data is converted into metapopulations, the simulation procedure follows the same as in section 4.3.4. We compared local and global strategies for the ST and LT scenarios, using the appropriate metrics in each case. Figures 48 and 49 show the results both for the Brazilian (upper plots) and Spanish (lower plots) datasets. In both countries, the seeded subpopulation is the most populous one: São Paulo state for Brazil, and Madrid for Spain.

Multiple insights can be extracted from the plot of results. First, for the ST scenario, the conclusion that a local intervention strategy is better than a global one remains valid, although the difference between them is smaller than in our theoretical setup, especially for Spain. Second, the LT scenario now presents a simpler conclusion: local strategies are better for the seeded subpopulation, while global ones are better for the other regions. This result is reasonable because, in a global strategy, distant subpopulations anticipate the arrival of the disease in a global scheme, reducing the peak size. However, the seeded subpopulation must act earlier, thus mak-

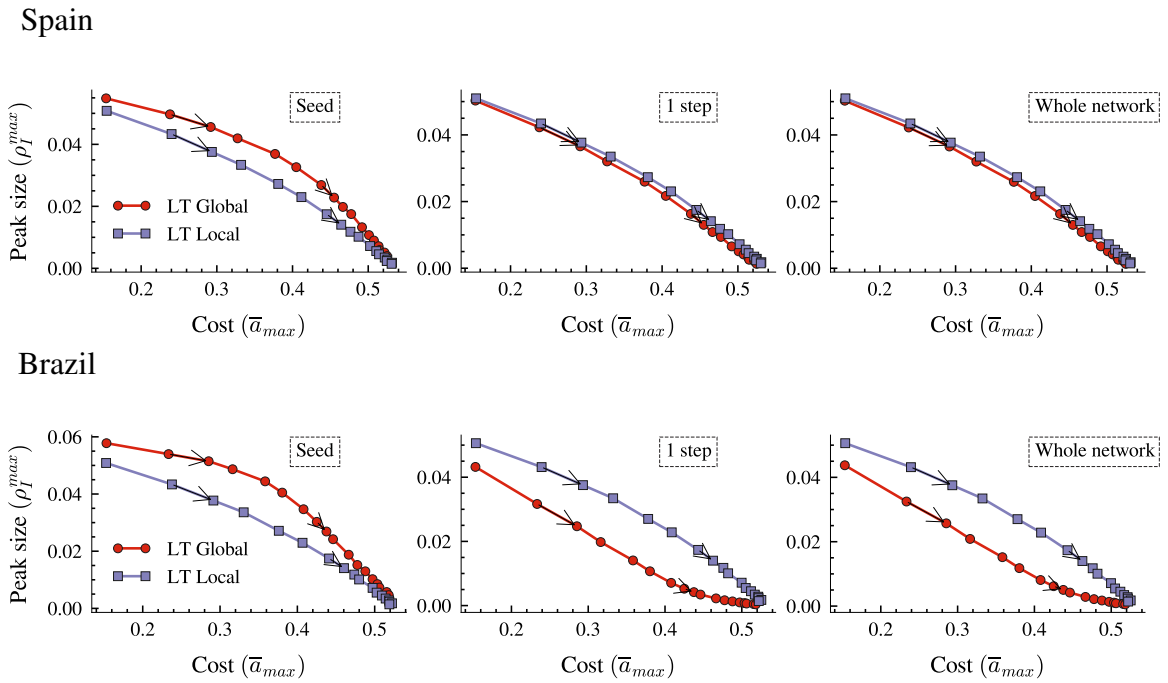

Figure 49 – Parametric effectiveness/cost curves of local and global strategies with LT scenario, using metapopulations from real data (upper plot: Spain; lower plot: Brazil). As every subpopulation is connected by at least one traveler, they are all one step far from the seed. Each point is an average over 1000 executions.

Source: VENTURA *et al.*[289]

ing a local strategy more plausible. We postulate that a strategy in which the seeded subpopulation locally implements strong contention measures while other subpopulations implement milder measures in a global scheme can overcome the results of pure local/global strategies.

Finally, an important insight is about the idea of *scale*. The differences between global and local strategies are clearly milder in the Spanish metapopulation than in the Brazilian one. In a broad sense, this means that our conclusions are more relevant for populations of larger scales. In more depth, notice that Brazil has a larger population and geographical extension then Spain, with mobility between federative units proportionally smaller from those between Spanish provinces. Besides, in our dataset, the larger Brazilian subpopulation has roughly the same population of the whole Spain, meaning that the former is a coarser representation of reality. It is intuitive to conclude that global and local strategies will diverge more for populations of larger scale.

4.3.6 Discussions

We have presented a model that incorporates dynamical behavioral responses to epidemics, which could be driven by governmental policies or by the endogenous response of

individuals (e.g. fear of infection), in the context of metapopulations. The emerging features of the model are very rich, showing a complex landscape of outcomes depending on the implemented strategy.

First, we have shown that for isolated populations, strong and long lasting social distancing measures (LT) are able to ablate the epidemic, however leave the population vulnerable to secondary outbreaks. Indeed, as long as the prevalence is below the herd immunity threshold, a reintroduction of the pathogen after the measures are lifted will lead to a second wave. On the other hand, soft social distancing measures (ST), aimed at reducing the peak without eradicating the disease, contain the exponential growth of the epidemic and leave the system over the herd immunity threshold, preventing further outbreaks. Note, however, that for a severe disease in which the infection fatality rate is substantial, larger prevalence implies a larger number of deaths. Thus, stronger social distancing policies will reduce the number of deaths at the expense of leaving the system vulnerable, while softer measures will control the spread but increase the number of deaths. These observations are particularly important in the context of metapopulations. Since subpopulations are not isolated, in the absence of additional control measures, the disease might be seeded again in disease-free areas by individuals who where infected in other regions. Thus, besides long and short term strategies, we also need to incorporate whether the contention measures use global or local information.

We compared the LT and ST scenarios of our model, in an attempt to address the question of whether the contention measures are more efficient if implemented and managed locally (at each subpopulation) or globally (equally to the whole population). For the ST strategy, we measured its cost by the J metric that quantifies the intensity and duration of the contention measures, and used the maximum number of simultaneous infections (i.e., the peak size) to quantify the strategy's performance. We showed that the local strategy always outperformed the global one, which is valid for any value of the mobility parameter. This also holds for real network topologies, although the difference is milder in a smaller scale country like Spain.

For the LT scenario, we quantified the cost by the maximum intensity reached by the contention measures, and the performance by the peak size. In this case, the cost/benefit relationship was more complex, and depended on the mobility rate and the distance to the seeded subpopulation. Global strategies are generally better for distant subpopulations (with respect to the seed). This situation was precisely the one that emerged in the first wave of infections in 2020 during the COVID-19 pandemic in countries that imposed country-wide lockdowns even if only one region was severely affected.[292–294] Yet, this is reversed if the mobility is low enough so that the local strategy can stop the epidemics before these nodes are reached. For the seeded subpopulation, local strategies are typically preferred, while global strategies are better for more distant subpopulations. This was also backed up by the results with real networks. For this type of scenario, therefore, the choice between global and local strategies is not trivial and should be addressed appropriately.

5 CONCLUSIONS

At this point, we are ready to recall our main goals for the present thesis, as well as how we made our way into achieving them. The common objective for all of our works was to address the problem of host behavioral reactions to the spreading of epidemics, through mathematical and computational modeling. This goal was sought in a variety of situations and approaches, which resulted in multiple works, not all of them presented in this thesis. Each work had its own set of specific goals which, together with the main goal, created an audacious research schedule.

As discussed in the introduction (Chapter 1), behavioral responses to epidemics may come in a great variety of ways. Complexity science and network science come as great tools to assess this problem, providing methods to deal with the complexity and chaoticity of interactions and behaviors of host populations. We hope that the arguments presented in the introduction were sufficient to motivate the reader to understand in more detail complex systems and the problem of disease-behavior dynamics.

In Chapter 2, we introduced the fundamentals of two important fields to our work: complex networks and epidemic models. In Section 2.1, we presented the basic and extended definitions of networks, some important statistical metrics and the fundamental models used to build synthetic networks. In Section 2.2, we presented multiple approaches to implement and study epidemic models: homogeneously mixed rate equations, heterogeneous mean field, quenched mean field, Markov chain approach and stochastic simulations. We mostly used the SIS model to exemplify each approach, as it is the most used model through our work, but the formulations are also applicable to the SIR-like model family. We hope that this Chapter of fundamentals can be useful for new researchers from both epidemiology and complex networks, even if their research interests are different than ours.

Following up, we divided our selected research work into two major chapters, according to their common points. In Chapter 3, we discuss epidemic dynamics that interact. In the literature review (Section 3.1), we present a great range of works regarding (i) the interaction between two or more spreading processes, and (ii) the interaction between diseases and human behavior in multiple aspects. Even though these two topics deal, in practice, with different problems, we believe that they should be seen as adjacent in a theoretical point of view, because they deal with closely related models and often come to overlapping conclusions.

Our first contribution, described in Section 3.2, is a great example of this proximity: it deals with both interacting spreading phenomena and disease-behavior coupling. We study an epidemic model with information-based awareness, by which individuals try to protect themselves from infection. We tackle two research gaps of the field by that time: (i) the inclusion

of stiflers and a rumor-like recovery transition, and (ii) the role of the epidemic-to-information relative time scale. We found that, when the information runs at a longer time scale (intrinsic clock) than the epidemics, it is more effective at reducing the disease prevalence, in agreement with another recent work.[187] Moreover, with a modification to the basic model, we found that it is possible that, for the same disease, one population can be more informed than another but still have greater disease prevalence; this is an effect of adding stiflers to the information model, which hinders its propagation. These conclusions further advance our understanding of the disease-information interaction, and the work is published in Physical Review E,[182] with a sequel in the same journal.[186]

After this work, we kept our motivation on the subject and decided to better understand the gaps left from it. Could the relationship between prevalence and relative time scale be an artifact of the specific model that we constructed? Did it depend on the multiplex topology? We addressed these questions by first "downgrading" from multiplex networks to homogeneously mixed populations, and then looking at different models to investigate the time scale relationship. These models should consider an asymmetric interaction between two spreading agents and, after some preliminary research, we ended with two representative models: model A, similar to that of our first work, and model B, which implemented the asymmetrical interaction in a different fashion.

These two models were found to present different behaviors regarding the relative time scale and the prevalence of the "prey" disease. This did not invalidate the results of our first work, but pointed that they were not valid for all classes of asymmetrically interacting models. As the same effect of our awareness model was observed for a homogeneously mixed population, we also concluded that it was intrinsic to the model and not an effect of topology. Finally, we used the achieved momentum to further investigate these models. We numerically evaluated their transient oscillations, determined a global maximum for model B, and derived analytical expressions that show the robustness of our conclusions. We believe that this work can be of great use for researchers interested in asymmetrical contagion, either between diseases, between disease and information, or any other similar system.

In Chapter 4, we dive into another important topic: host mobility. In general, mobility is known to promote disease spreading, and understanding its patterns is crucial to study the geographical disease spreading, such as in the Black Death example. We merge host behavior with host mobility using two different approaches: individual mobility models and net mobility flows. In our literature review (Section 4.1), we first present how scientists have tried to capture human and animal mobility with models, and then discuss the literature on epidemic models both at the individual level and with metapopulations.

Both of our works on the topic of mobility were started during an internship in Zaragoza – Spain.In the first one, we adapted a previously implemented model of random walking agents to include a social distancing-alike behavioral response. We used the literature on adaptive

networks, started by Gross and others,[73] as a guideline to our model. Despite some considerable differences, we could reproduce the bistable behavior reported with adaptive networks and caused by increased clustering of susceptible individuals when avoiding infectious ones. We developed a semi-analytical approach, decoupling the mobility and epidemic dynamics, which allowed us to precisely determine the phase diagrams and bifurcations of the system, as well as to relate its phenomenology to some network metrics. This is a notorious achievement, as epidemics with random walking agents can rarely be approached beyond the basic homogeneous mixing hypothesis.

Moving to our latest described work (in Section 4.3), we address behavioral responses to epidemics in metapopulations, which are massively used in realistic epidemic simulations. By adapting a model for contention measures first proposed in homogeneously mixed populations,[89] we show that behavioral responses produce heterogeneous outbreak sizes through subpopulations, contrasting with a simple reduction to the reproduction number, which is a widely used approach. We then use our framework to compare the effectiveness of employing the contention measures locally and globally, using both scenarios proposed by Eksin.[89] We conclude that, in the ST scenario (where the prevalence can be controlled until natural herd immunity is produced), it is always better to use a local strategy, while in the LT scenario (where the contention measures seek to extinguish the disease until artificial immunization is available), the choice between global and local intervention depends on many factors and details, with a global scheme in general being better for network as a whole but worse for the seeded subpopulations. These results are further validated by the use of data-driven metapopulations of Spain and Brazil.

After reviewing our work, we are confident that we contributed to the problem of disease-behavior coupling in multiple theoretical contexts. Each of our works provided valuable knowledge on how to model these situations, and we expect that this knowledge can be used by other researchers. We also provided some insights about the situations that we model, such as the “more informed yet more infected population” effect described in Section 3.2, and the evaluation of local and global strategies with the metapopulation model.

Yet in the theoretical domain, we unveil many open questions and follow-ups from our works, which are described in the discussions of each corresponding sections. Most of all, our greatest hope is that our contributions can be utilized by researchers that work with more realistic epidemic models. These, as we are witnessing, can have very prominent impacts into policy-making, resource planning and even individual attitude against infectious diseases, paving the way to a more developed society.

REFERENCES

1 SANZ, J. *et al.* Dynamics of interacting diseases. **Physical Review X**, v. 4, n. 4, p. 041005, 2014.

2 FU, F. *et al.* Imitation dynamics of vaccination behaviour on social networks. **Proceedings of the Royal Society B**, v. 278, n. 1702, p. 42–49, 2011.

3 SONG, C. *et al.* Modelling the scaling properties of human mobility. **Nature Physics**, v. 6, n. 10, p. 818–823, 2010.

4 FRASCA, M. *et al.* Dynamical network model of infective mobile agents. **Physical Review E**, v. 74, n. 3, p. 036110, 2006.

5 BUSCARINO, A. *et al.* Disease spreading in populations of moving agents. **Europhysics Letters**, v. 82, n. 3, p. 38002, 2008.

6 WATTS, D. J.; STROGATZ, S. H. Collective dynamics of 'small-world' networks. **Nature**, v. 393, n. 6684, p. 440–442, 1998.

7 ANDERSON, P. W. More is different: broken symmetry and the nature of the hierarchical structure of science. **Science**, v. 177, n. 4047, p. 393–396, 1972.

8 ANDERSON, P. W. Is complexity physics? Is it science? What is it? **Physics Today**, v. 44, n. 7, p. 9–11, 1991.

9 IÑIGUEZ, G.; BATTISTON, F.; KARSAI, M. Bridging the gap between graphs and networks. **Communications Physics**, v. 3, n. 1, p. 1–3, 2020.

10 SPORNS, O. Contributions and challenges for network models in cognitive neuroscience. **Nature Neuroscience**, v. 17, n. 5, p. 652–660, 2014.

11 VITALI, S.; GLATTFELDER, J. B.; BATTISTON, S. The network of global corporate control. **Plos One**, v. 6, n. 10, p. e25995, 2011.

12 HIDALGO, C. A.; HAUSMANN, R. The building blocks of economic complexity. **Proceedings of the National Academy of Sciences**, v. 106, n. 26, p. 10570–10575, 2009.

13 CHRETIEN, J.-P. *et al.* Influenza forecasting in human populations: a scoping review. **Plos One**, v. 9, n. 4, p. e94130, 2014.

14 DESAI, A. N. *et al.* Real-time epidemic forecasting: challenges and opportunities. **Health Security**, v. 17, n. 4, p. 268–275, 2019.

15 ROSTER, K.; CONNAUGHTON, C.; RODRIGUES, F. A. Predicting dengue fever in brazilian cities. **bioRxiv**, 2021. Available at: https://www.biorxiv.org/content/10.1101/2021.02.17.430949v1. Access at: 28 Nov. 2021.

16 PASTOR-SATORRAS, R. *et al.* Epidemic processes in complex networks. **Reviews of Modern Physics**, v. 87, n. 3, p. 925–979, 2015.

17 DALEY, D. J.; KENDALL, D. G. Stochastic rumours. **IMA Journal of Applied Mathematics**, v. 1, n. 1, p. 42–55, 1965.

18 FUNK, S. *et al.* Nine challenges in incorporating the dynamics of behaviour in infectious diseases models. **Epidemics**, v. 10, p. 21–25, 2015.

19 MORAN, K. R. *et al.* Epidemic forecasting is messier than weather forecasting: the role of human behavior and internet data streams in epidemic forecast. **The Journal of Infectious Diseases**, v. 214, n. Suppl 4, p. S404–S408, 2016.

20 HOLLAND, P. W.; LEINHARDT, S. Transitivity in structural models of small groups. **Comparative Group Studies**, v. 2, n. 2, p. 107–124, 1971.

21 TILMAN, D. Competition and biodiversity in spatially structured habitats. **Ecology**, v. 75, n. 1, p. 2–16, 1994.

22 MAY, R. M.; NOWAK, M. A. Superinfection, metapopulation dynamics, and the evolution of diversity. **Journal of Theoretical Biology**, v. 170, n. 1, p. 95–114, 1994.

23 BARABÁSI, A. L.; ALBERT, R. Emergence of scaling in random networks. **Science**, v. 286, n. 5439, p. 509–512, 1999.

24 BOCCALETTI, S. *et al.* Complex networks: structure and dynamics. **Physics Reports**, v. 424, n. 4, p. 175–308, 2006.

25 ALBERT, R.; BARABÁSI, A. L. Statistical mechanics of complex networks. **Reviews of Modern Physics**, v. 74, n. 1, p. 47–97, 2002.

26 NEWMAN, M. E. J. **Networks**: an introduction. New York: Oxford University Press, 2010. ISBN 978-0-19-920665-0.

27 DOROGOVTSEV, S. N.; GOLTSEV, A. V.; MENDES, J. F. F. Critical phenomena in complex networks. **Reviews of Modern Physics**, v. 80, n. 4, p. 1275–1335, 2008.

28 COSTA, L. F. *et al.* Analyzing and modeling real-world phenomena with complex networks: a survey of applications. **Advances in Physics**, v. 60, n. 3, p. 329–412, 2011.

29 BARABÁSI, A. L.; PÓSFAI, M. **Network science**. Cambridge: Cambridge University Press, 2016. ISBN 978-1-107-07626-6.

30 NEWMAN, M. E. J. The structure and function of complex networks. **SIAM Review**, v. 45, n. 2, p. 167–256, 2003.

31 BAVELAS, A. Communication patterns in task-oriented groups. **The Journal of the Acoustical Society of America**, v. 22, n. 6, p. 725–730, 1950.

32 WASSERMAN, S.; FAUST, K. **Social network analysis**: methods and applications. Cambridge: Cambridge University Press, 1994. (Structural analysis in the social sciences, 8). ISBN 978-0-521-38269-4.

33 HOLME, P. Congestion and centrality in traffic flow on complex networks. **Advances in Complex Systems**, v. 6, n. 2, p. 163–176, 2003.

34 BONACICH, P. Factoring and weighting approaches to status scores and clique identification. **The Journal of Mathematical Sociology**, v. 2, n. 1, p. 113–120, 1972.

35 MARCHIORI, M.; LATORA, V. Harmony in the small-world. **Physica A**, v. 285, n. 3, p. 539–546, 2000.

36 MARTIN, T.; ZHANG, X.; NEWMAN, M. E. J. Localization and centrality in networks. **Physical Review E**, v. 90, n. 5, p. 052808, 2014.

37 NEWMAN, M. E. J. Assortative mixing in networks. **Physical Review Letters**, v. 89, n. 20, p. 208701, 2002.

38 NEWMAN, M. E. J. Mixing patterns in networks. **Physical Review E**, v. 67, n. 2, p. 026126, 2003.

39 JEONG, H. *et al.* Lethality and centrality in protein networks. **Nature**, v. 411, n. 6833, p. 41–42, 2001.

40 ERDŐS, P.; RÉNYI, A. On random graphs, I. **Publicationes Mathematicae**, v. 6, p. 290–297, 1959.

41 ERDŐS, P.; RÉNYI, A. On the evolution of random graphs. **Publication of the Mathematical Institute of the Hungarian Academy of Sciences**, v. 5, n. 1, p. 17–60, 1960.

42 ERDŐS, P.; RÉNYI, A. On the evolution of random graphs. **Bulletin de l'Institut International de Statistique**, v. 38, n. 4, p. 343–347, 1961.

43 ERDŐS, P.; RÉNYI, A. On the strength of connectedness of a random graph. **Acta Mathematica Academiae Scientiarum Hungaricae**, v. 12, n. 1-2, p. 261–267, 1964.

44 REDNER, S. How popular is your paper? An empirical study of the citation distribution. **The European Physical Journal B**, v. 4, n. 2, p. 131–134, 1998.

45 ALBERT, R.; JEONG, H.; BARABÁSI, A. L. Diameter of the World-Wide Web. **Nature**, v. 401, n. 6749, p. 130–131, 1999.

46 MOLLOY, M.; REED, B. A critical point for random graphs with a given degree sequence. *In*: NEWMAN, M.; BARABÁSI, A. L.; WATTS, D. J. (ed.). **The structure and dynamics of networks**. 2nd. ed. Princeton: Princeton University Press, 2011. p. 240–258. ISBN 978-1-4008-4135-6.

47 MOLLOY, M.; REED, B. The size of the giant component of a random graph with a given degree sequence. **Combinatorics, Probability and Computing**, v. 7, n. 3, p. 295–305, 1998.

48 CATANZARO, M.; BOGUÑÁ, M.; PASTOR-SATORRAS, R. Generation of uncorrelated random scale-free networks. **Physical Review E**, v. 71, n. 2, p. 027103, 2005.

49 WATTS, D. J. **Six degrees**: the science of a connected age. New York: Norton, 2003. ISBN 978-0-393-04142-2.

50 PENROSE, M. **Random geometric graphs**. New York: Oxford University Press, 2003. (Oxford Studies in Probability, 5). ISBN 978-0-19-850626-3.

51 BIANCONI, G.; GULBAHCE, N.; MOTTER, A. E. Local structure of directed networks. **Physical Review Letters**, v. 100, n. 11, p. 118701, 2008.

52 ZHANG, Q.-M. *et al.* Potential theory for directed networks. **Plos One**, v. 8, n. 2, p. e55437, 2013.

53 FAGIOLO, G. Clustering in complex directed networks. **Physical Review E**, v. 76, n. 2, p. 026107, 2007.

54 LEICHT, E. A.; NEWMAN, M. E. J. Community structure in directed networks. **Physical Review Letters**, v. 100, n. 11, p. 118703, 2008.

55 CSERMELY, P.; ÁGOSTON, V.; PONGOR, S. The efficiency of multi-target drugs: the network approach might help drug design. **Trends in Pharmacological Sciences**, v. 26, n. 4, p. 178–182, 2005.

56 BARTHÉLEMY, M. *et al.* Characterization and modeling of weighted networks. **Physica A**, v. 346, n. 1, p. 34–43, 2005.

57 ALMAAS, E. *et al.* Global organization of metabolic fluxes in the bacterium Escherichia coli. **Nature**, v. 427, n. 6977, p. 839–843, 2004.

58 BARMAK, D. H. *et al.* Dengue epidemics and human mobility. **Physical Review E**, v. 84, n. 1, p. 011901, 2011.

59 MAROTTA, L. *et al.* Bank-firm credit network in Japan: an analysis of a bipartite network. **Plos One**, v. 10, n. 5, p. e0123079, 2015.

60 ZHOU, T. *et al.* Bipartite network projection and personal recommendation. **Physical Review E**, v. 76, n. 4, p. 046115, 2007.

61 DOMENICO, M. D. *et al.* Mathematical formulation of multilayer networks. **Physical Review X**, v. 3, n. 4, p. 041022, 2013.

62 BOCCALETTI, S. *et al.* The structure and dynamics of multilayer networks. **Physics Reports**, v. 544, n. 1, p. 1–122, 2014.

63 KIVELÄ, M. *et al.* Multilayer networks. **Journal of Complex Networks**, v. 2, n. 3, p. 203–271, 2014.

64 NICOSIA, V. *et al.* Collective phenomena emerging from the interactions between dynamical processes in multiplex networks. **Physical Review Letters**, v. 118, n. 13, p. 138302, 2017.

65 ARRUDA, G. F. *et al.* Disease localization in multilayer networks. **Physical Review X**, v. 7, n. 1, p. 011014, 2017.

66 HOLME, P.; SARAMÄKI, J. Temporal networks. **Physics Reports**, v. 519, n. 3, p. 97–125, 2012.

67 LI, A. *et al.* The fundamental advantages of temporal networks. **Science**, v. 358, n. 6366, p. 1042–1046, 2017.

68 ANTENEODO, C.; MALMGREN, R. D.; CHIALVO, D. R. Poissonian bursts in e-mail correspondence. **The European Physical Journal B**, v. 75, n. 3, p. 389–394, 2010.

69 STEHLÉ, J.; BARRAT, A.; BIANCONI, G. Dynamical and bursty interactions in social networks. **Physical Review E**, v. 81, n. 3, p. 035101, 2010.

70 STARNINI, M.; BARONCHELLI, A.; PASTOR-SATORRAS, R. Modeling human dynamics of face-to-face interaction networks. **Physical Review Letters**, v. 110, n. 16, p. 168701, 2013.

71 CATTUTO, C. *et al.* Dynamics of person-to-person interactions from distributed rfid sensor networks. **Plos One**, v. 5, n. 7, p. e11596, 2010.

72 STEHLÉ, J. *et al.* Simulation of an SEIR infectious disease model on the dynamic contact network of conference attendees. **BMC Medicine**, v. 9, n. 1, p. 87, 2011.

73 GROSS, T.; D'LIMA, C. J. D.; BLASIUS, B. Epidemic dynamics on an adaptive network. **Physical Review Letters**, v. 96, n. 20, p. 208701, 2006.

74 ZANETTE, D. H.; RISAU-GUSMÁN, S. Infection spreading in a population with evolving contacts. **Journal of Biological Physics**, v. 34, n. 1-2, p. 135–148, 2008.

75 ZHOU, J. *et al.* Epidemic reemergence in adaptive complex networks. **Physical Review E**, v. 85, n. 3, p. 036107, 2012.

76 SAYAMA, H. *et al.* Modeling complex systems with adaptive networks. **Computers & Mathematics with Applications**, v. 65, n. 10, p. 1645–1664, 2013.

77 BERNOULLI, D. Essai d'une nouvelle analyse de la mortalité causée par la petite vérole, et des avantages de l'inoculation pour la prévenir. **Histoire de L'Academie Royale des Sciences:** avec les memoires de mathematique & de physique, pour la meme annee, p. 1–45, 1760.

78 KERMACK, W. O.; MCKENDRICK, A. G. A contribution to the mathematical theory of epidemics. **Proceedings of the Royal Society of London**, v. 115, n. 772, p. 700–721, 1927.

79 ABBEY, H. An examination of the Reed-Frost theory of epidemics. **Human Biology**, v. 24, n. 3, p. 201, 1952.

80 ANDERSON, R. M.; MAY, R. M. **Infectious diseases of humans**: dynamics and control. Oxford: Oxford University Press, 1992. ISBN 978-0-19-854040-3.

81 COSTA, L. F. *et al.* Characterization of complex networks: a survey of measurements. **Advances in Physics**, v. 56, n. 1, p. 167–242, 2007.

82 BALCAN, D. *et al.* Seasonal transmission potential and activity peaks of the new influenza A(H1N1): a Monte Carlo likelihood analysis based on human mobility. **BMC Medicine**, v. 7, n. 1, p. 45, 2009.

83 KRAEMER, M. U. G. *et al.* The effect of human mobility and control measures on the COVID-19 epidemic in China. **Science**, v. 368, n. 6490, p. 493–497, 2020.

84 KEELING, M. J.; ROHANI, P. **Modeling infectious diseases in humans and animals**. Princeton: Princeton University Press, 2008. ISBN 978-0-691-11617-4.

85 KUZNETSOV, Y. A. **Elements of applied bifurcation theory**. 3rd. ed. New York: Springer, 2010. (Applied mathematical sciences, 112). ISBN 978-1-4419-1951-9.

86 FINE, P. E. Herd immunity: history, theory, practice. **Epidemiologic Reviews**, v. 15, n. 2, p. 265–302, 1993.

87 PASTOR-SATORRAS, R.; VESPIGNANI, A. Epidemic spreading in scale-free networks. **Physical Review Letters**, v. 86, n. 14, p. 3200–3203, 2001.

88 CHEN, L.; GHANBARNEJAD, F.; BROCKMANN, D. Fundamental properties of cooperative contagion processes. **New Journal of Physics**, v. 19, n. 10, p. 103041, 2017.

89 EKSIN, C.; PAARPORN, K.; WEITZ, J. S. Systematic biases in disease forecasting – the role of behavior change. **Epidemics**, v. 27, p. 96–105, 2019.

90 VENTURA, P. C.; MORENO, Y.; RODRIGUES, F. A. Role of time scale in the spreading of asymmetrically interacting diseases. **Physical Review Research**, v. 3, n. 1, p. 013146, 2021.

91 PASTOR-SATORRAS, R.; VESPIGNANI, A. Epidemic dynamics and endemic states in complex networks. **Physical Review E**, v. 63, n. 6, p. 066117, 2001.

92 BOGUÑÁ, M.; PASTOR-SATORRAS, R. Epidemic spreading in correlated complex networks. **Physical Review E**, v. 66, n. 4, p. 047104, 2002.

93 MORENO, Y.; GÓMEZ, J. B.; PACHECO, A. F. Epidemic incidence in correlated complex networks. **Physical Review E**, v. 68, n. 3, p. 035103, 2003.

94 GOLTSEV, A. V. *et al.* Localization and spreading of diseases in complex networks. **Physical Review Letters**, v. 109, n. 12, p. 128702, 2012.

95 FERREIRA, S. C.; CASTELLANO, C.; PASTOR-SATORRAS, R. Epidemic thresholds of the susceptible-infected-susceptible model on networks: a comparison of numerical and theoretical results. **Physical Review E**, v. 86, n. 4, p. 041125, 2012.

96 COTA, W.; FERREIRA, S. C.; ÓDOR, G. Griffiths effects of the susceptible-infected-susceptible epidemic model on random power-law networks. **Physical Review E**, v. 93, n. 3, p. 032322, 2016.

97 PASTOR-SATORRAS, R.; CASTELLANO, C. Eigenvector localization in real networks and its implications for epidemic spreading. **Journal of Statistical Physics**, v. 173, n. 3, p. 1110–1123, 2018.

98 CHAKRABARTI, D. *et al.* Epidemic thresholds in real networks. **ACM Transactions on Information and System Security**, v. 10, n. 4, p. 1–26, 2008.

99 MIEGHEM, P. V.; OMIC, J.; KOOIJ, R. Virus spread in networks. **IEEE/ACM Transactions on Networking**, v. 17, n. 1, p. 1–14, 2009.

100 DORMAND, J. R.; PRINCE, P. J. A family of embedded Runge-Kutta formulae. **Journal of Computational and Applied Mathematics**, v. 6, n. 1, p. 19–26, 1980.

101 GOH, K.-I.; KAHNG, B.; KIM, D. Spectra and eigenvectors of scale-free networks. **Physical Review E**, v. 64, n. 5, p. 051903, 2001.

102 DOROGOVTSEV, S. N. *et al.* Spectra of complex networks. **Physical Review E**, v. 68, n. 4, p. 046109, 2003.

103 WANG, Y. *et al.* Epidemic spreading in real networks: an eigenvalue viewpoint. *In*: INTERNATIONAL SYMPOSIUM ON RELIABLE DISTRIBUTED SYSTEMS, 22., 2003. **Proceedings[...]**. Florence, 2003. p. 25–34. ISSN 1060-9857.

104 PASTOR-SATORRAS, R.; CASTELLANO, C. Distinct types of eigenvector localization in networks. **Scientific Reports**, v. 6, n. 1, p. 18847, 2016.

105 SILVA, D. H.; FERREIRA, S. C. Dissecting localization phenomena of dynamical processes on networks. **Journal of Physics:** complexity, v. 2, n. 2, p. 025011, 2021.

106 MATA, A. S.; FERREIRA, S. C. Multiple transitions of the susceptible-infected-susceptible epidemic model on complex networks. **Physical Review E**, v. 91, n. 1, p. 012816, 2015.

107 GOMEZ, S. *et al.* Discrete-time Markov chain approach to contact-based disease spreading in complex networks. **Europhysics Letters**, v. 89, n. 3, p. 38009, 2010.

108 GILLESPIE, D. T. A general method for numerically simulating the stochastic time evolution of coupled chemical reactions. **Journal of Computational Physics**, v. 22, n. 4, p. 403–434, 1976.

109 GILLESPIE, D. T. Exact stochastic simulation of coupled chemical reactions. **The Journal of Physical Chemistry**, v. 81, n. 25, p. 2340–2361, 1977.

110 GILLESPIE, D. T. Approximate accelerated stochastic simulation of chemically reacting systems. **The Journal of Chemical Physics**, v. 115, n. 4, p. 1716–1733, 2001.

111 CASTELLANO, C.; PASTOR-SATORRAS, R. Thresholds for epidemic spreading in networks. **Physical Review Letters**, v. 105, n. 21, p. 218701, 2010.

112 LÜBECK, S.; HEGER, P. C. Universal finite-size scaling behavior and universal dynamical scaling behavior of absorbing phase transitions with a conserved field. **Physical Review E**, v. 68, n. 5, p. 056102, 2003.

113 DICKMAN, R.; TOMÉ, T.; OLIVEIRA, M. J. Sandpiles with height restrictions. **Physical Review E**, v. 66, n. 1, p. 016111, 2002.

114 OLIVEIRA, M. M.; DICKMAN, R. How to simulate the quasistationary state. **Physical Review E**, v. 71, n. 1, p. 016129, 2005.

115 DICKMAN, R.; OLIVEIRA, M. M. Quasi-stationary simulation of the contact process. **Physica A**, v. 357, n. 1, p. 134–141, 2005.

116 MAKI, D. P.; THOMPSON, M. **Mathematical models and applications**: with emphasis on the social, life, and management sciences. Englewood Cliffs: Prentice-Hall, 1973. ISBN 978-0-13-561670-3.

117 ANDREASEN, V.; LIN, J.; LEVIN, S. A. The dynamics of cocirculating influenza strains conferring partial cross-immunity. **Journal of Mathematical Biology**, v. 35, n. 7, p. 825–842, 1997.

118 NUÑO, M. *et al.* On the role of cross-immunity and vaccines on the survival of less fit flu-strains. **Theoretical Population Biology**, v. 71, n. 1, p. 20–29, 2007.

119 NELSON, J. A.; GHAZAL, P.; WILEY, C. A. Role of opportunistic viral infections in AIDS. **AIDS**, v. 4, n. 1, p. 1–10, 1990.

120 KASPER, L. H.; BUZONI-GATEL, D. Some opportunistic parasitic infections in AIDS: candidiasis, pneumocystosis, cryptosporidiosis, toxoplasmosis. **Parasitology Today**, v. 14, n. 4, p. 150–156, 1998.

121 WATT, G.; KANTIPONG, P.; JONGSAKUL, K. Decrease in human immunodeficiency virus type 1 load during acute dengue fever. **Clinical Infectious Diseases**, v. 36, n. 8, p. 1067–1069, 2003.

122 XIANG, J. *et al.* Viruses within the flaviviridae decrease CD4 expression and inhibit HIV replication in human CD4+ cells. **The Journal of Immunology**, v. 183, n. 12, p. 7860–7869, 2009.

123 MOSS, W. J. *et al.* Suppression of human immunodeficiency virus replication during acute measles. **The Journal of Infectious Diseases**, v. 185, n. 8, p. 1035–1042, 2002.

124 MANFREDI, P.; D'ONOFRIO, A. (ed.). **Modeling the interplay between human behavior and the spread of infectious diseases**. New York: Springer, 2013. ISBN 978-1-4614-5473-1.

125 WANG, Z. *et al.* Coupled disease–behavior dynamics on complex networks: a review. **Physics of Life Reviews**, v. 15, p. 1–29, 2015.

126 ELVEBACK, L. *et al.* An extension of the Reed-Frost epidemic model for the study of competition between viral agents in the presence of interference. **American Journal of Epidemiology**, v. 80, n. 3, p. 356–64, 1964.

127 DIETZ, K. Epidemiologic interference of virus populations. **Journal of Mathematical Biology**, v. 8, n. 3, p. 291–300, 1979.

128 CASTILLO-CHAVEZ, C.; HUANG, W.; LI, J. Competitive exclusion in gonorrhea models and other sexually transmitted diseases. **SIAM Journal on Applied Mathematics**, v. 56, n. 2, p. 494–508, 1996.

129 NUÑO, M. *et al.* Dynamics of two-strain influenza with isolation and partial cross-immunity. **SIAM Journal on Applied Mathematics**, v. 65, n. 3, p. 964–982, 2005.

130 FOX, J. P. Interference phenomena observed in the field. *In*: GIBBONS, N. E. (ed.) **Recent Progress in Microbiology**. Toronto: University of Toronto, 1963. cap.9, p. 443.

131 NEWMAN, M. E. J. Threshold effects for two pathogens spreading on a network. **Physical Review Letters**, v. 95, n. 10, p. 108701, 2005.

132 KARRER, B.; NEWMAN, M. E. J. Competing epidemics on complex networks. **Physical Review E**, v. 84, n. 3, p. 036106, 2011.

133 POLETTO, C. *et al.* Characterising two-pathogen competition in spatially structured environments. **Scientific Reports**, v. 5, n. 1, p. 7895, 2015.

134 FUNK, S.; JANSEN, V. A. A. Interacting epidemics on overlay networks. **Physical Review E**, v. 81, n. 3, p. 036118, 2010.

135 MARCEAU, V. *et al.* Modeling the dynamical interaction between epidemics on overlay networks. **Physical Review E**, v. 84, n. 2, p. 026105, 2011.

136 SAHNEH, F. D.; SCOGLIO, C. Competitive epidemic spreading over arbitrary multilayer networks. **Physical Review E**, v. 89, n. 6, p. 062817, 2014.

137 WANG, Y.; XIAO, G.; LIU, J. Dynamics of competing ideas in complex social systems. **New Journal of Physics**, v. 14, n. 1, p. 013015, 2012.

138 YE, Y. *et al.* Optimal vaccination program for two infectious diseases with cross-immunity spreading on a network. **Europhysics Letters**, v. 133, n. 4, p. 46001, 2021.

139 NEWMAN, M. E. J.; FERRARIO, C. R. Interacting epidemics and coinfection on contact networks. **Plos One**, v. 8, n. 8, p. 8, 2013.

140 CHEN, L. *et al.* Outbreaks of coinfections: the critical role of cooperativity. **Europhysics Letters**, v. 104, n. 5, p. 50001, 2013.

141 CAI, W. *et al.* Avalanche outbreaks emerging in cooperative contagions. **Nature Physics**, v. 11, n. 11, p. 936–940, 2015.

142 HÉBERT-DUFRESNE, L.; ALTHOUSE, B. M. Complex dynamics of synergistic coinfections on realistically clustered networks. **Proceedings of the National Academy of Sciences**, v. 112, n. 33, p. 10551–10556, 2015.

143 CUI, P.-B.; COLAIORI, F.; CASTELLANO, C. Mutually cooperative epidemics on power-law networks. **Physical Review E**, v. 96, n. 2, p. 022301, 2017.

144 WANG, W. *et al.* Coevolution spreading in complex networks. **Physics Reports**, v. 820, p. 1–51, 2019.

145 NOH, J. D.; PARK, H. Asymmetrically coupled directed percolation systems. **Physical Review Letters**, v. 94, n. 14, p. 145702, 2005.

146 AHN, Y.-Y. *et al.* Epidemic dynamics of two species of interacting particles on scale-free networks. **Physical Review E**, v. 74, n. 6, p. 066113, 2006.

147 WU, Q.; SMALL, M.; LIU, H. Superinfection behaviors on scale-free networks with competing strains. **Journal of Nonlinear Science**, v. 23, n. 1, p. 113–127, 2013.

148 ZHU, Q. *et al.* A mixing propagation model of computer viruses and countermeasures. **Nonlinear Dynamics**, v. 73, n. 3, p. 1433–1441, 2013.

149 FRIENDLY Welchia worm wreaking havoc. 2003. Available at: http://www.internetnews.com/ent-news/article.php/3065761/Friendly+Welchia+Worm+Wreaking+Havoc.htm. Access at: 30 Aug. 2021.

150 SORIANO-PAÑOS, D. *et al.* Markovian approach to tackle the interaction of simultaneous diseases. **Physical Review E**, v. 100, n. 6, p. 062308, 2019.

151 DANZIGER, M. M. *et al.* Dynamic interdependence and competition in multilayer networks. **Nature Physics**, v. 15, n. 2, p. 178–185, 2019.

152 WU, Q.; CHEN, S. Spreading of two interacting diseases in multiplex networks. **Chaos**, v. 30, n. 7, p. 073115, 2020.

153 OLIVARES, P.; CREIXELL, W.; FUJIWARA, N. Dynamical impacts of the coupling in a model of interactive infectious diseases. **Chaos**, v. 30, n. 9, p. 093144, 2020.

154 SUN, H.; SAAD, D.; LOKHOV, A. Y. Competition, collaboration, and optimization in multiple interacting spreading processes. **Physical Review X**, v. 11, n. 1, p. 011048, 2021.

155 BRÓDKA, P.; MUSIAL, K.; JANKOWSKI, J. Interacting spreading processes in multilayer networks: a systematic review. **IEEE Access**, v. 8, p. 10316–10341, 2020.

156 FUNK, S.; SALATHÉ, M.; JANSEN, V. A. A. Modelling the influence of human behaviour on the spread of infectious diseases: a review. **Journal of The Royal Society Interface**, v. 7, n. 50, p. 1247–1256, 2010.

157 DUBÉ, E.; VIVION, M.; MACDONALD, N. E. Vaccine hesitancy, vaccine refusal and the anti-vaccine movement: influence, impact and implications. **Expert Review of Vaccines**, v. 14, n. 1, p. 99–117, 2015.

158 BAUCH, C. T.; EARN, D. J. D. Vaccination and the theory of games. **Proceedings of the National Academy of Sciences**, v. 101, n. 36, p. 13391–13394, 2004.

159 RELUGA, T. C. Game theory of social distancing in response to an epidemic. **PLoS Computational Biology**, v. 6, n. 5, p. e1000793, 2010.

160 CHEN, X. *et al.* Suppressing epidemic spreading in multiplex networks with social-support. **New Journal of Physics**, v. 20, n. 1, p. 013007, 2018.

161 KUGA, K.; TANAKA, M.; TANIMOTO, J. Pair approximation model for the vaccination game: predicting the dynamic process of epidemic spread and individual actions against contagion. **Proceedings of the Royal Society A**, v. 477, n. 2246, p. 20200769, 2021.

162 SALATHÉ, M.; BONHOEFFER, S. The effect of opinion clustering on disease outbreaks. **Journal of The Royal Society Interface**, v. 5, n. 29, p. 1505–1508, 2008.

163 EAMES, K. T. D. Networks of influence and infection: parental choices and childhood disease. **Journal of The Royal Society Interface**, v. 6, n. 38, p. 811–814, 2009.

164 VELÁSQUEZ-ROJAS, F.; VAZQUEZ, F. Interacting opinion and disease dynamics in multiplex networks: discontinuous phase transition and nonmonotonic consensus times. **Physical Review E**, v. 95, n. 5, p. 052315, 2017.

165 PIRES, M. A.; OESTEREICH, A. L.; CROKIDAKIS, N. Sudden transitions in coupled opinion and epidemic dynamics with vaccination. **Journal of Statistical Mechanics:** theory and experiment, v. 2018, n. 5, p. 053407, 2018.

166 BAGNOLI, F.; LIÒ, P.; SGUANCI, L. Risk perception in epidemic modeling. **Physical Review E**, v. 76, n. 6, p. 061904, 2007.

167 WU, Q. *et al.* The impact of awareness on epidemic spreading in networks. **Chaos**, v. 22, n. 1, p. 013101, 2012.

168 MASSARO, E.; BAGNOLI, F. Epidemic spreading and risk perception in multiplex networks: a self-organized percolation method. **Physical Review E**, v. 90, n. 5, p. 052817, 2014.

169 POLETTI, P.; AJELLI, M.; MERLER, S. Risk perception and effectiveness of uncoordinated behavioral responses in an emerging epidemic. **Mathematical Biosciences**, v. 238, n. 2, p. 80–89, 2012.

170 MOINET, A.; PASTOR-SATORRAS, R.; BARRAT, A. Effect of risk perception on epidemic spreading in temporal networks. **Physical Review E**, v. 97, n. 1, p. 012313, 2018.

171 FUNK, S. *et al.* The spread of awareness and its impact on epidemic outbreaks. **Proceedings of the National Academy of Sciences**, v. 106, n. 16, p. 6872–6877, 2009.

172 GRANELL, C.; GÓMEZ, S.; ARENAS, A. Dynamical interplay between awareness and epidemic spreading in multiplex networks. **Physical Review Letters**, v. 111, n. 12, p. 128701, 2013.

173 GRANELL, C.; GÓMEZ, S.; ARENAS, A. Competing spreading processes on multiplex networks: awareness and epidemics. **Physical Review E**, v. 90, n. 1, p. 012808, 2014.

174 WANG, W. *et al.* Asymmetrically interacting spreading dynamics on complex layered networks. **Scientific Reports**, v. 4, n. 1, p. 5097, 2015.

175 WANG, W. *et al.* Suppressing disease spreading by using information diffusion on multiplex networks. **Scientific Reports**, v. 6, n. 1, p. 29259, 2016.

176 GUO, Q. *et al.* Two-stage effects of awareness cascade on epidemic spreading in multiplex networks. **Physical Review E**, v. 91, n. 1, p. 012822, 2015.

177 SAMANTA, S. *et al.* Effect of awareness programs by media on the epidemic outbreaks: a mathematical model. **Applied Mathematics and Computation**, v. 219, n. 12, p. 6965–6977, 2013.

178 TIWARI, P. K. *et al.* Dynamics of infectious diseases: local versus global awareness. **International Journal of Bifurcation and Chaos**, v. 31, n. 07, p. 2150102, 2021.

179 WANG, X. *et al.* Anomalous role of information diffusion in epidemic spreading. **Physical Review Research**, v. 3, n. 1, p. 013157, 2021.

180 WANG, J.; QIN, X.; FANG, H. Virus-information coevolution spreading dynamics on multiplex networks. **Complexity**, v. 2021, p. e6624612, 2021.

181 WANG, H. *et al.* Effects of asymptomatic infection and self-initiated awareness on the coupled disease-awareness dynamics in multiplex networks. **Applied Mathematics and Computation**, v. 400, p. 126084, 2021.

182 SILVA, P. C. V. *et al.* Epidemic spreading with awareness and different timescales in multiplex networks. **Physical Review E**, v. 100, n. 3, p. 032313, 2019.

183 NEKOVEE, M. *et al.* Theory of rumour spreading in complex social networks. **Physica A**, v. 374, n. 1, p. 457–470, 2007.

184 NJOZING, B. N. *et al.* "If the patients decide not to tell what can we do?"- TB/HIV counsellors' dilemma on partner notification for HIV. **BMC International Health and Human Rights**, v. 11, n. 1, p. 6, 2011.

185 BENDER, E. A.; CANFIELD, E. The asymptotic number of labeled graphs with given degree sequences. **Journal of Combinatorial Theory A**, v. 24, n. 3, p. 296–307, 1978.

186 VELÁSQUEZ-ROJAS, F. *et al.* Disease and information spreading at different speeds in multiplex networks. **Physical Review E**, v. 102, n. 2, p. 022312, 2020.

187 WANG, H. *et al.* Epidemic mitigation via awareness propagation in communication networks: the role of time scales. **New Journal of Physics**, v. 19, n. 7, p. 073039, 2017.

188 FULTZ, P. N. *et al.* Superinfection of a chimpanzee with a second strain of human immunodeficiency virus. **Journal of Virology**, v. 61, n. 12, p. 4026, 1987.

189 SMITH, D. M.; RICHMAN, D. D.; LITTLE, S. J. HIV Superinfection. **The Journal of Infectious Diseases**, v. 192, n. 3, p. 438–444, 2005.

190 RAMOS, A. *et al.* Intersubtype human immunodeficiency virus type 1 superinfection following seroconversion to primary infection in two injection drug users. **Journal of Virology**, v. 76, n. 15, p. 7444–7452, 2002.

191 FELDMEIER, H. *et al.* Bacterial superinfection in human tungiasis. **Tropical Medicine and International Health**, v. 7, n. 7, p. 559–564, 2002.

192 NOWAK, M. A.; MAY, R. M. Superinfection and the evolution of parasite virulence. **Proceedings of the Royal Society B**, v. 255, n. 1342, p. 81–89, 1994.

193 IANNELLI, M.; MARTCHEVA, M.; LI, X.-Z. Strain replacement in an epidemic model with super-infection and perfect vaccination. **Mathematical Biosciences**, v. 195, n. 1, p. 23–46, 2005.

194 MARTCHEVA, M.; BOLKER, B. M.; HOLT, R. D. Vaccine-induced pathogen strain replacement: what are the mechanisms? **Journal of The Royal Society Interface**, v. 5, n. 18, p. 3–13, 2008.

195 NOWAK, M. A. **Evolutionary dynamics**: exploring the equations of life. Cambridge: Harvard University Press, 2006. ISBN 0-674-02338-2.

196 BRAUER, F.; CASTILLO-CHAVEZ, C. **Mathematical models in population biology and epidemiology**. 2nd. ed. New York: Springer, 2012.

197 CHEN, L.-C.; CARLEY, K. The impact of countermeasure propagation on the prevalence of computer viruses. **IEEE Transactions on Systems, Man and Cybernetics:** part B, v. 34, n. 2, p. 823–833, 2004.

198 GOLDENBERG, J. *et al.* Distributive immunization of networks against viruses using the 'honey-pot' architecture. **Nature Physics**, v. 1, n. 3, p. 184–188, 2005.

199 YANG, L.-X.; YANG, X. The pulse treatment of computer viruses: a modeling study. **Nonlinear Dynamics**, v. 76, n. 2, p. 1379–1393, 2014.

200 SNOWDEN, F. M. **Epidemics and society**: from the black death to the present. New Haven: Yale University Press, 2019. ISBN 978-0-300-19221-6.

201 EISEN, R. J. *et al.* Early-phase transmission of Yersinia pestis by unblocked fleas as a mechanism explaining rapidly spreading plague epizootics. **Proceedings of the National Academy of Sciences**, v. 103, n. 42, p. 15380–15385, 2006.

202 BLACK Death: definition, cause, symptoms, effects, death toll, & facts. 2021. Available at: https://www.britannica.com/event/Black-Death. Access at: 29 Sept. 2021.

203 GÓMEZ, J. M.; VERDÚ, M. Network theory may explain the vulnerability of medieval human settlements to the Black Death pandemic. **Scientific Reports**, v. 7, n. 1, p. 43467, 2017.

204 EAGLE, N.; PENTLAND, A. S. Reality mining: sensing complex social systems. **Personal and Ubiquitous Computing**, v. 10, n. 4, p. 255–268, 2006.

205 SKELDON, R. **Population mobility in developing countries.** London: Belhaven Press, 1990.

206 RAVENSTEIN, E. G. The laws of migration. **Journal of the Statistical Society of London**, v. 48, n. 2, p. 167–235, 1885.

207 ZIPF, G. K. The P_1P_2/D hypothesis: on the intercity movement of persons. **American Sociological Review**, v. 11, n. 6, p. 677–686, 1946.

208 BARTHÉLEMY, M. Spatial networks. **Physics Reports**, v. 499, n. 1, p. 1–101, 2011.

209 ERLANDER, S.; STEWART, N. F. **The gravity model in transportation analysis**: theory and extensions. [*S.l.*]: CRC Press, 1990. ISBN 978-90-6764-089-3.

210 JUNG, W.-S.; WANG, F.; STANLEY, H. E. Gravity model in the Korean highway. **Europhysics Letters**, v. 81, n. 4, p. 48005, 2008.

211 THIEMANN, C. *et al.* The structure of borders in a small world. **Plos One**, v. 5, n. 11, p. e15422, 2010.

212 MARTINEZ-ZARZOSO, I. Gravity model: an application to trade between regional blocs. **Atlantic Economic Journal**, v. 31, n. 2, p. 174–187, 2003.

213 MARTINEZ-ZARZOSO, I.; NOWAK-LEHMANN, F. Augmented gravity model: an empirical application to mercosur-european union trade flows. **Journal of Applied Economics**, v. 6, n. 2, p. 291–316, 2003.

214 BERGSTRAND, J. H. The gravity equation in international trade: some microeconomic foundations and empirical evidence. **The Review of Economics and Statistics**, v. 67, n. 3, p. 474–481, 1985.

215 SIMINI, F. *et al.* A universal model for mobility and migration patterns. **Nature**, v. 484, n. 7392, p. 96–100, 2012.

216 BARBOSA, H. *et al.* Human mobility: models and applications. **Physics Reports**, v. 734, p. 1–74, 2018.

217 NOULAS, A. *et al.* A tale of many cities: universal patterns in human urban mobility. **Plos One**, v. 7, n. 5, p. e37027, 2012.

218 STOUFFER, S. A. Intervening opportunities: a theory relating mobility and distance. **American Sociological Review**, v. 5, n. 6, p. 845–867, 1940.

219 SCHNEIDER, M. Gravity models and trip distribution theory. **Papers in Regional Science**, v. 5, n. 1, p. 51–56, 1959.

220 SPADON, G. *et al.* Reconstructing commuters network using machine learning and urban indicators. **Scientific Reports**, v. 9, n. 1, p. 11801, 2019.

221 CODLING, E. A.; PLANK, M. J.; BENHAMOU, S. Random walk models in biology. **Journal of The Royal Society Interface**, v. 5, n. 25, p. 813–834, 2008.

222 OTHMER, H. G.; DUNBAR, S. R.; ALT, W. Models of dispersal in biological systems. **Journal of Mathematical Biology**, v. 26, n. 3, p. 263–298, 1988.

223 MURRAY, J. D. **Mathematical biology**. 3rd. ed. New York: Springer, 2002. (Interdisciplinary Applied Mathematics). ISBN 978-0-387-95228-4.

224 WANG, W.; ZHAO, X.-Q. Basic reproduction numbers for reaction-diffusion epidemic models. **SIAM Journal on Applied Dynamical Systems**, v. 11, n. 4, p. 1652–1673, 2012.

225 GONZÁLEZ, M. C.; HIDALGO, C. A.; BARABÁSI, A. L. Understanding individual human mobility patterns. **Nature**, v. 453, n. 7196, p. 779–782, 2008.

226 VISWANATHAN, G. M. *et al.* Lévy flight search patterns of wandering albatrosses. **Nature**, v. 381, n. 6581, p. 413–415, 1996.

227 SIMS, D. W. *et al.* Scaling laws of marine predator search behaviour. **Nature**, v. 451, n. 7182, p. 1098–1102, 2008.

228 HUMPHRIES, N. E. *et al.* Environmental context explains Lévy and Brownian movement patterns of marine predators. **Nature**, v. 465, n. 7301, p. 1066–1069, 2010.

229 RAMOS-FERNÁNDEZ, G. *et al.* Lévy walk patterns in the foraging movements of spider monkeys (Ateles geoffroyi). **Behavioral Ecology and Sociobiology**, v. 55, n. 3, p. 223–230, 2004.

230 BERTRAND, S. *et al.* Lévy trajectories of Peruvian purse-seiners as an indicator of the spatial distribution of anchovy (Engraulis ringens). **ICES Journal of Marine Science**, v. 62, n. 3, p. 477–482, 2005.

231 VISWANATHAN, G. M. *et al.* Optimizing the success of random searches. **Nature**, v. 401, n. 6756, p. 911–914, 1999.

232 VISWANATHAN, G. M.; RAPOSO, E. P.; LUZ, M. G. E. da. Lévy flights and superdiffusion in the context of biological encounters and random searches. **Physics of Life Reviews**, v. 5, n. 3, p. 133–150, 2008.

233 EDWARDS, A. M. *et al.* Revisiting Lévy flight search patterns of wandering albatrosses, bumblebees and deer. **Nature**, v. 449, n. 7165, p. 1044–1048, 2007.

234 PYKE, G. H. Understanding movements of organisms: it's time to abandon the Lévy foraging hypothesis. **Methods in Ecology and Evolution**, v. 6, n. 1, p. 1–16, 2015.

235 REYNOLDS, A. Liberating Lévy walk research from the shackles of optimal foraging. **Physics of Life Reviews**, v. 14, p. 59–83, 2015.

236 LEVERNIER, N. *et al.* Inverse square Lévy Walks are not optimal search strategies for $d \geq 2$. **Physical Review Letters**, v. 124, n. 8, p. 080601, 2020.

237 RHEE, I. *et al.* On the Levy-walk nature of human mobility. **IEEE/ACM Transactions on Networking**, v. 19, n. 3, p. 630–643, 2011.

238 BARONCHELLI, A.; RADICCHI, F. Lévy flights in human behavior and cognition. **Chaos, Solitons & Fractals**, v. 56, p. 101–105, 2013.

239 GONZÁLEZ, M. C.; HERRMANN, H. J. Scaling of the propagation of epidemics in a system of mobile agents. **Physica A**, v. 340, n. 4, p. 741–748, 2004.

240 BUSCARINO, A. *et al.* Effects of motion on epidemic spreading. **International Journal of Bifurcation and Chaos**, v. 20, n. 03, p. 765–773, 2010.

241 XIA, C. *et al.* Influence of mobile agents on the spreading behavior of SIS model. **Physics Procedia**, v. 3, n. 5, p. 1825–1830, 2010.

242 ZHOU, J.; LIU, Z. Epidemic spreading in communities with mobile agents. **Physica A**, v. 388, n. 7, p. 1228–12369, 2009.

243 ZHOU, J. *et al.* Epidemic spreading induced by diversity of agents' mobility. **Physical Review E**, v. 86, n. 2, p. 026115, 2012.

244 BUSCARINO, A. *et al.* Local and global epidemic outbreaks in populations moving in inhomogeneous environments. **Physical Review E**, v. 90, n. 4, p. 042813, 2014.

245 HUANG, Y. *et al.* Epidemic spreading in random walkers with heterogeneous interaction radius. **Journal of Statistical Mechanics:** theory and experiment, v. 2016, n. 10, p. 103501, 2016.

246 FENG, Y.; DING, L.; HU, P. Epidemic spreading on random surfer networks with optimal interaction radius. **Communications in Nonlinear Science and Numerical Simulation**, v. 56, p. 344–353, 2017.

247 ICHINOSE, G. *et al.* Reduced mobility of infected agents suppresses but lengthens disease in biased random walk. **arXiv**, 2018. Available at: https://arxiv.org/pdf/1807.01195.pdf. Access at: 29 Nov. 2021.

248 PENG, X. L. *et al.* An SIS epidemic model with vaccination in a dynamical contact network of mobile individuals with heterogeneous spatial constraints. **Communications in Nonlinear Science and Numerical Simulation**, v. 73, p. 52–73, 2019.

249 KEELING, M. J.; BJØRNSTAD, O. N.; GRENFELL, B. T. Metapopulation dynamics of Infectious Diseases. *In*: HANSKI, I.; GAGGIOTTI, O. E. (ed.). **Ecology, genetics and evolution of metapopulations**. Burlington: Academic Press, 2004. p. 415–445. ISBN 978-0-12-323448-3.

250 FAHRIG, L.; MERRIAM, G. Habitat patch connectivity and population survival. **Ecology**, v. 66, n. 6, p. 1762–1768, 1985.

251 KAREIVA, P. Population dynamics in spatially complex environments: theory and data. **Philosophical Transactions of the Royal Society B**, v. 330, n. 1257, p. 175–190, 1990.

252 FLAHAULT, A.; VALLERON, A.-J. A method for assessing the global spread of HIV-1 infection based on air travel. **Mathematical Population Studies**, v. 3, n. 3, p. 161–171, 1992.

253 LLOYD, A. L.; MAY, R. M. Spatial heterogeneity in epidemic models. **Journal of Theoretical Biology**, v. 179, n. 1, p. 1–11, 1996.

254 GRENFELL, B.; HARWOOD, J. (Meta)population dynamics of infectious diseases. **Trends in Ecology & Evolution**, v. 12, n. 10, p. 395–399, 1997.

255 COLIZZA, V.; PASTOR-SATORRAS, R.; VESPIGNANI, A. Reaction–diffusion processes and metapopulation models in heterogeneous networks. **Nature Physics**, v. 3, n. 4, p. 276–282, 2007.

256 COLIZZA, V.; VESPIGNANI, A. Invasion threshold in heterogeneous metapopulation networks. **Physical Review Letters**, v. 99, n. 14, p. 148701, 2007.

257 TANG, M.; LIU, Z.; LI, B. Epidemic spreading by objective traveling. **Europhysics Letters**, v. 87, n. 1, p. 18005, 2009.

258 NI, S.; WENG, W. Impact of travel patterns on epidemic dynamics in heterogeneous spatial metapopulation networks. **Physical Review E**, v. 79, n. 1, p. 016111, 2009.

259 POLETTO, C.; TIZZONI, M.; COLIZZA, V. Human mobility and time spent at destination: impact on spatial epidemic spreading. **Journal of Theoretical Biology**, v. 338, p. 41–58, 2013.

260 COLIZZA, V. *et al.* Modeling the worldwide spread of pandemic influenza: baseline case and containment interventions. **PLOS Medicine**, v. 4, n. 1, p. e13, 2007.

261 BALCAN, D. *et al.* Multiscale mobility networks and the spatial spreading of infectious diseases. **Proceedings of the National Academy of Sciences**, v. 106, n. 51, p. 21484–21489, 2009.

262 BAJARDI, P. *et al.* Human mobility networks, travel restrictions, and the global spread of 2009 H1N1 pandemic. **Plos One**, v. 6, n. 1, p. e16591, 2011.

263 CALVETTI, D. *et al.* Metapopulation network models for understanding, predicting, and managing the coronavirus disease COVID-19. **Frontiers in Physics**, v. 8, p. 261, 2020.

264 ALETA, A. *et al.* A data-driven assessment of early travel restrictions related to the spreading of the novel COVID-19 within mainland China. **Chaos, Solitons & Fractals**, v. 139, p. 110068, 2020.

265 ALETA, A.; MORENO, Y. Evaluation of the potential incidence of COVID-19 and effectiveness of containment measures in Spain: a data-driven approach. **BMC Medicine**, v. 18, n. 1, p. 157, 2020.

266 COLETTI, P. *et al.* A data-driven metapopulation model for the Belgian COVID-19 epidemic: assessing the impact of lockdown and exit strategies. **BMC Infectious Diseases**, v. 21, n. 1, p. 503, 2021.

267 ALETA, A. *et al.* Modelling the impact of testing, contact tracing and household quarantine on second waves of COVID-19. **Nature Human Behaviour**, v. 4, n. 9, p. 964–971, 2020.

268 VENTURA, P. C. *et al.* Epidemic spreading in populations of mobile agents with adaptive behavioral response. **Chaos, Solitons & Fractals**, v. 156, p. 111849, 2022.

269 GROSS, T.; D'LIMA, C. J. D.; BLASIUS, B. Epidemic dynamics on an adaptive network. **Physical Review Letters**, v. 96, n. 20, p. 208701, 2006.

270 GROSS, T.; KEVREKIDIS, I. G. Robust oscillations in SIS epidemics on adaptive networks: Coarse graining by automated moment closure. **Europhysics Letters**, v. 82, n. 3, p. 38004, 2008.

271 MARCEAU, V. *et al.* Adaptive networks: coevolution of disease and topology. **Physical Review E**, v. 82, n. 3, p. 036116, 2010.

272 GUERRA, B.; GÓMEZ-GARDEÑES, J. Annealed and mean-field formulations of disease dynamics on static and adaptive networks. **Physical Review E**, v. 82, n. 3, p. 035101, 2010.

273 SHAW, L. B.; SCHWARTZ, I. B. Fluctuating epidemics on adaptive networks. **Physical Review E**, v. 77, n. 6, p. 066101, 2008.

274 RISAU-GUSMÁN, S.; ZANETTE, D. H. Contact switching as a control strategy for epidemic outbreaks. **Journal of Theoretical Biology**, v. 257, n. 1, p. 52–60, 2009.

275 ZHOU, J. *et al.* Epidemic reemergence in adaptive complex networks. **Physical Review E**, v. 85, n. 3, p. 036107, 2012.

276 WIELAND, S.; AQUINO, T.; NUNES, A. The structure of coevolving infection networks. **Europhysics Letters**, v. 97, n. 1, p. 18003, 2012.

277 COLIZZA, V.; VESPIGNANI, A. Epidemic modeling in metapopulation systems with heterogeneous coupling pattern: theory and simulations. **Journal of Theoretical Biology**, v. 251, n. 3, p. 450–467, 2008.

278 MELONI, S. *et al.* Modeling human mobility responses to the large-scale spreading of infectious diseases. **Scientific Reports**, v. 1, n. 1, p. 62, 2011.

279 ALETA, A. *et al.* Human mobility networks and persistence of rapidly mutating pathogens. **Royal Society Open Science**, v. 4, n. 3, p. 160914, 2017.

280 IANNELLI, F. *et al.* Effective distances for epidemics spreading on complex networks. **Physical Review E**, v. 95, n. 1, p. 012313, 2017.

281 RISAU-GUSMÁN, S.; ZANETTE, D. H. Contact switching as a control strategy for epidemic outbreaks. **Journal of Theoretical Biology**, v. 257, n. 1, p. 52–60, 2009.

282 FOFANA, A. M.; HURFORD, A. Mechanistic movement models to understand epidemic spread. **Philosophical Transactions of the Royal Society B**, v. 372, n. 1719, p. 20160086, 2017.

283 WANG, L.; LI, X. Spatial epidemiology of networked metapopulation: an overview. **Chinese Science Bulletin**, v. 59, n. 28, p. 3511–3522, 2014.

284 PARK, J. Changes in subway ridership in response to COVID-19 in Seoul, South Korea: implications for social distancing. **Cureus**, v. 12, n. 4, p. e7668, 2020.

285 WAITZBERG, R. *et al.* Israel's response to the COVID-19 pandemic: tailoring measures for vulnerable cultural minority populations. **International Journal for Equity in Health**, v. 19, n. 1, p. 71, 2020.

286 GOLLWITZER, A. *et al.* Partisan differences in physical distancing are linked to health outcomes during the COVID-19 pandemic. **Nature Human Behaviour**, v. 4, n. 11, p. 1186–1197, 2020.

287 BALL, F. Seven challenges for metapopulation models of epidemics, including households models. **Epidemics**, v. 10, p. 63–67, 2015.

288 WANG, B. *et al.* Epidemic spread on interconnected metapopulation networks. **Physical Review E**, v. 90, n. 3, p. 032806, 2014.

289 VENTURA, P. C. *et al.* Modeling the effects of social distancing on the large-scale spreading of diseases. **Epidemics**, v. 38, p. 100544, 2022.

290 PERRA, N. *et al.* Towards a characterization of behavior-disease models. **Plos One**, v. 6, n. 8, p. e23084, 2011.

291 LU, D. *et al.* Data-driven estimate of SARS-CoV-2 herd immunity threshold in populations with individual contact pattern variations. **medRxiv**, 2021. Available at: https://www.medrxiv.org/content/10.1101/2021.03.19.21253974v1.full.pdf. Access at: 30 Nov. 2021.

292 POLLÁN, M. *et al.* Prevalence of SARS-CoV-2 in Spain (ENE-COVID): a nationwide, population-based seroepidemiological study. **The Lancet**, v. 396, n. 10250, p. 535–544, 2020.

293 RICCARDO, F. *et al.* Epidemiological characteristics of COVID-19 cases and estimates of the reproductive numbers 1 month into the epidemic, Italy, 28 January to 31 March 2020. **Eurosurveillance**, v. 25, n. 49, p. 2000790, 2020.

294 CHINAZZI, M. *et al.* The effect of travel restrictions on the spread of the 2019 novel coronavirus (COVID-19) outbreak. **Science**, v. 368, n. 6489, p. 395–400, 2020.

APPENDIX

APPENDIX A – MARKOV CHAIN APPROACH FOR THE SIS/UARU MODEL

In order to predict the behavior of the SIS/UARU model in a double-layer network, as described in section 3.2 of the main text, we developed a microscopic Markov chain approach to write dynamical equations for relevant probabilities of our system. For that purpose, we followed the methodology described in.[107]

A.1 The Markov chain equations

For each node i of the network and for each time stamp t, the probabilities that it is in each possible state of the model is defined as p. Such state can either be from a single process (e.g., $p_I^i(t)$ is the probability that node i is infected (I) at time t) or a "composite" state (e.g., $p_{SU}^i(t)$, $p_{IA}^i(t)$, etc.). For convenience, we label the corresponding nodes in different layers with the same number.

The first step is to build the transition trees for all possible changes of states and their respective transition probabilities. For each tree, we represent the root as one of the possible composite states of a node (SU, SA, SR, IU, IA and IR) at time t, and the leaves at each of the possible resulting states at time $t + 1$, starting from the state at time t. The branches represent each of the possible transitions. The probabilities of such transitions are written above the corresponding branches.

As described previously for the numerical simulations, we separate the transitions into two groups - the epidemic and informational - and only one of the transitions groups is performed in a time step. Figure 50 shows the trees for the SIS/UARU model. The baseline model corresponds to all the factors in black. The modified model has the same factors of the baseline model, except for the IR $\rightarrow$ IU transition, in which the correct factors are displayed in red. The modification is interpreted as a reduction on the forgetting probability for IR nodes.

The probability of each event on the informational side of Figure 50 is multiplied by π, which is the probability that the informational group is chosen to be updated in the current time step. On the other hand, probabilities from the epidemic side carry a factor of $1 - \pi$. Therefore, for instance, the probability that an infected-aware (IA) node gets healed and becomes susceptible-aware (SA) is of $(1 - \pi) \cdot \mu$, following the corresponding probability tree on the epidemic group.

The transition probabilities for processes which involve contact with neighboring nodes, namely q_U^i (infection of an unaware node), q_A^i (infection of an aware node), r_U^i (awareness by contacting an aware neighbor) and r_A^i ("stifling" - lost of interest) are defined by the following

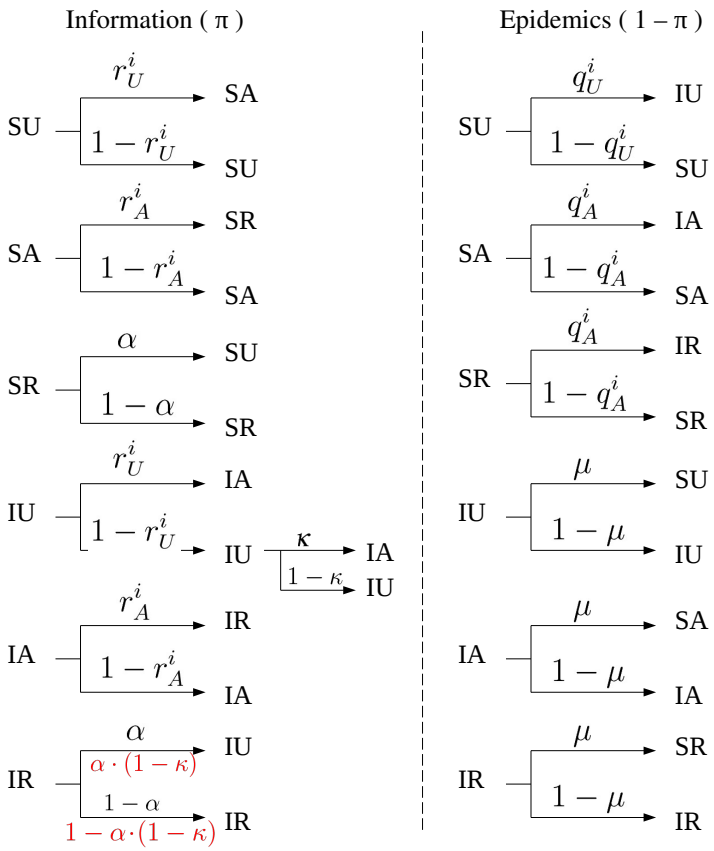

Figure 50 – Probability trees with all the possible transitions for each state. The informational group has an associated probability of π, whereas the epidemic group carries the complementary probability $1 - \pi$. For the modified model, the IR $\rightarrow$ IU transition follows the factors in red (instead of the ones in black).

Source: SILVA *et al.*[182]

set of equations:

$$q_U^i = 1 - \prod_j (1 - A_{ij}\, p_I^j\, \beta), \tag{A.1}$$

$$q_A^i = 1 - \prod_j (1 - A_{ij}\, p_I^j\, \Gamma\beta), \tag{A.2}$$

$$r_U^i = 1 - \prod_j (1 - B_{ij}\, p_A^j\, \gamma), \tag{A.3}$$

$$r_A^i = 1 - \prod_j (1 - B_{ij}\, (p_A^j + p_R^j)\, \sigma) \tag{A.4}$$

where A_{ij} and B_{ij} represent the adjacency matrices for the epidemic and informational layers, respectively. Here, we point out that our goal is to study the stationary state of the system, in which all probabilities do not change in time. Therefore, the time label t of all probabilities defined here (e.g, $p_{SU}^i(t), r_U^i(t)$) were removed.

Based on the transition trees drawn in Fig. 50, we can write down the Markov chain equations for the probabilities of each node i being in each of the six compartments (SU, SA, SR, IU, IA, IR) of the model as a fixed point set of equations, in which the time dependence is already removed:

$$
\begin{aligned}
p^i_{SU} &= p^i_{SU}[\pi(1-r^i_U)+(1-\pi)(1-q^i_U)]+ \\
&+ p^i_{SR}[\pi\alpha]+ \\
&+ p^i_{IU}[(1-\pi)\mu] && \text{(A.5)} \\
p^i_{SA} &= p^i_{SU}[\pi r^i_U]+ \\
&+ p^i_{SA}[\pi(1-r^i_A)+(1-\pi)(1-q^i_A)]+ \\
&+ p^i_{IA}[(1-\pi)\mu] && \text{(A.6)} \\
p^i_{SR} &= p^i_{SA}[\pi r^i_A]+ \\
&+ p^i_{SR}[\pi(1-\alpha)+(1-\pi)(1-q^i_A)]+ \\
&+ p^i_{IR}[(1-\pi)\mu] && \text{(A.7)} \\
p^i_{IU} &= p^i_{SU}[(1-\pi)q^i_U]+ \\
&+ p^i_{IU}[\pi(1-r^i_U)(1-\kappa)+(1-\pi)(1-\mu)]+ \\
&+ p^i_{IR}[\pi\alpha(1-\kappa)] && \text{(A.8)} \\
p^i_{IA} &= p^i_{SA}[(1-\pi)q^i_A]+ \\
&+ p^i_{IU}[\pi(r^i_U+(1-r^i_U)\kappa)]+ \\
&+ p^i_{IA}[\pi(1-r^i_A)+(1-\pi)(1-\mu)] && \text{(A.9)} \\
p^i_{IR} &= p^i_{SR}[(1-\pi)q^i_A]+ \\
&+ p^i_{IA}[\pi r^i_A]+ \\
&+ p^i_{IR}[\pi(\alpha\kappa+1-\alpha)+(1-\pi)(1-\mu)] && \text{(A.10)}
\end{aligned}
$$

Equations A.6 to A.10 represent the baseline model. For the modified model, in which the IR $\rightarrow$ IU has a modified probability, Equations A.8 and A.10 are respectively replaced by:

$$
\begin{aligned}
p^i_{IU} &= p^i_{SU}[(1-\pi)q^i_U] + \\
&+ p^i_{IU}[\pi(1-r^i_U)(1-\kappa) + (1-\pi)(1-\mu)] + \\
&+ p^i_{IR}[\pi\alpha] \qquad \text{(A.11)} \\
p^i_{IR} &= p^i_{SR}[(1-\pi)q^i_A] + \\
&+ p^i_{IA}[\pi r^i_A] + \\
&+ p^i_{IR}[\pi(1-\alpha) + (1-\pi)(1-\mu)] \qquad \text{(A.12)}
\end{aligned}
$$

We solve the system of $6N$ equations (where N is the number of nodes on the network) by the fixed point method, in which the LHS values are updated by applying previous values at the RHS expressions. As explained in the main text, the initial conditions are set to: $p^i_{IA} = 0.2$, $p^i_{SU} = 0.8$ and $p^i_{IU} = p^i_{IR} = p^i_{SA} = p^i_{SR} = 0$, for $i = 0, 1, ..., N-1$. The solutions of these equations are shown in Figures 10, 11 and 12 as solid lines, where we can see a good agreement between the Markov chain predictions and Monte Carlo simulations.

A.2 Epidemic critical point

From the Markov chain equations, we can derive the epidemic critical point between the healthy and the endemic phases. The basic idea is to analyze the stability of the healthy solution $p^i_I = 0$, $i = 1, 2, ..., N$, using a perturbative approach.

We first add Equations A.8 to A.10 to obtain the evolution of the probability $p^i_I = p^i_{IU} + p^i_{IA} + p^i_{IR}$ that node i is infected:

$$
\begin{aligned}
p^i_I = \quad & (1-\pi)[p^i_I(1-\mu) + p^i_{SU}q^i_U + \\
& + (p^i_{SA} + p^i_{SR})q^i_A] \; + \; \pi p^i_I \qquad \text{(A.13)}
\end{aligned}
$$

Notice that this equation holds both for the baseline and modified models, as the informational terms add up to πp^i_I in any case. We now use the following approximation for the q^i_U and q^i_A transition probabilities, which is valid when p^i_I is sufficiently small for any node i:

$$
q^i_U \approx \beta \sum_j A_{ij} p^j_I \qquad \text{(A.14)}
$$

$$
q^i_A \approx \Gamma\beta \sum_j A_{ij} p^j_I \qquad \text{(A.15)}
$$

Rewriting Equation A.13 with these approximations yields:

$$p_I^i \approx (1-\pi)\Big\{p_I^i(1-\mu) + \beta\,[p_{SU}^i + \\ +\ \Gamma(p_{SA}^i + p_{SR}^i)]\sum_j A_{ij}p_I^j\Big\}\ +\ \pi p_I^i \tag{A.16}$$

Sending the terms with p_I^i to LHS and leaving the terms with $\sum_j A_{ij}p_I^i$ on the RHS, we end up with the following self-consistent relation for p_I^i, which does not depend on the time scale π:

$$p_I^i \approx \frac{\beta}{\mu}[p_{SU}^i + \Gamma(p_{SA}^i + p_{SR}^i)]\sum_j A_{ij}p_I^j \tag{A.17}$$

Equation A.17 is a matrix equation of the shape $\overrightarrow{p} = (\beta/\mu)H\overrightarrow{p}$. The trivial solution $p_I^i = 0$ for every node i is stable on Equation A.17 if all eigenvalues of the matrix H, with elements defined as:

$$H_{ij} = [p_U^i + \Gamma(p_A^i + p_R^i)]A_{ij} = \\ = [1 - (p_A^i + p_R^i)(1-\Gamma)]A_{ij} \tag{A.18}$$

Are not greater than μ/β. Noticed that we also approximated $p_U^i = p_{SU}^i + p_{IU}^i \approx p_{SU}^i$, and the same for A and R compartments. Therefore, the expression for the healthy/endemic phase transition curve is:

$$\frac{\beta}{\mu} = \frac{1}{\Lambda_{\max}(H)} \tag{A.19}$$

The values of p_A^i and p_R^i can be found by solving the Markov chain equations for the informational model only, with no interference of the disease.

APPENDIX B – ANALYTICAL DERIVATIONS FOR THE INTERACTING DISEASES MODELS

In section 3.3, we discussed two models for interacting diseases in the asymmetrical regime, studying their dynamics in homogeneously mixed populations. This formulation provides much greater analytical power, and most of our results were based on closed-form equations or simple numerically tractable expressions. In this appendix, we show some intermediate steps that conduct to the results we discussed in the main text.

For simplicity, and to avoid a heavily loaded notation (specially in the two last sections), we represent by u, v and w the *fixed point* values of the prevalences (this is, their values in the stationary state), and use the explicit time dependence ($u(t)$, $v(t)$ and $w(t)$) to represent the actual dynamical variables. As a reminder: u is the prevalence of disease I ("prey"), v is the prevalence of disease II ("predator") and w is the prevalence of coinfection (only for model A);

B.1 Phase transition curves

The phase diagrams in Figure 19 were drawn based on analytical expressions, which can be derived from a simple stability analysis of the dynamical system of each model. In general, stability analysis involves the calculation of the Jacobian matrix, but here we show that this can be done with a simple perturbative analysis, which is highly analogous to the Jacobian method, yet offers a more intuitive perspective.

B.1.1 Model A

The phase transitions in an epidemic model are typically determined by changes in the stability of the trivial solution (i.e., for which the prevalence is zero), commonly called the *disease-free equilibrium* (DFE) in math jargon. For a model of two diseases, we have to analyze the DFE stability of each disease. We shall start with disease I, but due to the symmetry of Model A, the exact same procedure is valid for the DFE of disease II.

Consider the dynamical equations for u and v (from Equations 3.16 and 3.17):

$$\dot{u}(t) = (1-\pi)\left[\beta_1(1-u(t)) + (\Gamma_1 - 1)\beta_1(v(t)-w(t)) - \mu_1\right] u(t) \tag{B.1}$$

$$\dot{v}(t) = \pi\left[\beta_2(1-v(t)) + (\Gamma_2 - 1)\beta_2(u(t)-w(t)) - \mu_2\right] v(t) \tag{B.2}$$

And assume that the system is close to the DFE of disease I, i.e.:

$$\begin{cases} u(t) = 0 + \epsilon_u(t) \\ v(t) = v + \epsilon_v(t) \\ w(t) = 0 + \epsilon_w(t) \end{cases} \tag{B.3}$$

Where ϵ_u, ϵ_v and ϵ_w are arbitrarily small dynamic variables, and v is the stationary prevalence of disease II with no influence of disease I. By applying Equation B.3 in Equations B.1 and B.2, we perform a variable change on the dynamical system. Retaining up to first order in Equation B.1 and zeroth order in Equation B.2, we get:

$$\dot{\epsilon}_u(t) \simeq (1-\pi)\left[\beta_1 \cdot (1) + (\Gamma_1 - 1)\beta_1 \cdot (v) - \mu_1\right] \epsilon_u(t) \tag{B.4}$$

$$0 = \pi \cdot [\beta_2(1-v) - \mu_2] \cdot v \tag{B.5}$$

Equation B.4 is a linear differential equation for $\epsilon_u(t)$ (notice that it decouples from the other variables), whose solution is $\epsilon_u(t) = \epsilon_u(0)\, e^{at}$, where $a = (1-\pi)[\beta_1 + (\Gamma_1 - 1)\beta_1 v - \mu_1]$. It will exponentially decay in time, meaning that disease I's DFE is stable, provided that $a < 0$. By setting $a = 0$, we get the critical value of $\lambda_1 = \beta_1/\mu_1$ in which the DFE changes its stability:

$$\begin{aligned} (1-\pi)[\beta_1 + (\Gamma_1 - 1)\beta_1 v - \mu_1] &= 0 \\ \mu_1 \cdot [\lambda_1 + (\Gamma_1 - 1)\lambda_1 v - 1] &= 0 \\ \lambda_1[1 + (\Gamma_1 - 1)v] &= 1 \\ \lambda_1 &= [1 + (\Gamma_1 - 1)v]^{-1} \end{aligned} \tag{B.6}$$

Where we had to assume that $\pi - 1 \neq 0 \neq \mu_1$. Equation B.5, in turn, only ensures that v is one of the stationary solutions of the simple SIS model with parameters β_2 and μ_2, as stated before. In particular, it must be the *stable* solution. If the DFE of disease II is the stable solution, then $v = 0$, and the critical value of λ_1 for disease I's DFE is $\lambda_1 = 1$, which is actually the frontier between phases P1 and P2 in Figure 19. * If disease II's DFE is unstable, then the stable solution is the one that solves $\beta_2(1-v) - \mu_2 = 0$, this is (for $\mu_2 \neq 0$):

$$v = 1 - \frac{1}{\lambda_2} \tag{B.7}$$

And the critical λ_1 for disease I's onset is, as reported in the main text, given by:

$$\frac{1}{\lambda_1} = 1 - (1 - \Gamma_1)\left(1 - \frac{1}{\lambda_2}\right)$$

* Indeed, this is the critical value for an SIS disease without interference of another disease.

Which is the expression for the edge between phases P3 and P4 in figure 19. Notice that we conveniently flipped a signal to indicate that, in the asymmetrical regime, $\Gamma_1 < 1$.

We can repeat the exact same procedure for disease II, as the shape of the dynamical equations is symmetric between the diseases. This would again result in the critical stability condition for the DFE of disease II to be $\lambda_2 = 1$ if $u = 0$ is the stable solution for disease I, and:

$$\frac{1}{\lambda_2} = 1 + (\Gamma_2 - 1)\left(1 - \frac{1}{\lambda_1}\right) \tag{B.8}$$

If $u = 1 - 1/\lambda_1$ is the stable solution instead. We again remark that, for Model A, none of the stability conditions depend on the relative time scale parameter π.

B.1.2 Model B

As discussed, the same is not true for Model B, as one of the phase edges depends on π. Let us perform the perturbative stability analysis to the DFE of disease I. The dynamical equations (Equations 3.22 and 3.23 in the main text) are:

$$\dot{u}(t) = (1-\pi)\,[\beta_1(1-u(t)-v(t)) - \mu_1]u(t) \;-\; \pi\alpha\beta_2 u(t)\,v(t) \tag{B.9}$$

$$\dot{v}(t) = \pi[\,\beta_2(1-u(t)-v(t)) - \mu_2]v(t) \;+\; \pi\alpha\beta_2 u(t)\,v(t). \tag{B.10}$$

Under the perturbative transformation around the DFE:

$$\begin{cases} u(t) = 0 + \epsilon_u(t) \\ v(t) = v + \epsilon_v(t) \end{cases} \tag{B.11}$$

Equations B.9 (up to first order) and B.10 (up to zeroth order) become:

$$\dot{\epsilon}_u(t) \cong (1-\pi)\,[\beta_1(1-v) - \mu_1]\cdot\epsilon_u(t) - \pi\alpha\beta_2\epsilon_u(t)\cdot(v) \tag{B.12}$$

$$0 = \pi[\beta_2(1-v) - \mu_2]\cdot v + 0 \tag{B.13}$$

By extracting $(1-\pi)\mu_1$ from the right-hand side of Equation B.12 and using $\lambda_1 = \beta_1/\mu_2$, $\lambda_2 = \beta_2/\mu_2$, we get:

$$\begin{aligned} \dot{\epsilon}_u(t) &\cong (1-\pi)\mu_1\left\{\left[\frac{\beta_1}{\mu_1}(1-v) - 1\right]\epsilon_u - \frac{\pi\mu_2}{(1-\pi)\mu_1}\alpha\frac{\beta_2}{\mu_2}v\epsilon_u\right\} \\ &\cong (1-\pi)\mu_1\;[\lambda_1(1-v) - 1 - \chi\alpha\lambda_2 v]\;\cdot\epsilon_u(t) \end{aligned} \tag{B.14}$$

Which, again, is a linear decoupled differential equation whose solution is exponential, which decays to zero provided that $\lambda_1(1-v) - 1 - \chi\alpha\lambda_2 v < 1$. As a remainder, χ is the time scale ratio between diseases II and I, defined as $\chi = \frac{\pi\mu_2}{(1-\pi)\mu_1}$ (Equation 3.28 from the main text). The critical condition for stability is such that:

$$\begin{aligned} \lambda_1(1-v) - 1 - \chi\alpha\lambda_2 v &= 0 \\ \lambda_1(1-v) &= 1 + \chi\alpha\lambda_2 v \end{aligned} \tag{B.15}$$

As in Model A, the value of v is given by the stable fixed point prevalence of disease II (i.e., the stable solution of Equation B.13). In the DFE of disease II, $v = 0$ and, according to equation B.15, the critical condition for disease 1 is $\lambda_1 = 1$. This is the edge between phases P1 and P2 in Figure 19. If the DFE of disease II is unstable, the solution is $v = 1 - 1/\lambda_2$, and the critical condition for disease I's onset is given by:

$$\begin{aligned} \lambda_1\left(1 - \left(1 - \frac{1}{\lambda_2}\right)\right) &= 1 + \chi\alpha\lambda_2\left(1 - \frac{1}{\lambda_2}\right) \\ \lambda_1 &= \lambda_2(1 + \chi\alpha(\lambda_2 - 1)) \end{aligned} \tag{B.16}$$

Which represents the edge between phases P3 and P4 in Figure 19. Notice the explicit dependence on the time scale χ, which is unique to this curve in the models that we studied here. Mathematically, this dependence comes from the superinfection term, as it can be seen in Equation B.14. More intuitively, it comes from the fact that *a process from disease II can directly affect the prevalence of disease I* (in Model A, the interaction only occurs through "indirect" ways). This essential difference between Models A and B is the key to determine whether the relative time scale will influence the critical curves of an interacting epidemic model.

To conclude this section, we calculate the stability condition for the DFE of disease II, as no longer the equations are symmetric in Model B. Applying the perturbative transformation:

$$\begin{cases} u(t) = u + \epsilon_u(t) \\ v(t) = 0 + \epsilon_v(t) \end{cases} \tag{B.17}$$

To Equations B.9 and B.10, we get:

$$0 = (1-\pi)[\beta_1(1-u) - \mu_1]u \; - \; 0 \tag{B.18}$$

$$\dot{\epsilon}_v(t) \cong \pi\,[\beta_2(1-u) - \mu_2]\epsilon_v(t) + \pi\alpha\beta_2 \cdot (u) \cdot \epsilon_v(t) \tag{B.19}$$

Extracting $\pi\mu_2$ from Equation B.19 and using $\lambda_2 = \beta_2/\mu_2$, we get the uncoupled linear differential equation:

$$\dot{\epsilon}_v(t) \cong \pi\mu_2[\lambda_2(1-u) - 1 + \alpha\lambda_2 u]\epsilon_u(t) \tag{B.20}$$

Whose solution will exponentially decay if $\lambda_2(1-u) - 1 + \alpha\lambda_2 u < 0$. The critical condition is:

$$\begin{aligned} \lambda_2(1-u) - 1 + \alpha\lambda_2 u &= 0 \\ \lambda_2[1 - u + \alpha u] &= 1 \\ \lambda_2 &= [1 + (\alpha - 1)u]^{-1} \end{aligned} \tag{B.21}$$

Which is very similar to the critical condition of disease II in model A (see Equation B.6). For $u = 0$ (disease I's DFE) being the stable solution, $\lambda_2 = 1$ is the critical condition for disease II's DFE stability, and the expression for the edge between phases P1 and P3 in figure 19. When the stable solution for disease I is $u = 1 - 1/\lambda_1$, Equation B.21 reads:

$$\frac{1}{\lambda_2} = 1 + (\alpha - 1)\left(1 - \frac{1}{\lambda_1}\right) \tag{B.22}$$

Which is the expression for the edges between phases P2 and P4 in Figure 19.

B.2 Coexistence fixed point

The stationary prevalences displayed in Figures 20 to 23 were all obtained from numerical evaluation of closed-form analytical expressions. While finding the stationary prevalence of a disease when the other is extinct is trivial, this is not as straightforward when both diseases coexist in the long term. In this section, we show how to analytically calculate the prevalences for the coexistence fixed points of both models. For simplicity, we shall continue to use u, v and w to denote the fixed point values of the prevalences, and $u(t)$, $v(t)$ and $w(t)$ to denote their time-dependent counterparts.

B.2.1 Model A

We find the fixed points by setting $\dot{u}(t) = \dot{v}(t) = \dot{w}(t) = 0$ in the dynamical equations 3.16 to 3.18. Using the fact that $u, v > 0$ at the coexistence, we divide equation 3.16 by $(1 - \pi)\mu_1 u$, equation 3.17 by $\pi\mu_2 v$ and equation 3.18 by $(1-\pi)\mu_1$, obtaining the following reduced system of equations:

$$0 = \lambda_1[1 - u + (\Gamma_1 - 1)(v - w)] - 1 \tag{B.23}$$

$$0 = \lambda_2[1 - v + (\Gamma_2 - 1)(u - w)] - 1 \tag{B.24}$$

$$0 = \lambda_1\Gamma_1(v - w)u - w + \chi[\lambda_2\Gamma_2(u - w)v - w] \tag{B.25}$$

in which only equation B.25 is non-linear. The disease II time scale factor χ is the same as defined in Eq. 3.28. Using also the definition:

$$s_i = 1 - \frac{1}{\lambda_i}, \quad i = 1, 2, \tag{B.26}$$

where s_i is the solution for a non-interacting SIS model with reproduction ratio λ_i, we can further simplify equations B.23 and B.24 respectively to:

$$u - (\Gamma_1 - 1)(v - w) = s_1 \tag{B.27}$$

$$v - (\Gamma_2 - 1)(u - w) = s_2, \tag{B.28}$$

from which it is intuitive to see that the interaction between the diseases (represented by Γ_1 and Γ_2) causes a deviation from the non-interacting solutions, s_1 and s_2.

At this point, we split the solution in two cases: (a) the simpler case $\Gamma_1 = 0$ (i.e., when disease II completely inhibits infection by disease I) and (b) the more general case $\Gamma_1 > 0$.

B.2.1.1 Case $\Gamma_1 = 0$

In this case, equation B.27 simplifies to:

$$u - w = s_1 - v \tag{B.29}$$

Combining this equation with B.28, we get a 2x2 system for v and $(u - w)$, for which the solution is:

$$v = \frac{s_2 + (\Gamma_2 - 1)s_1}{\Gamma_2} \tag{B.30}$$

$$u - w = \frac{s_1 - s_2}{\Gamma_2} \tag{B.31}$$

Now using that $\Gamma_1 = 0$ in Equation B.25, we obtain an expression for w in terms of known variables:

$$w = \frac{\chi}{1 + \chi} \lambda_2 \Gamma_2 (u - w) v \tag{B.32}$$

Plugging Equations B.30 and B.31 in the above equation, and then using it back to Equation B.31, we get the full expressions for the fixed points when $\Gamma_1 = 0$:

$$u = s_1 - \left[1 - \frac{\chi}{1 + \chi} \frac{s_1 - s_2}{1 - s_2}\right] \left[\frac{s_2 + (\Gamma_2 - 1)s_1}{\Gamma_2}\right] \tag{B.33}$$

$$v = \frac{s_2 + (\Gamma_2 - 1)s_1}{\Gamma_2} \tag{B.34}$$

$$w = \frac{\chi}{1 + \chi} \frac{s_1 - s_2}{1 - s_2} \left[\frac{s_2 + (\Gamma_2 - 1)s_1}{\Gamma_2}\right], \tag{B.35}$$

where we have also replaced $\lambda_2 = 1/(1 - s_2)$. With some analysis of the above expressions, noticing that $\chi/(1-\chi)$ is an increasing function of $\chi > 0$, we can infer that u and w increase with χ (and thus with π), whereas v does not depend on the time scale factor. This is in agreement with the plots in figure 21 (a) and (b). For the most general case, we argument about the increasing behavior of the prevalences with π in section B.3 of this Appendix.

B.2.1.2 Case $\Gamma_1 > 0$

In this case, the fact that equation B.25 is quadratic on its variables cannot be avoided. Our strategy is to use equations B.23 and B.24 to write u, v, $(u-w)$ and $(v-w)$ as functions of the variable w and the model parameters. This can be used in equation B.25 to find the solution for w and, consequently, for the other variables.

We can isolate v in equation B.28 and apply it to equation B.27, obtaining:

$$u = m[P_{12} - (\Gamma_1 - 1)\Gamma_2 w] \tag{B.36}$$

$$v = m[P_{21} - (\Gamma_2 - 1)\Gamma_1 w], \tag{B.37}$$

where we simplified the notation using the definitions

$$P_{12} = s_1 + (\Gamma_1 - 1)s_2 \tag{B.38}$$

$$P_{21} = s_2 + (\Gamma_2 - 1)s_1 \tag{B.39}$$

$$m = 1/[1 - (\Gamma_1 - 1)(\Gamma_2 - 1)]. \tag{B.40}$$

We can also manipulate equations B.36 and B.37 to obtain:

$$u - w = m[P_{12} - \Gamma_1 w] \tag{B.41}$$

$$v - w = m[P_{21} - \Gamma_2 w] \tag{B.42}$$

Now we plug the above expressions into equation B.25 which, after redistributing the terms and dividing them by $\Gamma_1\Gamma_2 m^2$ ($m > 0$ for asymmetrical interactions and, by hypothesis, $\Gamma_1 > 0$), becomes the quadratic equation $aw^2 + bw + c = 0$, where:

$$a = \lambda_1(\Gamma_1 - 1)\Gamma_2 + \chi\lambda_2(\Gamma_2 - 1)\Gamma_1 \tag{B.43}$$

$$b = -\Big\{\lambda_1[P_{12} + (\Gamma_1 - 1)P_{21}] + \\ +\chi\lambda_2[P_{21} + (\Gamma_2 - 1)P_{12}] + \frac{1+\chi}{m^2\Gamma_1\Gamma_2}\Big\} \tag{B.44}$$

$$c = \frac{P_{12}P_{21}}{\Gamma_1\Gamma_2}(\Gamma_1\lambda_1 + \chi\Gamma_2\lambda_2) \tag{B.45}$$

For asymmetrical interactions, it is possible that $a = 0$ in the coexistence region. Thus we write the coexistence fixed point of the system as:

$$w = \begin{cases} \frac{-b-\sqrt{b^2-4ac}}{2a} & a \neq 0 \\ \frac{-c}{b} & a = 0 \end{cases} \tag{B.46}$$

$$u = m[P_{12} - (\Gamma_1 - 1)\Gamma_2 w] \tag{B.47}$$

$$v = m[P_{21} - (\Gamma_2 - 1)\Gamma_1 w] \tag{B.48}$$

From the above expressions, it is difficult to extract the behavior of the prevalences with respect to the time scale parameter χ (or π). However, in appendix B.3 we present an alternative argument that reinforces the behavior observed in Fig. 21.

B.2.2 Model B

Model B has a much simpler procedure to find analytical expressions for the coexistence fixed point u and v, for general values of the parameters. Knowing that $u, v > 0$, one can divide eq. 3.22 by $(1-\pi)\mu_1 u$ and eq. 3.23 by $\pi\mu_2 v$ and set their left-hand sides to 0, obtaining:

$$0 = \lambda_1(1-u-v) - 1 - \chi\alpha\lambda_2 v \tag{B.49}$$

$$0 = \lambda_2(1-u-v) - 1 + \alpha\lambda_2 u \tag{B.50}$$

which is a 2x2 linear system in u and v. Passing convenient terms to the left side of each equation, one can write the system in terms of s_1 and s_2 as defined in B.26:

$$s_1 = u + \phi v \tag{B.51}$$

$$s_2 = (1-\alpha)u + v \tag{B.52}$$

where we define ϕ as:

$$\phi = 1 + \alpha\chi\lambda_2/\lambda_1 \tag{B.53}$$

The solution of this 2x2 system is:

$$u = \frac{s_1 - \phi s_2}{1 + \phi(\alpha - 1)} \tag{B.54}$$

$$v = \frac{(\alpha-1)s_1 + s_2}{1 + \phi(\alpha - 1)} \tag{B.55}$$

B.3 Behavior of the prevalences with π

By plotting the values of the fixed point prevalences, analytically derived in the previous section, we could analyze the behavior of such prevalences with the time scale parameter π for models A and B (e.g. Figure 20). However, as our plots can only cover a subset of the whole parameter space, a valid question is whether the observed increasing/decreasing behaviors with π are valid for any set of parameters (respecting the asymmetrical interaction condition). In this section, we analytically support the statement that the reported behaviors are robust in both models, i.e., they remain consistent throughout the parameter space.

B.3.1 Model A

A possible approach to determine the slope of the fixed point prevalences u, v, w with π is to differentiate the Equations B.46 to B.48 with respect to χ (notice, from the definition in Equation 3.28, that χ is an increasing function of π). This procedure, however, can be very tedious and provides little or no analytical insight. An alternative approach is to implicitly differentiate the reduced equations B.23 to B.25 w.r.t. χ, obtaining more insightful expressions.

Let us define here $u' = \partial u/\partial\chi$, $v' = \partial v/\partial\chi$ and $w' = \partial w/\partial\chi$. Implicit differentiation of equations B.23 to B.25 yield:

$$
\begin{aligned}
0 &= -\lambda_1 u' + (\Gamma_1 - 1)\lambda_1 v' - (\Gamma_1 - 1)\lambda_1 w' && \text{(B.56)}\\
0 &= -\lambda_2 v' + (\Gamma_2 - 1)\lambda_2 u' - (\Gamma_2 - 1)\lambda_2 w' && \text{(B.57)}\\
0 &= \Gamma_1\lambda_1(v' - w') + \Gamma_1\lambda_1(v - w)u' - w' + \\
&\quad [\Gamma_2\lambda_2(u - w)v - w] + \\
&\quad \chi[\Gamma_2\lambda_2(u' - w')v + \Gamma_2\lambda_2(u - w)v' - w'] && \text{(B.58)}
\end{aligned}
$$

With some rearrangement, the above expressions can be written as a linear system given by:

$$A\overrightarrow{x'} = \overrightarrow{b} \tag{B.59}$$

where $\overrightarrow{x'} = (u', v', w')^T$, and

$$A = \begin{bmatrix} -\lambda_1 & (\Gamma_1 - 1)\lambda_1 & -(\Gamma_1 - 1)\lambda_1 \\ (\Gamma_2 - 1)\lambda_2 & -\lambda_2 & -(\Gamma_2 - 1)\lambda_2 \\ A_{wu} & A_{wv} & A_{ww} \end{bmatrix} \tag{B.60}$$

with

$$A_{wu} = \Gamma_1\lambda_1(v-w) + \chi\Gamma_2\lambda_2 v \tag{B.61}$$
$$A_{wv} = \chi\Gamma_2\lambda_2(u-w) + \Gamma_1\lambda_1 u \tag{B.62}$$
$$A_{ww} = \Gamma_1\lambda_1 u + \chi\Gamma_2\lambda_2 v + 1 + \chi \tag{B.63}$$

Moreover, the vector of independent coefficients is

$$\overrightarrow{b} = (0, 0, -[\Gamma_2\lambda_2(u-w)v - w])^T = (0, 0, b_w)^T \tag{B.64}$$

Using Cramer's rule, we can obtain the χ-derivatives as functions of the model parameters and the prevalences:

$$u' = (b_w\lambda_1\lambda_2/\det A)\,(1-\Gamma_1)\Gamma_2 \tag{B.65}$$
$$v' = (b_w\lambda_1\lambda_2/\det A)\,(1-\Gamma_2)\Gamma_1 \tag{B.66}$$
$$w' = (b_w\lambda_1\lambda_2/\det A)\,[1-(\Gamma_1-1)(\Gamma_2-1)] \tag{B.67}$$

Thus, in the asymmetrically interacting regime ($0 \leq \Gamma_1 < 1$ and $\Gamma_2 > 1$), u' has the same sign as w' (thus u and w have the same slope with χ and π), whereas v' (v) has opposite sign (slope). By showing that the ratio $b_w/\det A$ is positive, we could demonstrate that u and w actually increase with π, while v decreases. Although we could not mathematically determine the signals of b_w and $\det A$ for arbitrary model parameters, we collected robust numerical evidence that b_w and $\det A$ are both negative in the coexistence phase (region (P4) in figure 19) for a wide set of model parameters, and so the ratio $b_w/\det A$ is positive. This suggests that the behaviors shown in figures 20.a) and 21 are robust and should remain for the whole coexistence region.

B.3.2 Model B

For model B, one can extract the dependence of the prevalences with π (or χ) directly from their analytical expressions (Equations B.54 and B.55), noticing that $\phi = 1 + \alpha\chi\lambda_2/\lambda_1$ is an increasing function of χ. The prevalence v of disease II, as in equation B.55, is clearly a decreasing function of ϕ for $\alpha > 1$ (which is the asymmetrically interacting case). From equation B.54, we can also directly infer that the prevalence u of disease I also decreases with ϕ for $s_2 > 0$ (or equivalently, $\lambda_2 \geq 1$). However, the coexistence phase (region (P4)) also comprehends a region at which $\lambda_2 < 1$, for which we should check the behavior with ϕ more carefully. Taking the partial derivative of u with respect to ϕ, we get:

$$\frac{\partial u}{\partial \phi} = \frac{-s_2\,[1+\phi(\alpha-1)] - (s_1 - \phi s_2)(\alpha-1)}{(1+\phi(\alpha-1)^2)} \tag{B.68}$$

From the above expression, the condition $\frac{\partial u}{\partial \phi} < 0$ can be simplified as:

$$s_2 + (\alpha - 1)s_1 > 0, \tag{B.69}$$

which is equivalent to the condition that λ_2 is above its critical value for coexistence, expressed by equation 3.26. This means that $\frac{\partial u}{\partial \phi} < 0$ in the whole coexistence region and, therefore, both prevalences v and u are decreasing functions of ϕ, χ and π. This is consistent with the observed behaviors in figures 20.b) and 22.